

Fixed-Order Robust Controller Design by Convex Optimization Using Spectral Models

THÈSE N° 4785 (2010)

PRÉSENTÉE LE 27 AOÛT 2010

À LA FACULTÉ SCIENCES ET TECHNIQUES DE L'INGÉNIEUR

LABORATOIRE D'AUTOMATIQUE

PROGRAMME DOCTORAL EN INFORMATIQUE, COMMUNICATIONS ET INFORMATION

ÉCOLE POLYTECHNIQUE FÉDÉRALE DE LAUSANNE

POUR L'OBTENTION DU GRADE DE DOCTEUR ÈS SCIENCES

PAR

Gorka GALDOS SANZ DE GALDEANO

acceptée sur proposition du jury:

Prof. D. Bonvin, président du jury
Prof. R. Longchamp, Dr A. Karimi, directeurs de thèse
Prof. S. Dormido Bencomo, rapporteur
Prof. L. Guzzella, rapporteur
Prof. A. Ijspeert, rapporteur



ÉCOLE POLYTECHNIQUE
FÉDÉRALE DE LAUSANNE

Suisse
2010

Aitta eta amari

Remerciements

La réussite de cette thèse a été possible grâce à l'aide de nombreuses personnes, et je voudrais saisir l'occasion de les remercier.

Tout d'abord, je tiens à remercier les professeurs Roland Longchamp et Dominique Bonvin ainsi que le Dr. Denis Gillet et le Dr. Alireza Karimi de m'avoir accueilli au sein du laboratoire. Cet ouvrage a également pu être réalisé grâce aux multiples discussions avec mes directeurs de thèse Roland Longchamp et Alireza Karimi. Je voudrais tout particulièrement remercier Ali qui m'a donné de nombreux conseils et qui a toujours trouvé les mots pour me motiver dans les moments difficiles.

Je tiens également à remercier vivement le président du jury Dominique Bonvin ainsi que les professeurs Auke Ijspeert, Lino Guzzella et Sebastián Dormido pour avoir accepté d'évaluer ce travail.

Si cette thèse ne comporte pas trop d'erreurs d'anglais, c'est grâce à la lecture attentive de Mark. Un grand merci pour tout ce temps investi!

Je voudrais remercier tous les collègues du Laboratoire d'Automatique de l'Ecole Polytechnique Fédérale de Lausanne pour l'excellente ambiance qui a toujours régné. Aux secrétaires Ruth, Francine, Homeira, Sol et Sara merci pour le soutien administrative. Merci

à François et Christophe pour trouver des solutions à mes multiples problèmes techniques. Aux amis indiens pour partager mes pauses de midi. Un merci tout particulier à Marc, Mark, Seb, Basile, Damien, Philippe, Christophe et Yvan pour les discussions de tout et de rien durant les cinq années passés.

Bere garaian, Suitzan geratzeko erabakia hartu banuen, neurri handi batean, mendiarekiko dudan loturagatik izan zen. Ezinbestekoa izan da mendian igarotako denbora lan honek eman dizkidan buruhaustek ahazteko. Xabi eskertu nahi dut alpinismoko lehen pausutan laguntzearen; Etxeba, Willy eta Josep mendian pasa ditugun uneengatik; Ilazki eski gainean egin ditugun desnibel kontaezinengatik. Espero dut aurrerantzean ere izango dugula horretarako parada.

Urte hauetan Lausannen elkartu garen lagun euskaldunei ere eskertu nahi diet bertan igarotako momentu guztiengatik.

Nahiz eta azkenengo zortzi urte hauetan herritik urrun izan, Torpedo lagun taldea eskertu nahiko nuke, bueltatzen naizen bakoitzean inoiz joan ez banintz bezala sentiaraztearen.

Ces années de thèse, je les ai partagées avec de nombreuses activités extra-professionnelles. Je tiens à remercier tout spécialement Marc et Mark pour m'avoir donné goût aux activités d'endurance pratiquées durant ces années. Nous avons passé plein de moments inoubliables ensemble, toujours de très bonne humeur. J'espère qu'à l'avenir on vivra encore d'autres aventures en gardant le même esprit!

Saioa, zuri ere eskerrak azken urte hauetan eman didazun laguntza eta babesagatik. Batez ere azkenengo urtean izan duzun pazientziagatik, nire ondoan egotea ez bait da lan erraza izan. Mil esker bihotzez!

Bukatzeko, Andoni, aitta eta ama eskertu nahi ditut. Bereziki gurasoak, nik nahi izan ditudan ikasketak egitea bultzatu eta laguntzearen. Eskerrik asko!

Abstract

This thesis proposes a new method to design fixed-order controllers in frequency domain using convex optimization. The method is based on the shaping of open-loop transfer function in the Nyquist diagram with infinity norm constraints on weighted closed-loop transfer functions. A parametric model is not required in this method as it directly uses frequency-domain data. Furthermore, systems with multi-model uncertainty as well as systems with frequency-domain uncertainties can be considered.

Fixed-order linearly parameterized controllers are designed with the proposed method for single-input single-output (SISO) linear time-invariant plants. The shaping of the open-loop transfer function is performed based on the minimization of the difference with a desired open-loop transfer function under H_∞ constraints on the closed-loop sensitivity functions. Since these constraints represent a nonconvex set in the space of the controller parameters, an inner convex approximation of this set is proposed using the desired open-loop transfer function. This approximation makes the problem of robust fixed-order controller design a convex optimization problem. An extension of the method is proposed to design two-degree-of-freedom (2DOF) controllers for SISO plants. The method is also extended to

tune fixed-order linearly parameterized multivariable controllers for multiple-input multiple-output (MIMO) linear time-invariant plants where the stability of the closed-loop system is guaranteed using Gershgorin bands. The control problem is solved only using a finite number of frequency-domain samples. However, the stability and performance conditions between frequency samples are also verified if a frequency-domain uncertainty is considered. It is shown that this adds some conservatism to the solution.

The proposed frequency-domain method has been tested on many simulation examples. The method has been applied to a flexible transmission benchmark for robust controller design giving extremely good results. Additionally, the method has also been implemented on an experimental high-precision double-axis positioning system. These results show the effectiveness of the proposed methods.

Keywords: robust controller; convex optimization; Nyquist diagram; spectral models; frequency-domain data; H_∞ .

Résumé

Dans cette thèse, une nouvelle méthode utilisant l'optimisation convexe est proposée afin de synthétiser des régulateurs d'ordre fixe dans le domaine fréquentiel. Cette méthode est basée sur le calibrage de la fonction de transfert en boucle ouverte dans le diagramme de Nyquist avec des contraintes de norme infinie sur les fonctions de transfert en boucle fermée pondérées. Cette méthode ne requiert pas de modèles paramétriques car elle peut directement utiliser des données fréquentielles. De plus, cette approche peut directement traiter des systèmes multi-modèles, ainsi que des systèmes comportant des incertitudes fréquentielles.

Des régulateurs d'ordre fixe linéairement paramétrés peuvent être synthétisés pour des systèmes ayant une seule entrée et une seule sortie (SISO), linéaires et stationnaires. Le calibrage de la fonction de transfert en boucle ouverte est réalisé en minimisant la différence entre cette dernière et une fonction de transfert en boucle ouverte désirée. Des contraintes H_∞ sur les fonctions de transfert en boucle fermées sont imposées. Ces contraintes représentent un ensemble non convexe dans l'espace des paramètres du régulateur. Une approximation interne de cet ensemble est proposée en utilisant la fonction de transfert en boucle ouverte désirée. Cette approximation permet de

transformer le problème de commande robuste en un problème d'optimisation convexe. Une extension de la méthode est proposée pour synthétiser des régulateurs à deux degrés de liberté (2DOF) pour des systèmes SISO. En utilisant la même méthodologie, une extension est proposée afin de synthétiser des régulateurs multivariables linéairement paramétrés pour des systèmes à plusieurs entrées à plusieurs sorties (MIMO), linéaires et stationnaires pour lesquels la stabilité de la boucle fermée est garantie en utilisant des bandes de Gershgorin. Le problème de commande est résolu en utilisant un nombre fini de données fréquentielles. Cependant, les conditions de stabilité et de performance entre les données fréquentielles peuvent aussi être vérifiées en ajoutant une incertitude. Cette incertitude ajoute du conservatisme à la solution.

Cette méthode basée dans le domaine fréquentiel a été testée sur de nombreux exemples. Elle a notamment été validée sur un système de transmission flexible servant de référence lors de l'évaluation de la performance des méthodes de commande robuste avec des résultats satisfaisants. En outre, cette méthode a aussi été implémentée sur un système expérimental de positionnement à deux axes de haute précision. Les résultats montrent l'efficacité des méthodes proposées.

Mots-clés : régulateur robuste; optimisation convexe; diagramme de Nyquist; modèles spectraux; données fréquentielles; H_∞ .

Contents

1	Introduction	1
1.1	Motivation	1
1.2	State of the Art	3
1.2.1	Frequency-domain data-based methods for SISO systems	3
1.2.2	Frequency-domain data-based 2DOF controller design methods	5
1.2.3	Frequency-domain data-based methods for MIMO systems	7
1.3	Organization and Contributions of the Thesis	9
2	Fixed-order H_∞ Controller Design for Spectral SISO Models	11
2.1	Introduction	11
2.2	Problem Formulation	12
2.2.1	Class of models	12
2.2.2	Class of controllers	13
2.2.3	Design specifications	15
2.3	Robust Controller Design in Nyquist Diagram	16
2.3.1	Robust performance convex constraints	16
2.3.2	Main result	19

2.3.3	Choice of $L_d(s)$	23
2.3.4	Optimization problem	27
2.4	Simulation Example	28
2.5	Discussion and Conclusions	31
2.5.1	Discussion	31
2.5.2	Conclusions	32
3	Fixed-order RST Controller Design for Spectral SISO Models	35
3.1	Introduction	35
3.2	Problem Formulation	36
3.2.1	Class of models	36
3.2.2	Class of controllers	37
3.2.3	Design specifications	38
3.2.4	Control problem	39
3.3	RST Controller Design in Nyquist Diagram	40
3.3.1	Convex approximation of the constraints on sensitivity functions	40
3.3.2	Optimization problem	44
3.4	Solution to a Flexible Transmission Benchmark	46
3.5	Application to an Industrial Double-Axis Positioning System	53
3.5.1	Non-parametric identification of the dynamics of the higher axis	55
3.5.2	RST controller design of the higher axis	56
3.6	Conclusions	60
4	Fixed-order H_∞ Controller Design for Spectral MIMO Models	65
4.1	Introduction	65
4.2	Problem Formulation	66
4.2.1	Class of models	66
4.2.2	Class of controllers	66
4.2.3	Control problem	67
4.3	MIMO Controller Design in Nyquist Diagram	67

4.3.1	Stability condition based on Gershgorin Bands	68
4.3.2	Main result	70
4.3.3	Optimization problem	72
4.4	Simulation Examples	74
4.4.1	Example 1	74
4.4.2	Example 2	77
4.5	Conclusions	82
5	Controller Design with Finite Number of Constraints	85
5.1	Approximate Approach	87
5.2	Probabilistic Approach	89
5.3	Exact Approach	90
5.3.1	Analysis of the inter-grid behavior	91
5.3.2	Controller design method	94
5.4	Simulation Results	101
5.5	Conclusions	103
6	Conclusions	105
6.1	Summary	105
6.2	Perspectives	107
A	Exact Approach with Integrators	109
A.1	Inter-grid behavior	109
A.2	Controller design method with integrator	113
	Curriculum Vitæ	123

List of Acronyms

2DOF	two-degree-of-freedom
BLT	biggest log modulus tuning
CbT	correlation based tuning
ETFE	empirical transfer function estimate
FRF	frequency response function
LFT	linear fractional transformation
LMI	linear matrix inequality
LPMSM	linear permanent magnet synchronous motor
LTI	linear time-invariant
MIMO	multi-input multi-output
PID	proportional-integral-derivative
PLL	phase locked loop
QFT	quantitative feedback theory
RHP	right half-plane
SDP	semi-definite programming
SIP	semi-infinite programming
SISO	single-input single-output
SSOE	sum of squared output error
Z-N	Ziegler-Nichols

Introduction

1.1 Motivation

Fundamentally, automatic control studies and develops algorithms to tune feedback loops in order to assure that the output tracks a desired trajectory even in presence of disturbances and uncertainty. Automatic control can be implemented on a large variety of systems and it is used extensively in industrial applications. Consequently, many researchers have studied this field in the last few centuries, proposing many methods to design feedback loops for different types of systems.

Many controller design methods have been proposed to tune controllers with different structures, even though most industrial applications using a feedback controller employ the well-known Proportional-Integral-Derivative (PID) controller. This controller has a very simple structure with only three parameters to be tuned. Each of the parameters has an intuitive behavior which makes them relatively easy to tune and, in most cases, they achieve the required specifications. However, nowadays many applications require very demanding specifications which need more sophisticated PID controller design methods or more complex controller structures, e.g.

two-degree-of-freedom controllers (2DOF). In these cases, the methods to be implemented are not simple enough, and experienced engineers are needed to apply them. This is typically the case when the desired specifications for which the controller has been tuned are changed or when the system is modified. If the controller structure or/and the method that have been used to tune it are complex, an engineer is needed to redesign the controller.

Some characteristics are desired for a controller design method to be easy to implement on an industrial system:

- Most of the controller design methods in the literature are parametric model based. This latter kind of model can be obtained either by first principles modeling or by parameter estimation techniques using measured data. However, it is usually too difficult or time consuming to obtain a parametric model based on physical laws. Identification of parametric models is based on much a priori information. The user needs to choose the sampling period, time-delay, number of parameters in the numerator and denominator of the plant and noise model, optimal excitation etc. which are neither easy to choose nor always available. Consequently, data-driven controller design methods using time-domain or frequency-domain data are preferred instead of model based methods. Moreover, frequency-domain data or spectral models are appropriate because stability conditions and several performance specifications can be defined in the frequency domain. Additionally, they need less a priori knowledge of the plant than the parametric models and are obtained directly from data. Furthermore, the information is not condensed into a small set of parameters avoiding errors of unmodeled dynamics that appear in parametric models.
- Many industrial applications can be approximated with a low-order system containing a pure time delay. However, most of the design methods in the literature that can deal with this type of systems approximate the pure time delay. Hence, a controller

design method considering pure time delay without any approximation is preferred.

- Usually, most industrial applications have more than one operating point and, generally, the dynamics of the system change at each operating point. Additionally, due to different types of error, the model at each operating point is not an exact representation of the real system at that point. This type of systems can be represented as a multi-model plant. This is a set of models where each of the models contains additionally a frequency-domain uncertainty. The controller design method should be able to deal directly with this set of uncertain systems.
- Nowadays, controllers are implemented in computers which have limited memory and computing power. The order of the controller plays a key role in this limitation. Many methods in the literature compute high-order controllers which are not implementable. The problem can be resolved using existing methods to reduce the order of the controller. However, it is difficult to guarantee that the reduced controller will satisfy the requirements in terms of stability and performance. Hence, it is desirable to implement methods that tune directly fixed-order controllers.

1.2 State of the Art

This thesis gives some contributions in the following domains: controller design based on frequency-domain data for single-input single-output (SISO) and multiple-input multiple-output (MIMO) systems and two degree-of-freedom (2DOF) controller design based on frequency-domain data.

1.2.1 Frequency-domain data-based methods for SISO systems

The first systematic controller design methods are based on graphical tools where loop-shaping techniques are used in the Bode di-

agram or Nichols chart. These methods are discussed in classical textbooks for the design and analysis of control systems. The well-known Ziegler-Nichols tuning method based on a single point on the frequency response of the plant model (the critical frequency) is still used to tune PID controllers in many practical situations. These approaches are very intuitive and work well for simple systems that can be approximated by a low-order model with a relatively small delay. However, for unstable and nonminimum-phase systems and systems with parametric and frequency-domain uncertainty the results are unsatisfactory. Additionally, stability is not guaranteed. There have been some attempts to modify the Ziegler-Nichols tuning algorithm which are reported in [4].

Recently, it has been shown that the set of all stabilizing PID controllers achieving a desired gain and phase margin or H_∞ norm can be obtained using only frequency-domain data [36]. However, this set is not a convex set and it is only applicable for three-term controllers. Another frequency-domain method is the well-known Quantitative Feedback Theory (QFT) [30] which is based on loop-shaping in the Nichols chart. This approach leads usually to low-order controllers but the design procedure needs some expertise and is based on trial and error. Although recently optimization approaches have been used to compute controllers in the QFT framework [6, 9, 24], H_2 and H_∞ control criteria for spectral models have not yet been considered.

Some iterative methods using specific points of the frequency response function have been developed in literature. A PI controller tuning method achieving a specified maximum sensitivity and phase margin using a Phase Locked Loop (PLL) identifier module for measuring some frequency points is presented in [11]. A PID controller tuning technique based on the minimization of the sum of square errors between the desired and measured specifications (gain margin, phase margin, maximum sensitivity and crossover frequency) has been proposed in [20, 34] based on simple relay experiments. A linear quadratic control criterion in the frequency domain is minimized iteratively using only the spectral models of the closed-loop system

in [33]. At each iteration the closed-loop system (with the controller from the previous iteration) is excited with a reference signal and the gradient and Hessian of the criterion are estimated using the spectral models identified by the measured data. It should be noted that all of the mentioned iterative methods use the Gauss-Newton algorithm and consequently they converge to a local optimum of their criteria. Moreover, they need many experiments on the real system and cannot consider multimodel uncertainty.

With new progress in numerical methods for solving convex optimization problems, new approaches for controller design with convex objectives and constraints have been developed. In [23] a convex optimization method for PID controller tuning by open-loop shaping in the frequency domain is proposed. The infinity-norm of the difference between the desired open-loop transfer function and the achieved one weighted by a so-called target sensitivity function is minimized. It is shown using the small gain theorem that if the infinity norm is less than 1 the nominal closed-loop system is stable. This is a sufficient condition and depends on the choice of the target sensitivity function. The condition for the stability of multiple models becomes more conservative as for each model a reasonable target sensitivity function should be available. In [35] a robust fixed-order controller design using linear programming is proposed. The main feature of this method is that the stability and some robustness margins are guaranteed by linear constraints in the Nyquist diagram and the method is applicable to multiple models as well. However, the performance specifications are limited to the choice of a lower bound for the crossover frequency and the minimization of the integral of the tracking error.

1.2.2 Frequency-domain data-based 2DOF controller design methods

Most of the control problems found in industry have specifications in terms of robustness, disturbance rejection and tracking of a given reference signal. It is very difficult to achieve all the specifications

using one-degree-of-freedom controllers, therefore, 2DOF controllers are preferred. The degree-of-freedom of a controller defines the number of closed-loop transfer functions that can be shaped independently [29], which allows good performance to be achieved whilst preserving robustness.

Typically, a two-step strategy is chosen in order to design the feedback and feedforward terms of 2DOF controllers. In the first step, the feedback term is designed to guarantee stability, robustness and disturbance rejection specifications. Then, the feedforward term is designed to achieve the desired tracking specifications. Many different methods can be found in the literature to tune the feedback or feedforward terms separately. An example is shown in [53] where a combined QFT/H_∞ design technique is proposed. The classical H_∞ method is used to tune the feedback controller to minimize the maximum value of the sensitivity function and the noise amplification for a desired frequency range. Then, the QFT techniques are applied to design the feedforward term to assure certain tracking specifications.

The general H_∞ control problem, where infinity norm constraints are defined for different weighted closed-loop transfer functions is a general representation of most controller design problems. Furthermore, it can be desirable to minimize one or more of these norms to achieve better performances. The classical H_∞ optimization method can deal with the mixed sensitivity controller design problem which is a particular case of the previously mentioned control problem. As it is shown in [58], this is achieved based on the linear fractional transformation (LFT). A controller design problem for a SISO system is transformed to an augmented MIMO system and the infinity norm of the closed-loop weighted transfer function matrix is minimized. This matrix contains many cross transfer functions between the different outputs and inputs of the augmented system which affects the norm to be minimized. Therefore, it is not possible to minimize the infinity norm of one of the weighted closed-loop transfer functions of the original SISO problem under some constraints on the other weighted sensitivity functions. It should be mentioned that

this method tunes both degrees of freedom simultaneously instead of tuning them in two different steps.

1.2.3 Frequency-domain data-based methods for MIMO systems

Many industrial plants, particularly in the process industry, consist of several interconnected loops, which are typically represented by MIMO models. One approach to design multivariable controllers is the classical optimal and robust control technique applied to a state space representation of these MIMO models. Unfortunately, these techniques leads to high-order multivariable controllers with a state-space representation. This type of controller structure is not common in industrial plants and their retuning is difficult for control technicians. Hence, they are rarely used in industry.

A two-step technique is commonly used in practice instead. In the first step the MIMO system is transformed into a diagonally dominant system using a decoupling precompensator. Once the system is diagonally dominant, SISO techniques are used to design the decoupled controllers for each diagonal element of the MIMO system. This strategy is easy to implement and maintain, and is very effective in practice. An example of a two-step approach is given in [48], where first a decoupler is obtained based on the adjoint of the system. Then, a diagonal PID controller is tuned minimizing the integrated absolute error for a step load disturbance for each decoupled system satisfying an upper bound on the sensitivity and complementary sensitivity functions. Many decoupling techniques have been proposed in the literature. The classical decoupling methods are based on the eigenvalue decomposition [45] or the singular value decomposition [31]. The minimization of a non-convex function of the weighted off-diagonals of the open-loop system in some given frequencies is considered in [55] to tune a decoupler. An appropriate choice of the weighting function provides a better decoupling around the crossover frequency.

Since the decoupling step is never perfect, several methods based on a detuning factor are proposed that take into account the coupling effects in the design of SISO controllers. The biggest log modulus tuning (BLT) method proposed in [44] is used to tune individual PI controllers for each decoupled loop using Ziegler-Nichols (Z-N) approach. Then, the proportional and integral terms are multiplied by a detuning factor so that the maximum modulus of the closed-loop transfer function has a specific value. A decentralized PID controller design method using Gershgorin bands is proposed in [28]. By solving a system of nonlinear equations involving the Gershgorin bands, the decentralized controllers are tuned so that desired gain and phase margins are guaranteed for the diagonal system. It should be noted that the global stability is not guaranteed because only two crossover frequencies associated with the gain and phase margins are considered for the Gershgorin bands shaping. The coupling effects for a particular loop from all other closed loops are incorporated in a so called effective transfer function, which is subsequently used to design decentralized controllers using single loop tuning techniques [57]. Several simulation examples show the effectiveness of this approach, however the stability of the multivariable system cannot be guaranteed.

All the above mentioned methods are based on parametric models. Few controller design methods based on MIMO spectral models are available in literature. For diagonally dominant or decoupled systems, in [19] a non-convex frequency criterion is defined as the weighted sum of the squared error between the desired and computed stability margins considering the Gershgorin bands. Then, this criterion is minimized iteratively using the measured data from some specific closed-loop relay tests. The Gershgorin bands are also used to compute the detuning factor for Z-N tuned controllers based on the calculation of the ultimate gains and ultimate frequencies of each loop using the frequency response of the system [10]. The minimization of a weighted difference between a desired diagonal closed-loop frequency response and the real response for a finite number of frequencies is presented in [21] to attain the decoupling and desired

performances via separate non-convex optimizations. Note that this method is only applicable to 2×2 systems. It should be noticed that these methods do not guarantee closed-loop stability.

1.3 Organization and Contributions of the Thesis

A new method to design fixed-order controllers based on open-loop shaping with H_∞ constraints on the weighted closed-loop transfer functions for SISO models is presented in Chapter 2. Using linearly parameterized controllers, every point of the open-loop transfer function is a linear function of the controller parameters in the Nyquist diagram. However, it is observed that the classical H_∞ conditions lead to non-convex constraints. Based on the available desired open-loop transfer function used for the loop shaping, the non-convex constraints are approximated by convex constraints (inner approximation). Hence, the controller design problem is solved using standard convex solvers. The method can deal directly with multi-model uncertainties. Furthermore, time delay systems can be also considered. Additionally, only frequency-domain data are needed to apply the method instead of a parametric model.

An extension of the method to design 2DOF controllers with RST structures is proposed in Chapter 3. The idea is to design RST controllers with a fixed feedback R polynomial by approximating the non-convex weighted sensitivity infinity norm constraints by convex constraints in the Nyquist diagram. The performance can be improved by minimizing one or more of those infinity norms.

Chapter 4 proposes an extension of the method presented in Chapter 2 to deal with systems consisting of several interconnected loops which can be represented as MIMO systems. A linearly parameterized MIMO controller is designed and the stability is guaranteed by approximating the eigenvalues of the transfer function matrix at each frequency using the Gershgorin Bands. The method needs only frequency-domain data and it can also deal with multi-model uncertainties.

In Chapters 2, 3 and 4 , the proposed controller design methods are formulated as convex Semi-Infinite Programming (SIP) problems. This type of optimization problem has a finite number of decision variables to be optimized subject to an infinite number of constraints. In Chapter 5, different solutions to deal with this optimization problem for our particular controller design problem are presented.

Finally, Chapter 6 concludes the manuscript and gives some perspectives related to the design methods proposed in this thesis.

Fixed-order H_∞ Controller Design for Spectral SISO Models

2.1 Introduction

In this chapter, a new approach to design a robust fixed-order controller based on the shaping of the open-loop transfer function is developed. It is shown that robust fixed-order linearly parameterized controllers for LTI-SISO systems represented by nonparametric spectral models can be computed by convex optimization. The stability and several performance conditions are assured with H_∞ constraints on the weighted closed-loop sensitivity transfer functions. It should be mentioned that the set of all fixed-order stabilizing controllers satisfying the infinity norm constraints is a nonconvex set. An inner convex approximation of this set is given by a set of linear constraints in the Nyquist diagram. The proposed method can be used for PID controllers as well as for higher order linearly parametrized controllers in discrete or continuous time. The case of unstable open-loop systems can also be considered if a stabilizing controller is available or the number of unstable poles of the plant is known. The main idea is to define new constraints such that the designed open-loop system has the winding number satisfying the Nyquist stability criterion. Another important feature is that, by contrast with the standard H_∞ problem, this approach can treat the

case of multi-model uncertainty. The effectiveness of the proposed approach is illustrated by comparison with the standard H_∞ control design in a simulation example.

This chapter is organized as follows: In Section 2.2 the class of models, the class of controllers and the control objectives are defined. Section 2.3 introduces the control design methodology based on the linear and convex constraints in the Nyquist diagram. The results of a simulation example are given in Section 2.4. Advantages and disadvantages of the proposed method are discussed in Section 2.5.

2.2 Problem Formulation

2.2.1 Class of models

The class of causal continuous-time LTI-SISO systems with bounded infinity norm is considered. It is assumed that the plant model belongs to a set \mathcal{G} that contains m spectral models with multiplicative unstructured uncertainty :

$$\mathcal{G} = \left\{ G_i(j\omega)[1 + W_{2i}(j\omega)\Delta]; i = 1, \dots, m; \omega \in \mathbb{R} \right\} \quad (2.1)$$

where $W_{2i}(j\omega)$ is the uncertainty weighting frequency function and Δ is a stable unknown transfer function with $\|\Delta\|_\infty < 1$. This type of models can be obtained from a parametric model or by spectral analysis from a set of input/output data.

Consider the input $u(t)$ and the output $y(t)$ of a discrete-time system $G(q^{-1})$ are available for a finite number of $t = 1, \dots, N_t$, where q^{-1} is backward shift operator. Assume that the data are noise-free and the initial and final conditions for u and y are zero, i.e $u(t) = y(t) = 0$ for $t \leq 0$ and $t > N_t$. Then

$$G(e^{-j\omega}) = \frac{Y(\omega)}{U(\omega)} \quad (2.2)$$

where $U(\omega)$ and $Y(\omega)$ are the periodograms of $u(t)$ and $y(t)$ defined by [43]:

$$U(\omega) = \frac{1}{\sqrt{N_t}} \sum_{t=1}^{N_t} u(t)e^{-j\omega t} \quad (2.3)$$

$$Y(\omega) = \frac{1}{\sqrt{N_t}} \sum_{t=1}^{N_t} y(t)e^{-j\omega t} \quad (2.4)$$

For noisy data (2.2) gives the so-called Empirical Transfer Function Estimate (ETFTE) which is asymptotically unbiased and has a variance of $\Phi_v(\omega)/|U(\omega)|^2$, with $\Phi_v(\omega)$ the spectrum of a stationary stochastic disturbance $v(t)$ at the output of the plant. In this case, the spectral model can be represented by a multiplicative uncertainty model $G(e^{-j\omega})[1 + W_2(e^{-j\omega})\Delta]$, where $|W_2(e^{-j\omega})|$ can be computed for a given probability level. It is clear that the quality of the ETFTE estimate can be improved by different ways of smoothing which are not discussed here.

In the sequel, for the sake of simplicity, we consider one of the models in \mathcal{G} with multiplicative frequency-domain uncertainty, $G(j\omega)[1 + W_2(j\omega)\Delta]$ and a continuous-time controller will be designed. Then the results are extended to the multi-model case and the convex combination of m spectral models. The results are also applicable to discrete-time models and other types of frequency-domain uncertainty.

2.2.2 Class of controllers

Linearly parameterized controllers are given by :

$$K(s, \rho) = \rho^T \phi(s) \quad (2.5)$$

where

$$\rho^T = [\rho_1, \rho_2, \dots, \rho_n] \quad (2.6)$$

$$\phi^T(s) = [\phi_0(s), \phi_1(s), \dots, \phi_{n-1}(s)] \quad (2.7)$$

n is the number of controller parameters and $\phi_i(s)$ are stable transfer functions with bounded infinity norm that may be chosen from a set of generalized orthonormal basis functions. Consider for example the Laguerre basis [1, 46]:

$$\phi_0(s) = 1, \phi_i(s) = \frac{\sqrt{2\xi}(s - \xi)^{i-1}}{(s + \xi)^i} \quad \text{for } i \geq 1 \quad (2.8)$$

with $\xi > 0$. It can be shown that for any stable rational finite order transfer function $F(s)$ and for arbitrary $\varepsilon > 0$ there exists a sufficiently large n such that

$$\|F - \rho^T \phi\|_p < \varepsilon \quad \text{for } 0 < p < \infty \quad (2.9)$$

Therefore, with this controller parameterization any finite order stable transfer function can be approximated with a desired accuracy by increasing the number of controller parameters. The quality of this approximation for a finite n , however, depends on the difference between the poles of $F(s)$ and ξ . An appropriate choice of ξ can lead to a better approximation for a given controller order. The optimal choice of basis functions has already been investigated in the context of modeling and identification [25] and will not be considered in this thesis. However, a practical guideline for an appropriate choice of the basis functions follows. First, a very high-order controller is designed with Laguerre basis functions and an arbitrary positive value for ξ . Then, the dominant poles of the optimal high-order controller are identified using the standard methods for model-order reduction. Next, the dominant poles are used as the poles of a low-order generalized orthogonal basis function (see [1]) and a second run of the optimization problem is performed.

The main reason to use a linearly parameterized controller is that every point on the Nyquist diagram of the open-loop transfer function $L(j\omega, \rho)$ can be written as a linear function of the controller parameters ρ :

$$L(j\omega, \rho) = K(j\omega, \rho)G(j\omega) = \rho^T \phi(j\omega)G(j\omega) \quad (2.10)$$

This property helps in obtaining a convex parameterization of fixed-order H_∞ controllers.

Remark: The bounded infinity-norm condition will be relaxed to allow possible poles on the imaginary axis for plant model and controller. It is clear that, in this case, PID controllers belong to the set of parameterized controllers.

2.2.3 Design specifications

The proposed approach is based on the shaping of the open-loop transfer function where H_∞ constraints on the closed-loop sensitivity functions are considered. It is assumed that a desired open-loop transfer function L_d is available which represents all or a part of the desired specifications. Consequently, it is judicious to minimize a norm of $L(\rho) - L_d$. Since $L(\rho)$ is linear with respect to ρ any norm of $L(\rho) - L_d$ is a convex function of ρ .

Let the sensitivity function $\mathcal{S}(s) = [1 + L(s)]^{-1}$ and the complementary sensitivity function $\mathcal{T}(s) = L(s)[1 + L(s)]^{-1}$ be defined. A standard robust control problem is to design a controller that satisfies $\|W_1\mathcal{S}\|_\infty < 1$ for a set of models, where $W_1(s)$ is the performance weighting filter. If the set of models is represented by multiplicative unstructured uncertainty, the necessary and sufficient condition for robust performance is given by [17]:

$$\|W_1\mathcal{S} + W_2\mathcal{T}\|_\infty < 1 \quad (2.11)$$

There is no analytical solution to this problem, however, in the standard H_∞ framework a solution to the following approximate problem can be found:

$$\left\| \begin{array}{c} W_1\mathcal{S} \\ W_2\mathcal{T} \end{array} \right\|_\infty < \frac{1}{\sqrt{2}} \quad (2.12)$$

This solution is conservative and leads to high-order controllers. Moreover, it cannot be applied to systems with multi-model uncertainty.

The proposed approach is based on the shaping of the open-loop transfer function satisfying an infinite number of linear or convex constraints on the Nyquist diagram such that the following robust performance constraint is satisfied:

$$|W_1(j\omega)\mathcal{S}(j\omega)| + |W_2(j\omega)\mathcal{T}(j\omega)| < 1 \quad \forall\omega \quad (2.13)$$

2.3 Robust Controller Design in Nyquist Diagram

2.3.1 Robust performance convex constraints

The basic idea is to represent the robust performance constraints in (2.13) in the Nyquist diagram and give a set of linear or convex constraints which guarantee that the robust performance condition is satisfied. This way, the controller design is represented by a convex optimization problem where a norm of the difference between the actual open-loop transfer function and the desired open-loop transfer function is minimized.

Multiplying the robust performance condition in (2.13) by $|1 + L(j\omega, \rho)|$ gives:

$$|W_1(j\omega)| + |W_2(j\omega)L(j\omega, \rho)| < |1 + L(j\omega, \rho)| \quad \forall\omega \quad (2.14)$$

Note that $|1 + L(j\omega, \rho)|$ is the distance between the critical point $(-1+0j)$ and $L(j\omega, \rho)$. Hence, this constraint is satisfied if and only if there is no intersection in the Nyquist diagram between a circle centered at the critical point with a radius of $|W_1(j\omega)|$ and a circle centered at $L(j\omega, \rho)$ with a radius of $|W_2(j\omega)L(j\omega, \rho)|$ for all ω [17].

Now, consider a straight line $d^*(\omega)$ which is tangent to the circle with radius $|W_1(j\omega)|$ and orthogonal to the line between the critical point $(-1+0j)$ and $L(j\omega, \rho)$. Therefore, the robust performance condition in (2.13) is satisfied if and only if the circle centered at $L(j\omega, \rho)$ does not intersect $d^*(\omega)$ and is completely on the side that excludes the critical point $(-1+0j)$ (on the right hand side in Fig. 2.1).

This condition cannot be represented as a convex constraint because $d^*(\omega)$ is a function of the controller parameters. Using $L_d(j\omega)$, $d^*(\omega)$ can be approximated by $d(\omega)$ which is tangent to the circle with radius $|W_1(j\omega)|$ but orthogonal to the line connecting the critical point $(-1+0j)$ to $L_d(j\omega)$ (see Fig. 2.1). This will be a good approximation if $L_d(j\omega)$ is “close” to $L(j\omega, \rho)$.

It should be noted that the equation of $d(\omega)$ at each frequency depends only on $W_1(j\omega)$ and $L_d(j\omega)$. If we name x and y , respectively, the real and imaginary parts of a point on the complex plane, the equation of $d(\omega)$ at each frequency becomes :

$$|W_1(j\omega)[1 + L_d(j\omega)]| - I_m\{L_d(j\omega)\}y - [1 + R_e\{L_d(j\omega)\}][1 + x] = 0 \quad (2.15)$$

where $R_e\{\cdot\}$ and $I_m\{\cdot\}$ represent real and imaginary parts of a complex value, respectively. Therefore, the condition that $L(j\omega, \rho)$ for all ω is located on the side of $d(\omega)$ that excludes the critical point $(-1 + 0j)$ can be given by the following linear constraints :

$$|W_1(j\omega)[1 + L_d(j\omega)]| - I_m\{L_d(j\omega)\}I_m\{L(j\omega, \rho)\} - [1 + R_e\{L_d(j\omega)\}][1 + R_e\{L(j\omega, \rho)\}] < 0 \quad \forall \omega \quad (2.16)$$

Replacing $R_e\{L_d(j\omega)\} = 1/2[L_d(j\omega) + L_d^*(j\omega)]$ and $I_m\{L_d(j\omega)\} = 1/2[L_d(j\omega) - L_d^*(j\omega)]$, the above linear constraints can be further simplified to:

$$|W_1(j\omega)[1 + L_d(j\omega)]| - R_e\{[1 + L_d^*(j\omega)][1 + L(j\omega, \rho)]\} < 0 \quad \forall \omega \quad (2.17)$$

where $L_d^*(j\omega)$ is the complex conjugate of $L_d(j\omega)$.

There exist two alternatives in order that this condition be satisfied for all models in the uncertainty set represented by a circle centered at $L(j\omega, \rho)$. The first alternative is to approximate the uncertainty circle by a polygon of $\nu > 2$ vertices. Then, the robust performance condition in (2.13) is satisfied if all vertices are located

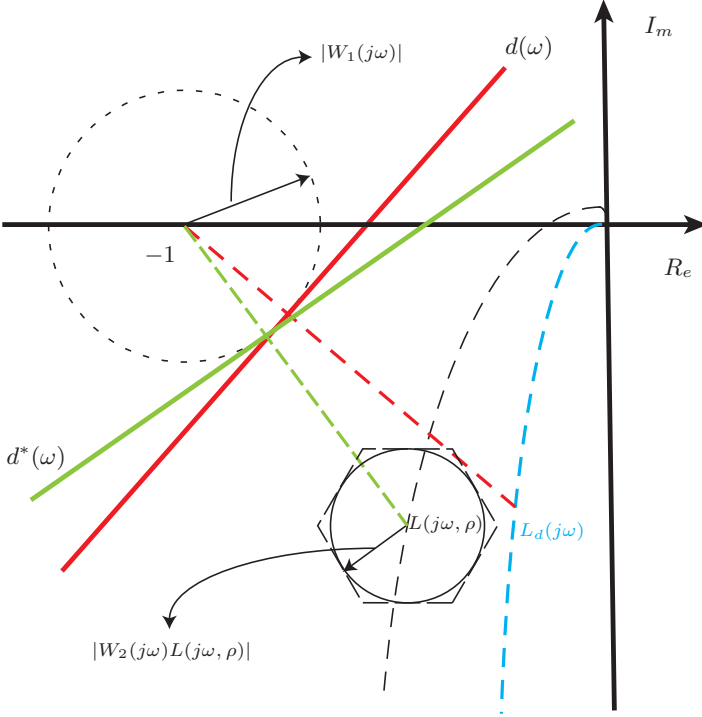


Fig. 2.1. Linear constraints for robust performance in Nyquist diagram

on the right side of $d(\omega)$. This can be represented by the following linear constraints :

$$|W_1(j\omega)[1 + L_d(j\omega)]| - \text{Re}\{[1 + L_d^*(j\omega)][1 + L_i(j\omega, \rho)]\} < 0$$

$$\forall \omega \text{ and } i = 1, \dots, \nu \quad (2.18)$$

where $L_i(j\omega, \rho) = K(j\omega, \rho)G_i(j\omega)$ and

$$G_i(j\omega) = G(j\omega) \left[1 + \frac{|W_2(j\omega)|}{\cos(\pi/\nu)} e^{j2\pi i/\nu} \right] \quad (2.19)$$

It can be observed that the number of linear constraints are multiplied by ν when the uncertainty circle is approximated by a polygon of ν vertices.

The second alternative is to increase the radius of the performance circle by $|W_2(j\omega)L(j\omega, \rho)|$ which leads to the following convex constraints:

$$\begin{aligned} & |W_1(j\omega)[1 + L_d(j\omega)]| + |W_2(j\omega)L(j\omega, \rho)[1 + L_d(j\omega)]| - \\ & R_e\{[1 + L_d^*(j\omega)][1 + L(j\omega, \rho)]\} < 0 \quad \forall \omega \quad (2.20) \end{aligned}$$

This alternative has less constraints and no conservatism but leads to a slightly more complex convex optimization problem (convex constraints instead of linear constraints).

It should be noted that the nonconvex constraint in (2.11) is convexified using the desired open-loop transfer function $L_d(s)$. In other words, the convex set in (2.20) is an inner approximation of the nonconvex set defined by the constraint in (2.11).

2.3.2 Main result

The main result of this chapter is presented in the following theorem:

Theorem 2.1 *Given the set of models \mathcal{G} in (2.1) with performance weighting functions $W_{1_i}(j\omega)$, the linearly parameterized controller in (2.5) stabilizes all models in \mathcal{G} and satisfies the following robust performance condition:*

$$\| |W_{1_i}\mathcal{S}_i| + |W_{2_i}\mathcal{T}_i| \|_\infty < 1 \quad \text{for } i = 1, \dots, m \quad (2.21)$$

if

$$\begin{aligned} & |W_{1_i}(j\omega)| + |W_{2_i}(j\omega)\rho^T\phi(j\omega)G_i(j\omega)| \\ & - \frac{R_e\{[1 + L_{d_i}^*(j\omega)][1 + \rho^T\phi(j\omega)G_i(j\omega)]\}}{|1 + L_{d_i}(j\omega)|} < 0 \\ & \forall \omega \quad \text{for } i = 1, \dots, m \quad (2.22) \end{aligned}$$

where $L_{d_i}(j\omega)$ is chosen such that the number of counterclockwise encirclements of the critical point by its Nyquist plot is equal to the number of unstable poles of $G_i(s)$ and $L_{d_i}^*(j\omega)$ is the complex conjugate of $L_{d_i}(j\omega)$.

Proof: Since the real value of a complex number is less than or equal to its magnitude, we have:

$$Re\{[1 + L_{d_i}^*(j\omega)][1 + \rho^T \phi(j\omega)G_i(j\omega)]\} \leq | [1 + L_{d_i}^*(j\omega)][1 + \rho^T \phi(j\omega)G_i(j\omega)] | \quad (2.23)$$

Then from (2.22) we obtain:

$$|W_{1_i}(j\omega)| + |W_{2_i}(j\omega)\rho^T \phi(j\omega)G_i(j\omega)| - |1 + \rho^T \phi(j\omega)G_i(j\omega)| < 0 \quad \forall \omega \quad \text{for } i = 1, \dots, m \quad (2.24)$$

which gives:

$$\left| \frac{W_{1_i}(j\omega)}{1 + L_i(j\omega, \rho)} \right| + \left| \frac{W_{2_i}(j\omega)L_i(j\omega, \rho)}{1 + L_i(j\omega, \rho)} \right| < 1 \quad \forall \omega \quad \text{for } i = 1, \dots, m \quad (2.25)$$

that leads directly to (2.21).

Now we should show that this controller stabilizes all models in \mathcal{G} . From (2.22), for $i = 1, \dots, m$, we have:

$$Re\{[1 + L_{d_i}^*(j\omega)][1 + \rho^T \phi(j\omega)G_i(j\omega)]\} > 0 \quad \forall \omega \quad (2.26)$$

or $wno\{[1 + L_{d_i}^*(j\omega)][1 + L_i(j\omega, \rho)]\} = 0$, where wno stands for winding number around the origin. It should be mentioned that $L_{d_i}^*(j\omega)$ and $L_i(j\omega, \rho)$ are zero or constant for the semicircle with infinity radius of the Nyquist contour so the wno depends only on the variation of s on the imaginary axis. Therefore:

$$wno[1 + L_{d_i}(j\omega)] = wno[1 + L_i(j\omega, \rho)] \quad (2.27)$$

Since $L_{d_i}(j\omega)$ satisfies the Nyquist criterion, $L_i(j\omega, \rho)$ will do so as well and all closed-loop systems are stable. ■

Corollary 2.1 *Consider the convex combination of m spectral models in \mathcal{G} :*

$$\sum_{i=1}^m \lambda_i G_i(j\omega) [1 + W_{2_i}(j\omega)\Delta] \triangleq G_\lambda(j\omega) [1 + W_2(j\omega)\Delta] \quad (2.28)$$

where

$$G_\lambda(j\omega) \triangleq \sum_{i=1}^m \lambda_i G_i(j\omega) \quad (2.29)$$

$$W_2(j\omega) \triangleq \frac{\sum_{i=1}^m \lambda_i G_i(j\omega) W_{2_i}(j\omega)}{G_\lambda(j\omega)} \quad (2.30)$$

$\lambda = [\lambda_1, \dots, \lambda_m]$, $\sum_{i=1}^m \lambda_i = 1$ and $\lambda_i \in [0, 1]$. Then, the linearly parameterized controller in (2.5) will stabilize this model for any admissible λ and satisfies the following robust performance condition:

$$\| |W_1 \mathcal{S}| + |W_2 \mathcal{T}| \|_\infty < 1 \quad (2.31)$$

where

$$W_1(j\omega) \triangleq \sum_{i=1}^m \lambda_i W_{1_i}(j\omega) \quad (2.32)$$

if (2.22) is satisfied with $L_{d_i}(j\omega) = L_d(j\omega)$ for $i = 1, \dots, m$. $L_d(j\omega)$ should be chosen such that the number of counterclockwise encirclements of the critical point by its Nyquist plot is equal to the number of unstable poles of $G_\lambda(s)$. A fixed $L_d(j\omega)$ means that the number of unstable poles of $G_\lambda(s)$ should be fixed for all λ .

Proof: Multiplying (2.22) by λ_i and adding the m constraints we obtain:

$$\begin{aligned} & \sum_{i=1}^m \lambda_i |W_{1_i}(j\omega)| + \sum_{i=1}^m |W_{2_i}(j\omega) \rho^T \phi(j\omega) \lambda_i G_i(j\omega)| - \\ & \frac{Re\{[1 + L_d^*(j\omega)][1 + \rho^T \phi(j\omega) \sum_{i=1}^m \lambda_i G_i(j\omega)]\}}{|1 + L_d(j\omega)|} < 0 \quad \forall \omega \quad (2.33) \end{aligned}$$

We have : $|W_1(j\omega)| \leq \sum_{i=1}^m \lambda_i |W_{1_i}(j\omega)|$ and

$$\left| \rho^T \phi(j\omega) \sum_{i=1}^m \lambda_i G_i(j\omega) W_{2_i}(j\omega) \right| \leq \sum_{i=1}^m |W_{2_i}(j\omega) \rho^T \phi(j\omega) \lambda_i G_i(j\omega)| \quad (2.34)$$

Therefore :

$$\begin{aligned} & |W_1(j\omega)| + |\rho^T \phi(j\omega) G_\lambda(j\omega) W_2(j\omega)| \\ & - \frac{R_e\{[1 + L_d^*(j\omega)][1 + \rho^T \phi(j\omega) G_\lambda(j\omega)]\}}{|1 + L_d(j\omega)|} < 0 \quad \forall \omega \end{aligned} \quad (2.35)$$

The rest of the proof is similar to that of Theorem 2.1. \blacksquare

Remarks:

1. The results of Theorem 2.1 are valid if $L_i(s, \rho)$ has some poles on the imaginary axis, say $\{jp_1, jp_2, \dots\}$. In this case $\omega \in \mathbb{R} - \{[p_1 - \epsilon, p_1 + \epsilon], [p_2 - \epsilon, p_2 + \epsilon], \dots\}$ where ϵ is a small positive value. The stability is guaranteed if $L_{d_i}(s)$ contains the poles on the imaginary axis of $L_i(s, \rho)$ because they will have the same behavior at the small semicircular detour of the Nyquist contour at these poles.
2. The same approach can be applied when an additive uncertainty model is available i.e.

$$\tilde{G}_i(s) = G_i(s) + W_{3_i}(s)\Delta(s) \quad (2.36)$$

The robust performance condition is given by:

$$\left\| |W_{1_i} \mathcal{S}_i| + \left| \frac{W_{3_i}}{G_i} \mathcal{T}_i \right| \right\|_\infty < 1 \quad \text{for } i = 1, \dots, m \quad (2.37)$$

In this case the convex constraints in (2.22) can be used with the difference that

$$|W_{2_i}(j\omega)| = \frac{|W_{3_i}(j\omega)|}{|G_i(j\omega)|} \quad (2.38)$$

3. Individual shaping of the sensitivity functions is also possible using the constraints in (2.22) with one of the filters equal to zero.
4. Instead of minimizing a norm of $L(\rho) - L_d$, the robust performance can be improved by minimizing the upper bound of the infinity norm of the weighted sensitivity function. Consider the following optimization problem for a single model:

$$\begin{aligned} \min \gamma \\ \||W_1\mathcal{S}| + |W_2\mathcal{T}|\|_\infty < \gamma \end{aligned} \quad (2.39)$$

This optimization can be solved by an iterative bisection algorithm. At each i -th iteration, for a fixed γ_i , we replace W_1 and W_2 with W_1/γ_i and W_2/γ_i and we solve the feasibility problem represented by the linear constraints in (2.18) or convex constraints in (2.20). If the problem is feasible, γ_{i+1} will be chosen smaller than γ_i and if the problem is infeasible γ_{i+1} will be increased.

2.3.3 Choice of $L_d(s)$

Open-loop shaping

The choice of $L_d(s)$ should be coherent with respect to plant, controller structure and design specifications. For example, if we design a PID controller for open-loop stable systems with no pole on the imaginary axis a good choice is $L_d(s) = \omega_c/s$ with ω_c the desired closed-loop crossover frequency. It is clear that $L_d(s)$ contains only one integrator that reflects the integrator of the PID controller. This choice is coherent with the choice of desired open-loop transfer function in the classical open-loop shaping methods that suggest

the magnitude of the open-loop transfer function should be large at low frequencies and small at high frequencies. If a desired reference model $\mathcal{M}(s)$ for the closed-loop system is available, $L_d(s)$ can be chosen equal to $\mathcal{M}(s)[1 - \mathcal{M}(s)]^{-1}$. If $W_1(s)$ is designed as the inverse of a target sensitivity function, a good choice of $L_d(s)$ is $W_1(s) - 1$.

The choice of $L_d(s)$ is more important for unstable systems. In this case, according to Theorem 2.1, the winding number of the Nyquist plot of $L_d(s)$ around the critical point should satisfy the Nyquist stability criterion. For this purpose, the number of unstable poles of the plant model should be known or a stabilizing controller $K_0(s)$ should be available. In the latter, $L_d(j\omega) = K_0(j\omega)G(j\omega)$ is a good choice that satisfies the Nyquist criterion.

H_∞ control problem

In some control problems, such as feasibility problem satisfying H_∞ constraints or a performance minimization problem as explained in Remark 4, $L_d(s)$ might not be considered as a performance specification (e.g. as the example 2.4). In these cases, $L_d(s)$ is only chosen to convexify the nonconvex constraints in (2.11) giving the convex set in (2.20). $L_d(s)$ plays an intermediate role in reducing the conservatism of the solution.

The following Proposition shows under what condition a feasible point of the nonconvex set in (2.11) is also a feasible point of the convex inner approximation set in (2.20).

Proposition 2.1 *Consider that ρ° belongs to the non-convex set (2.11), i.e. :*

$$\| |W_1\mathcal{S}(\rho^\circ)| + |W_2\mathcal{T}(\rho^\circ)| \|_\infty = \gamma(\rho^\circ) < 1 \quad (2.40)$$

then ρ° satisfies the constraints in (2.20) if and only if :

$$\begin{aligned} & |\angle(1 + L_d(j\omega)) - \angle(1 + L(j\omega, \rho^\circ))| < \\ & \cos^{-1} (|W_1(j\omega)\mathcal{S}(j\omega, \rho^\circ)| + |W_2(j\omega)\mathcal{T}(j\omega, \rho^\circ)|) \quad \forall \omega \end{aligned} \quad (2.41)$$

The above inequality is satisfied if

$$|\angle(1 + L_d(j\omega)) - \angle(1 + L(j\omega, \rho^\circ))| < \cos^{-1} \gamma(\rho^\circ) \quad \forall \omega \quad (2.42)$$

Proof: The proof is straightforward using the following relation:

$$\begin{aligned} R_e\{[1 + L_d^*(j\omega)][1 + L(j\omega, \rho^\circ)]\} = \\ |1 + L_d^*(j\omega)||1 + L(j\omega, \rho^\circ)| \cos \alpha \end{aligned} \quad (2.43)$$

where

$$\alpha = |\angle[1 + L(j\omega, \rho^\circ)] - \angle[1 + L_d(j\omega)]| \quad (2.44)$$

Replacing the right hand side of (2.43) in (2.20) gives:

$$\begin{aligned} |W_1(j\omega)| + |W_2(j\omega)L(j\omega, \rho^\circ)| < \\ |1 + L(j\omega, \rho^\circ)| \cos \alpha \quad \forall \omega \end{aligned} \quad (2.45)$$

Dividing both sides by $|1 + L(j\omega, \rho^\circ)|$ leads to :

$$|W_1(j\omega)\mathcal{S}(j\omega, \rho^\circ)| + |W_2(j\omega)\mathcal{T}(j\omega, \rho^\circ)| < \cos \alpha \quad \forall \omega \quad (2.46)$$

which is equivalent to (2.41). A sufficient condition for the above inequality is that the maximum value of the left hand side be smaller than $\cos \alpha$ or:

$$\gamma(\rho^\circ) < \cos \alpha \quad (2.47)$$

from which (2.42) can be concluded. ■

Suppose for example that ρ° is a feasible point of the nonconvex set with $\gamma(\rho^\circ) = 0.7$, then α , the phase difference of $1 + L_d(j\omega)$ and $1 + L(j\omega, \rho^\circ)$, should be less than $\cos^{-1} 0.7 = 45^\circ$. This represents a very large set (one quarter of the complex plane) of admissible $L_d(j\omega)$ for which ρ° is in the feasibility set of the inner approximation (see Fig. 2.2). It is clear that if the specifications are too tight (which means that for any feasible point ρ° , $\gamma(\rho^\circ)$ is very close to 1),

and controller (including the poles on the imaginary axis) will be “close” to $L(s, \rho^*)$ and the convex set generated based on this $L_d(s)$ probably contains the optimal controller. In this case the optimal controller can be found by minimizing a criterion $J(\rho) = \|L(\rho) - L_d\|$ under the robust performance constraint in (2.22).

If the first choice of $L_d(j\omega)$ leads to a non feasible set, the iterative windsurfing approach [3] can be used to compute an appropriate $L_d(s)$. In this approach we start with modest specifications by reducing the gain of W_1 and W_2 so that a feasible solution ρ_1 is obtained. Then $L_d(j\omega) = L(j\omega, \rho_1)$ is chosen and the specifications will be tightened by increasing the gain of W_1 and W_2 . A feasible solution ρ_2 for the second feasibility problem will be used to compute a new $L_d(j\omega) = L(j\omega, \rho_2)$. Although the convergence of this iterative approach to the optimal solution cannot be proved, good results in practice can be obtained.

It should be mentioned that a nonrealistic choice of $L_d(s)$ (with respect to plant model and controller structure) will only increase the conservatism of the approach and never leads to a destabilizing controller. As a result, a badly chosen $L_d(s)$ may lead to an infeasible solution.

2.3.4 Optimization problem

Any norm of $L - L_d$ can be minimized subject to the linear or convex constraints proposed in (2.18) or in (2.20) respectively. A convex optimization approach is proposed in which the system two norm of $L - L_d$ is minimized under the convex constraints in (2.20):

$$\min_{\rho} \|L(\rho) - L_d\|_2$$

Subject to: (2.48)

$$\begin{aligned} & |W_1(j\omega)[1 + L_d(j\omega)]| + |W_2(j\omega)L(j\omega, \rho)[1 + L_d(j\omega)]| - \\ & R_e\{[1 + L_d^*(j\omega)][1 + L(j\omega, \rho)]\} < 0 \quad \forall \omega \end{aligned}$$

This optimization problem is known as the convex SIP problem where a finite number of decision variables (the parameters of the

controller) should be optimized subject to an infinite number of constraints. Different approaches to solving this type of optimization problem are discussed in Chapter 5. A practical solution to solving (2.48) is to choose a finite number of frequencies and define a finite set of convex constraints in (2.20) for $\omega \in \{\omega_1, \omega_2, \dots, \omega_N\}$. The two norm is replaced by $\|L(\rho) - L_d\|_2^2$ which at the same time is approximated by $\sum_{k=1}^N |L(j\omega_k, \rho) - L_d(j\omega_k)|^2$ to obtain a quadratic objective function. Thus, the following optimization problem is considered:

$$\min_{\rho} \sum_{k=1}^N |L(j\omega_k, \rho) - L_d(j\omega_k)|^2$$

Subject to:

$$\begin{aligned} & |W_1(j\omega_k)[1 + L_d(j\omega_k)]| + |W_2(j\omega_k)L(j\omega_k, \rho)[1 + L_d(j\omega_k)]| - \\ & R_e\{[1 + L_d^*(j\omega_k)][1 + L(j\omega_k, \rho)]\} < 0 \quad \text{for } k = 1, \dots, N \end{aligned} \quad (2.49)$$

where $L_d^*(j\omega_k)$ is the complex conjugate of $L_d(j\omega_k)$.

2.4 Simulation Example

This example is a classical H_∞ control problem and it is shown that the proposed approach gives better performance with a lower order controller. Additionally, it shows that the proposed method is applicable to unstable systems. The example is taken from [16] where a robust performance problem is defined for an unstable plant.

Consider the family of plants described by the following multiplicative uncertainty model:

$$\tilde{G}(s) = \frac{(s+1)(s+10)}{(s+2)(s+4)(s-1)} [1 + W_2(s)\Delta(s)] \quad (2.50)$$

where

$$W_2(s) = 0.8 \frac{1.1337s^2 + 6.8857s + 9}{(s+1)(s+10)} \quad (2.51)$$

The nominal performance is defined by $\|W_1\mathcal{S}\|_\infty < 1$ with :

$$W_1(s) = \frac{2}{(20s + 1)^2} \quad (2.52)$$

The objective is to compute a controller $K(s)$ that optimizes the robust performance by minimizing γ in (2.39).

The standard H_∞ solution solves an approximate problem and leads to $\gamma_{\text{opt}} = 0.844$ for this problem with the controller $K(s) = N_\infty/D_\infty$, where

$$N_\infty = 7.409e6s^6 + 1.266e8s^5 + 6.335e8s^4 + 1.152e9s^3 + 6.911e8s^2 + 5.442e7s + 9.37e5 \quad (2.53)$$

$$D_\infty = s^7 + 9.07e5s^6 + 1.901e7s^5 + 1.043e8s^4 + 4.416e7s^3 - 4.682e7s^2 - 4.962e6s - 1.262e5 \quad (2.54)$$

This 7th-order controller is unstable and has a pair of complex conjugate poles very close to the imaginary axis.

Now, the method proposed in this chapter is applied to design a PID controller represented by :

$$K(s) = [K_p \ K_i \ K_d] \left[1 \ \frac{s}{1 + T_f s} \right]^T \quad (2.55)$$

where the time constant of the derivative part of the PID controller T_f is set to 0.01 s. The frequency response of the model is computed at $N = 500$ linearly spaced frequency points between 10^{-3} and 10^3 rad/s. The uncertainty circle at each frequency is approximated by an outbounding polygon with $\nu = 8$ vertices. The plant model contains one unstable pole and the controller contains an integrator, so the desired open-loop transfer function is chosen as

$$L_d(s) = \beta \frac{s + \alpha}{s(s - 1)} \quad (2.56)$$

This is the simplest choice of $L_d(s)$ that contains a stable zero to ensure the Nyquist stability criterion. The characteristic polynomial of the closed-loop system with $L_d(s)$ is given by: $s^2 - s + \beta s + \beta\alpha$.

Taking $\alpha = 1$ for simplicity, the stability criterion is satisfied for $L_d(s)$ with $\beta > 1$. For instance, we choose $\beta = 2$ and we will study later the sensitivity of the solution for different values of β .

In order to obtain the controller giving the minimal value for γ , the bisection algorithm explained in Remark 4 of Subsection 2.3.2 is used with the linear constraints in (2.18) and leads to

$$\| |W_1 \mathcal{S}| + |W_2 \mathcal{T} \|_\infty = 0.7262 \quad (2.57)$$

The resulting PID controller is :

$$K_0(s) = \frac{2.074s^2 + 9.702s + 6.425}{0.01s^2 + s} \quad (2.58)$$

It is interesting to observe that this PID controller gives better performance than the H_∞ controller. Moreover, it is stable and easily implementable on a real system. The performance can be further improved using a new $L_d(s)$ based on $K_0(s)$. With this new $L_d(s) = K_0(s)G(s)$ the optimal controller is given by :

$$K(s) = \frac{2.643s^2 + 23.500s + 8.589}{0.01s^2 + s} \quad (2.59)$$

which leads to $\gamma_{\text{opt}} = 0.7247$.

In order to study the sensitivity of the solutions to the choice of $L_d(s)$, the value of β in (2.56) is changed from 2 to 97 with a step size of 5. For each value of β the minimum of γ is computed. The mean value of optimal γ 's is 0.7611 and its standard deviation 0.0394. This shows that although the optimal solution depends on the choice of $L_d(s)$, it is not very sensitive to this choice. Moreover, the results obtained by this approach, whatever the choice of β between 2 and 97, are better than the standard H_∞ optimal solution.

2.5 Discussion and Conclusions

2.5.1 Discussion

It should be mentioned that the problem of robust fixed-order controller design is a non-convex NP-hard problem and all solutions to this problem are based on some approximations. For example, if we consider the standard H_∞ control problem for design of fixed-order controllers for systems with multi-model and frequency-domain uncertainty, we have the following approximations :

- Approximation of the structured multi-model uncertainty with unstructured frequency-domain uncertainty.
- Approximation of the frequency-domain uncertainty with a rational weighting filter.
- Approximation of the real robust performance condition in (2.11) with the condition given in (2.12).
- Approximation of the resulting high-order controller with a fixed-order controller. In this operation, it is difficult to even guarantee the stability and performance for the reduced-order controller.

The proposed method considers directly the multi-model and frequency-domain uncertainty and designs a fixed-order controller. Systems with time-delay can also be considered. However, it seems that this method has some drawbacks which are discussed below :

1. The proposed optimization problem has an infinite number of constraints. However, in practice, a finite number of frequency points is sufficient for almost all applications. Different approaches to deal with this problem are discussed in Chapter 5.
2. The controller is linearly parameterized, so the denominator of the controller is fixed and it should be chosen prior to design. In practice, some of the poles of the controller are usually fixed to achieve certain closed-loop performances. For example a pole at origin, an integrator, or a pair of complex poles in a certain frequency are fixed in order to reject the disturbances (internal model principle). Therefore, this condition is not restrictive for

low-order controller design. For higher order controller design the use of a set of orthogonal basis function is proposed. It is known that by increasing the controller order any stable transfer function can be approximated with such a set. On the other hand, this restriction ensures the stability of the controller which is required in many applications and cannot be guaranteed by a full controller parameterization. This means that this parameterization cannot be applied to systems which are not stabilizable by stable controllers.

3. The robust performance condition in (2.11) is transformed to a set of linear constraints in (2.18) or convex constraints in (2.20) which adds some conservatism.

2.5.2 Conclusions

It is very difficult (if not impossible) to compare, by a theoretical analysis, the overall approximation or conservatism of different approaches to fixed-order controller design. However, the effectiveness of the proposed approach has been shown by the simulation example. The advantages of this approach are summarized below:

- The method uses only the frequency response of the system and no parametric model is required. The frequency response of the model and the uncertainty at each frequency can be obtained directly by the discrete Fourier transform from a set of data, so the method can be considered as completely “data-driven”. Of course, the method can be applied as well if a parametric model with a pure time delay and an uncertainty set is available.
- PID controllers as well as higher order controllers with H_∞ type specifications can also be designed within the same framework.
- Unstable systems can also be considered if the number of unstable poles or a stabilizing controller is known.
- The method is very simple, at least as simple as open-loop shaping methods in Bode diagram or in Nichols chart currently used

in textbooks for undergraduate courses in control systems. Moreover, the case of multi-model uncertainty can be handled easily just by increasing the number of linear constraints while the mentioned classical frequency-domain approaches cannot deal with this type of uncertainty.

Fixed-order RST Controller Design for Spectral SISO Models

3.1 Introduction

Basically, a two-step strategy can be considered to extend the proposed method in Chapter 2 to tune 2DOF controllers. First, a linearly parameterized feedback controller can be obtained by applying directly the method proposed in the previous chapter. Then, by a second optimization, a linearly parameterized feedforward controller can be tuned subject to convex constraints assuring desired upper bounds on the magnitude of the closed-loop sensitivity functions. The main drawback of tuning a 2DOF controller in two different steps is that there is no guarantee of achieving the optimal solution for the original problem. The first optimization result influences the solution of the second optimization problem. Consequently, it is desirable to tune both degrees of freedom simultaneously.

In this chapter, the idea presented in Chapter 2 is extended to design robust fixed-order RST controllers based on open-loop shaping with H_∞ constraints on the weighted closed-loop sensitivity functions. An RST controller is a polynomial controller which was first proposed in [5], and where R , S and T are polynomials in q^{-1} (time shift operator) (see Fig. 3.1). It can be shown that any 2DOF controller can be represented in an RST form choosing the correct

feedback and feedforward terms. In this approach, we consider that the R polynomial is fixed a priori, for example as an integrator. The performance specifications are presented as loop shaping of the open-loop transfer function with H_∞ constraints on the weighted closed-loop sensitivity functions. The set of all fixed-order stabilizing RST controllers satisfying these conditions is a nonconvex set. This set is approximated by an inner convex one represented by a set of convex constraints in the Nyquist diagram. In this chapter, a discrete-time approach is considered, however, the results are also applicable to continuous-time systems.

This chapter is organized as follows: In Section 3.2 the class of models, controllers, the design specifications and the control problem are defined. Section 3.3 introduces the RST control design methodology based on the convex constraints in the Nyquist diagram. A simulation example of a robust controller design benchmark problem for a flexible transmission system is presented in Section 3.4. The proposed method is applied to a double-axis Linear Permanent Magnet Synchronous Motor (LPMSM) in Section 3.5. Some conclusions are given in Section 3.6.

3.2 Problem Formulation

3.2.1 Class of models

The class of causal discrete-time LTI-SISO systems is considered. It is assumed that the plant model belongs to a set \mathcal{G} containing m spectral models:

$$\mathcal{G} = \{G_i(e^{-j\omega}); \quad i = 1, \dots, m; \quad \forall \omega \in [0, \pi]\} \quad (3.1)$$

which are presented in normalized frequencies. This type of model can be obtained from a parametric model or by spectral analysis from a set of input/output data as presented in Subsection 2.2.1.

In the sequel, for the sake of simplicity, we consider a nominal model $G \in \mathcal{G}$ and a discrete-time controller will be designed. However, the results are also applicable to the multi-model case.

3.2.2 Class of controllers

The controller to be designed is a discrete-time 2DOF controller of the RST-type (Figure 3.1). The R polynomial is fixed a priori, which is typically chosen as an integrator:

$$R(q^{-1}) = 1 - q^{-1} \quad (3.2)$$

The S and T polynomials are given by :

$$S(q^{-1}, \rho) = \rho_1 + \rho_2 q^{-1} + \dots + \rho_{n_S} q^{-n_S+1} \quad (3.3)$$

$$T(q^{-1}, \rho) = \rho_{n_S+1} + \rho_{n_S+2} q^{-1} + \dots + \rho_{n_S+n_T} q^{-n_T+1} \quad (3.4)$$

where

$$\rho^T = [\rho_1, \rho_2, \dots, \rho_{n_S+n_T}] \quad (3.5)$$

and n_S and n_T are the number of parameters for S and T polynomials, respectively.

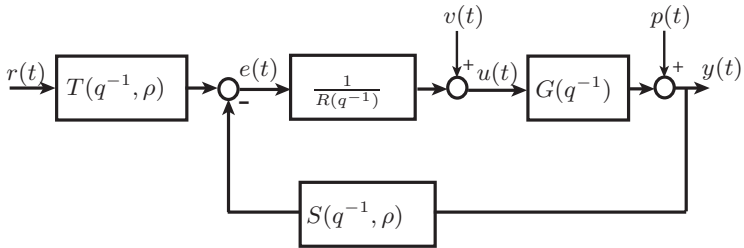


Fig. 3.1. Structure of 2DOF controller of the RST-type

As in the previous chapter, the main property of this parameterization is that every point on the Nyquist diagram of the open-loop transfer function $L(q^{-1}, \rho)$ can be written as a linear function of the parameters ρ :

$$L(q^{-1}, \rho) = \frac{S(q^{-1}, \rho)}{R(q^{-1})} G(q^{-1}) \quad (3.6)$$

3.2.3 Design specifications

As in the previous section, a desired open-loop transfer function L_d is available which represents all or a part of the desired specifications and a norm of $L(\rho) - L_d$ is minimized subject to the constraints on the weighted closed-loop sensitivity functions.

Following the controller structure given in Figure 3.1, different sensitivity functions can be defined between external inputs: $r(t)$ (the reference signal), $v(t)$ (the input disturbance) and $p(t)$ (the output disturbance) and outputs: $y(t)$ (the plant output) and $u(t)$ (the control input).

The following 5 sensitivity functions can be considered:

$$\mathcal{S}_{yr}(q^{-1}, \rho) = \mathcal{S}_1(q^{-1}, \rho) = \frac{\frac{T(q^{-1}, \rho)}{R(q^{-1})}G(q^{-1})}{1 + \frac{S(q^{-1}, \rho)}{R(q^{-1})}G(q^{-1})} \quad (3.7)$$

$$\mathcal{S}_{yv}(q^{-1}, \rho) = \mathcal{S}_2(q^{-1}, \rho) = \frac{G(q^{-1})}{1 + \frac{S(q^{-1}, \rho)}{R(q^{-1})}G(q^{-1})} \quad (3.8)$$

$$\mathcal{S}_{yp}(q^{-1}, \rho) = \mathcal{S}_{uv}(q^{-1}, \rho) = \mathcal{S}_3(q^{-1}, \rho) = \frac{1}{1 + \frac{S(q^{-1}, \rho)}{R(q^{-1})}G(q^{-1})} \quad (3.9)$$

$$\mathcal{S}_{ur}(q^{-1}, \rho) = \mathcal{S}_4(q^{-1}, \rho) = \frac{\frac{T(q^{-1}, \rho)}{R(q^{-1})}}{1 + \frac{S(q^{-1}, \rho)}{R(q^{-1})}G(q^{-1})} \quad (3.10)$$

$$\mathcal{S}_{up}(q^{-1}, \rho) = \mathcal{S}_5(q^{-1}, \rho) = -\frac{\frac{S(q^{-1}, \rho)}{R(q^{-1})}}{1 + \frac{S(q^{-1}, \rho)}{R(q^{-1})}G(q^{-1})} \quad (3.11)$$

A small tracking error for a given reference signal is usually a desired specification in many control problems. The tracking error sensitivity function can be defined as:

$$\mathcal{S}_6(q^{-1}, \rho) = \mathcal{S}_1(q^{-1}, \rho) - 1 = \frac{\frac{T(q^{-1}, \rho) - S(q^{-1}, \rho)}{R(q^{-1})}G(q^{-1}) - 1}{1 + \frac{S(q^{-1}, \rho)}{R(q^{-1})}G(q^{-1})} \quad (3.12)$$

The performance and robust stability of most control problems can be defined by constraints on the infinity norm of the weighted sensitivity functions. A standard nominal performance control problem designs a controller satisfying $\|W_1\mathcal{S}_{yp}\|_\infty < 1$ where W_1 represents the performance filter. If the system's uncertainty is represented by a multiplicative uncertainty

$$\tilde{G}(q^{-1}) = G(q^{-1})[1 + W_2(q^{-1})\Delta(q^{-1})] \text{ with } \|\Delta\|_\infty < 1 \quad (3.13)$$

the robust stability is given by [17]:

$$\|W_2\mathcal{S}_{yr}\|_\infty < 1 \quad (3.14)$$

In general, any upper bound condition on the previously mentioned sensitivity functions can be defined by the following constraints:

$$\|W_p\mathcal{S}_p\|_\infty < 1 \quad \text{for } p = 1, \dots, 6 \quad (3.15)$$

These constraints are however non-convex on the controller parameters ρ . In this chapter, convex constraints are proposed on the Nyquist diagram to guarantee the following performance conditions:

$$|W_p(e^{-j\omega})\mathcal{S}_p(e^{-j\omega})| < 1 \quad \forall \omega \in [0, \pi] \text{ and for } p = 1, \dots, 6 \quad (3.16)$$

3.2.4 Control problem

The following non-convex controller design problem is treated in this chapter:

$$\begin{aligned} & \min \|L - L_d\|_2 \\ & \text{Subject to:} \\ & \|W_p\mathcal{S}_p\|_\infty < 1 \quad \text{for } \forall p \in P \end{aligned} \quad (3.17)$$

where P is a subset of the set $\{1, \dots, 6\}$.

To illustrate the advantage of tuning both degrees of freedom simultaneously over tuning them in two steps, the following example is considered. The 2-norm of $L - L_d$ is minimized subject to infinity

norm constraints on the weighted tracking error sensitivity function $W_6\mathcal{S}_6$ and on the weighted output sensitivity function $W_3\mathcal{S}_3$. If a two-step strategy is applied to solve the control problem, first the $S(q^{-1}, \rho)$ polynomial is designed minimizing $\|L - L_d\|_2$ satisfying the constraints in the weighted output sensitivity function $W_3\mathcal{S}_3$. Then, $T(q^{-1}, \rho)$ is designed with a feasibility problem where the constraints in $W_6\mathcal{S}_6$ are satisfied with the fixed $S(q^{-1}, \rho)$ tuned previously. In this example, the feasibility problem of the second step might not be feasible. However, in the case that it is feasible, the solution would be optimal. Obviously, if $S(q^{-1}, \rho)$ and $T(q^{-1}, \rho)$ polynomials are designed in the same optimization problem better results can be obtained. This will be shown in Section 3.5 with an experimental example.

3.3 RST Controller Design in Nyquist Diagram

The constraints presented in (3.16) and in the optimization problem (3.17) are non-convex on controller parameters ρ . The idea is to approximate these constraints by a set of convex constraints guaranteeing the robustness and/or performance conditions in the Nyquist diagram. This approximation is similar to that given for the robust performance problem presented in Chapter 2. However, a generalization is presented where the individual shaping of the different closed-loop transfer functions are proposed which permits also to tune RST controllers.

3.3.1 Convex approximation of the constraints on sensitivity functions

Let the inequality in (3.16) be multiplied by $|1 + \frac{S(e^{-j\omega}, \rho)}{R(e^{-j\omega})}G(e^{-j\omega})|$. Then, define:

$$\begin{aligned} \tilde{W}_p(e^{-j\omega})X_p(e^{-j\omega}, \rho) \equiv \\ W_p(e^{-j\omega})\mathcal{S}_p(e^{-j\omega}, \rho) \left[1 + \frac{S(e^{-j\omega}, \rho)}{R(e^{-j\omega})}G(e^{-j\omega}) \right] \\ \omega \in [0, \pi] \quad \text{and for } p = 1, \dots, 6 \quad (3.18) \end{aligned}$$

where $\tilde{W}_p(e^{-j\omega})$ and $X_p(e^{-j\omega}, \rho)$ are respectively the fixed term and the term depending linearly on ρ . Then, the constraint in (3.16) can be written as:

$$\begin{aligned} |\tilde{W}_p(e^{-j\omega})X_p(e^{-j\omega}, \rho)| < \left| 1 + \frac{S(e^{-j\omega}, \rho)}{R(e^{-j\omega})}G(e^{-j\omega}) \right| \\ \forall \omega \in [0, \pi] \quad \text{and for } p = 1, \dots, 6 \quad (3.19) \end{aligned}$$

Note that $\left| 1 + \frac{S(e^{-j\omega}, \rho)}{R(e^{-j\omega})}G(e^{-j\omega}) \right|$ is the distance in the Nyquist diagram between the critical point $(-1 + 0j)$ and $L(e^{-j\omega}, \rho)$. Hence, the constraints in (3.19) are satisfied if and only if, in the Nyquist diagram, the circle centered at the critical point $(-1 + 0j)$ with a radius of $|\tilde{W}_p(e^{-j\omega})X_p(e^{-j\omega}, \rho)|$ does not contain the point $L(e^{-j\omega}, \rho)$ for all ω .

The condition that the point $L(e^{-j\omega}, \rho)$ is outside the circle centered at the critical point with a radius of $|\tilde{W}_p(e^{-j\omega})X_p(e^{-j\omega}, \rho)|$ is a non-convex constraint on controller parameters ρ . The non-convex constraint can be approximated with a convex one by replacing the circle of radius $|\tilde{W}_p(e^{-j\omega})X_p(e^{-j\omega}, \rho)|$ by a fixed line $d(\omega)$ tangent to the circle (Fig. 3.2). The line $d(\omega)$ divides the Nyquist complex plane in two parts at each frequency ω . Now, the condition that the point $L(e^{-j\omega}, \rho)$ is at the side of the line $d(\omega)$, excluding the critical point $(-1 + 0j)$, is a convex constraint on controller parameters ρ . The conservatism of this approximation can be reduced if the slope of $d(\omega)$ changes with frequency. A progressive variation of the slope is proposed using the frequency response of $L_d(e^{-j\omega})$. The line $d(\omega)$ at each frequency ω can be defined orthogonal to the line connecting the critical point $(-1 + 0j)$ to $L_d(e^{-j\omega})$ and tangent to the circle centered at the critical point $(-1 + 0j)$ with a radius

of $|\tilde{W}_p(e^{-j\omega})X_p(e^{-j\omega}, \rho)|$. As it has been already discussed in Sub-section 2.3.3, $L_d(e^{-j\omega})$ represents the desired specifications and it should be coherent with respect to the plant, controller structure and design specifications.

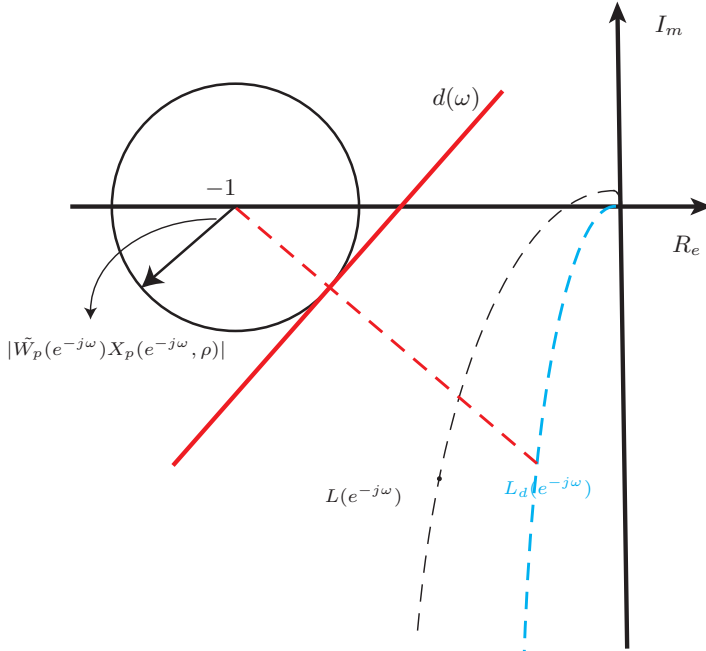


Fig. 3.2. Convex constraint for performance condition in Nyquist diagram

If we name x and y respectively, the real and imaginary parts of a point on the complex plane, the equation of $d(\omega)$ is given by:

$$\begin{aligned}
& |\tilde{W}_p(e^{-j\omega})X_p(e^{-j\omega}, \rho)[1 + L_d(e^{-j\omega})]| \\
& \quad - I_m\{L_d(e^{-j\omega})\}y - [1 + R_e\{L_d(e^{-j\omega})\}](1 + x) = 0 \\
& \quad \forall \omega \in [0, \pi] \quad \text{and} \quad \text{for } p = 1, \dots, 6 \quad (3.20)
\end{aligned}$$

where $R_e\{\cdot\}$ and $I_m\{\cdot\}$ represent respectively the real and imaginary parts of a complex value. The condition that the point $L(e^{-j\omega}, \rho)$ is on the side of the line $d(\omega)$ excluding the critical point $(-1 + 0j)$ is given by the following convex constraints:

$$\begin{aligned}
& |\tilde{W}_p(e^{-j\omega})X_p(e^{-j\omega}, \rho)[1 + L_d(e^{-j\omega})]| \\
& \quad - I_m\{L_d(e^{-j\omega})\}I_m\{L(e^{-j\omega}, \rho)\} \\
& \quad - [1 + R_e\{L_d(e^{-j\omega})\}](1 + R_e\{L(e^{-j\omega}, \rho)\}) < 0 \\
& \quad \forall \omega \in [0, \pi] \quad \text{and} \quad \text{for } p = 1, \dots, 6 \quad (3.21)
\end{aligned}$$

These convex constraints can be simplified to:

$$\begin{aligned}
& |\tilde{W}_p(e^{-j\omega})X_p(e^{-j\omega}, \rho)[1 + L_d(e^{-j\omega})]| - \\
& \quad R_e\{[1 + L_d^*(e^{-j\omega})][1 + \frac{S(e^{-j\omega}, \rho)}{R(e^{-j\omega})}G(e^{-j\omega})]\} < 0 \\
& \quad \omega \in [0, \pi] \quad \text{and for } p = 1, \dots, 6 \quad (3.22)
\end{aligned}$$

where $L_d^*(e^{-j\omega})$ is the complex conjugate of $L_d(e^{-j\omega})$.

These convex constraints can be used for systems with multi-model uncertainty by repeating the constraints for each system.

Remark: These constraints can also be presented in Theorem 2.1 if $W_{1i} = 0$, $T_i(j\omega) = \mathcal{S}_{p_i}(e^{-j\omega})$, $W_{2i}(j\omega)\rho^T\phi(j\omega)G_i(j\omega) = \tilde{W}_{p_i}(e^{-j\omega})X_{p_i}(e^{-j\omega}, \rho)$ and $\rho^T\phi(j\omega) = \frac{S(e^{-j\omega}, \rho)}{R(e^{-j\omega})}$ are considered. As in this case, discrete-time controller design problems are considered, the wno of $[1 + L_d^*(e^{-j\omega})]$ and $[1 + \frac{S(e^{-j\omega}, \rho)}{R(e^{-j\omega})}G_i(e^{-j\omega})]$ depend only on the variation of $e^{-j\omega}$ on the unit circle.

3.3.2 Optimization problem

Any norm of $L - L_d$ can be minimized subject to the convex constraints proposed in (3.22). Multi-model uncertainty can be directly considered by repeating the constraints for each of the models of the uncertainty. The following convex optimization problem is proposed where the two norm of $L_i - L_{d_i}$ is minimized under the convex constraints to solve the control problem given in (3.17) for a system with multi-model uncertainty:

$$\min \sum_{i=1}^m \|L_i(\rho) - L_{d_i}\|_2$$

$$\begin{aligned} \text{Subject to:} & \\ |\tilde{W}_{p_i}(e^{-j\omega})X_{p_i}(e^{-j\omega}, \rho)[1 + L_{d_i}(e^{-j\omega})]| - & \quad (3.23) \\ R_e\{[1 + L_{d_i}^*(e^{-j\omega})][1 + \frac{S(e^{-j\omega}, \rho)}{R(e^{-j\omega})}G_i(e^{-j\omega})]\} < 0 & \\ \text{for } \omega \in [0, \pi], \quad \forall p \in P \text{ and for } i = 1, \dots, m & \end{aligned}$$

where P is a subset of the set and $L_{d_i}^*(e^{-j\omega})$ is the complex conjugate of $L_{d_i}(e^{-j\omega})$.

Remarks:

1. It should be mentioned that $X_p(e^{-j\omega}, \rho) = 1$ for $p = 2, 3$ leads to linear constraints on controller parameters ρ .
2. In many cases, the aim is to minimize one of the upper bounds of the infinity norm of the weighted closed-loop sensitivity functions under infinity norm constraints on the other weighted closed-loop sensitivity functions. This control problem is solved with the following optimization problem:

min γ

Subject to:

$$\begin{aligned} & \left| \frac{\tilde{W}_\kappa(e^{-j\omega})}{\gamma} X_\kappa(e^{-j\omega}, \rho) [1 + L_d(e^{-j\omega})] \right| - \\ & R_e \left\{ [1 + L_d^*(e^{-j\omega})] \left[1 + \frac{S(e^{-j\omega}, \rho)}{R(e^{-j\omega})} G(e^{-j\omega}) \right] \right\} < 0 \\ & \text{for } \omega \in [0, \pi] \end{aligned} \quad (3.24)$$

$$\begin{aligned} & \left| \tilde{W}_p(e^{-j\omega}) X_p(e^{-j\omega}, \rho) [1 + L_d(e^{-j\omega})] \right| - \\ & R_e \left\{ [1 + L_d^*(e^{-j\omega})] \left[1 + \frac{S(e^{-j\omega}, \rho)}{R(e^{-j\omega})} G(e^{-j\omega}) \right] \right\} < 0 \\ & \text{for } \omega \in [0, \pi] \quad \text{and} \quad \forall p \in P \end{aligned}$$

where P is a subset of the set $\{[1, \dots, 6] \setminus \kappa\}$ where $\setminus \kappa$ defines the exclusion of κ .

This optimization problem can be solved with an iterative bisection algorithm. At the i -th iteration, a feasibility optimization problem is solved with the constraints given in (3.24) for a fixed value of γ_i . If the problem is feasible, γ_{i+1} will be chosen smaller than γ_i , and if the problem is infeasible, γ_{i+1} will be increased. This is solved using standard solvers. Note that for fixed values of γ , the constraints in the optimization problem (3.24) are convex on controller parameters ρ .

3. This optimization problem is also an SIP problem. As in the Subsection 2.3.4, a practical solution is chosen with N finite number of frequencies $\omega \in \{\omega_1, \omega_2, \dots, \omega_N\}$ to solve the problem. The two norm is replaced by $\|L_i(\rho) - L_{d_i}\|_2^2$ which at the same time is approximated by $\sum_{k=1}^N |L_i(j\omega_k, \rho) - L_{d_i}(j\omega_k)|^2$ to obtain a quadratic objective function. Thus, the following optimization problem is considered for multi-model case:

$$\min \sum_{i=1}^m \sum_{k=1}^N |L_i(e^{-j\omega_k}, \rho) - L_{d_i}(e^{-j\omega_k})|^2$$

Subject to:

$$\begin{aligned} & |\tilde{W}_{p_i}(e^{-j\omega_k})X_{p_i}(e^{-j\omega_k}, \rho)[1 + L_{d_i}(e^{-j\omega_k})]| - \\ & R_e\{[1 + L_{d_i}^*(e^{-j\omega_k})][1 + \frac{S(e^{-j\omega_k}, \rho)}{R(e^{-j\omega_k})}G_i(e^{-j\omega_k})]\} < 0 \end{aligned} \quad (3.25)$$

for $k = 1, \dots, N$, for $i = 1, \dots, m$ and $\forall p \in P$

where P is a subset of the set $\{1, \dots, 6\}$ and $L_{d_i}^*(e^{-j\omega_k})$ is the complex conjugate of $L_{d_i}(e^{-j\omega_k})$.

3.4 Solution to a Flexible Transmission Benchmark

One of the well-known benchmarks for robust controller design was presented in the second European Control Conference in Rome (ECC 1995) and the results were published in a special issue of European Journal of Control (Vol. 1 No. 2, 1995). The benchmark problem is to design a low-order robust controller for a flexible transmission system in three different loadings [41]. The model of the system contains two low-damped resonance modes whose frequencies change drastically with load. The control specifications are given in terms of time-domain performances for tracking and disturbance rejection and frequency-domain performances in terms of the constraints on the magnitude of the sensitivity functions. The problem is challenging, because the large model uncertainty is located at low frequencies where the performances are required.

Many robust control design approaches have been already applied to the flexible transmission benchmark. Some of them are published in the special issue dedicated to the benchmark and the others ulteriorly with new progress in robust control approaches. The following solutions can be found in literature: four H_∞ solutions [18, 32, 38, 56], two controllers based on Quantitative Feedback Theory (QFT) [37, 49], three controllers using pole placement with

sensitivity shaping [39, 40, 42], one Generalized Predictive Controller (GPC) [13], one fractional order controller by CRONE control [50] and one model-free approach based on Iterative Feedback Tuning (IFT) [27]. Although all the methods stabilize the system and achieve good performance, only two controllers meet all required specifications for all loadings with relatively high-order controllers. The first controller that satisfied all specifications was a QFT controller with 20 parameters. Later on, a controller using convex optimization achieved the same performances with 16 parameters.

System description

The flexible transmission system is a laboratory setup designed and constructed in Laboratoire d'Automatique de Grenoble (INPG-CNRS), France. This system consists of three horizontal pulleys connected by two elastic belts. The input of the system is the reference position for the first pulley controlled by a DC motor in closed-loop. The output of the system is the position of the third pulley measured by a potentiometer. The schematic diagram of the system is given in Figure 3.3. The goal is to control the position of the third pulley which can be loaded with small disks. A PC is used to control the system with a sampling frequency of 20 Hz.

The system has two oscillatory modes with damping factors of less than 0.05 that vary significantly in different loadings. The discrete time models of the system for the no load, half load (1.8 kg) and full load (3.6 kg) configurations have been identified with a low magnitude Pseudo Random Binary Sequence (PRBS) input. The amplitude of the frequency characteristics is represented in Figure 3.4 where the frequency axis is normalized. The discrete-time transfer functions of the system are given by:

$$G_i(q^{-1}) = \frac{q^{-d}B_i(q^{-1})}{A_i(q^{-1})} \quad i = 1, 2, 3 \quad (3.26)$$

where q^{-1} is the backward shift operator and the pure time delay $d = 2$ for all models. The corresponding identified and validated models are :

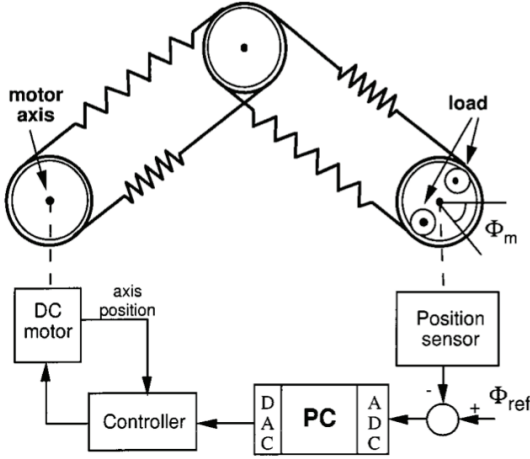


Fig. 3.3. Schematic diagram of the flexible transmission.

Unloaded model:

$$\begin{aligned} A_1(q^{-1}) &= 1 - 1.14833q^{-1} + 1.58939q^{-2} \\ &\quad - 1.31608q^{-3} + 0.88642q^{-4} \\ B_1(q^{-1}) &= 0.28261q^{-1} + 0.50666q^{-2} \end{aligned} \quad (3.27)$$

Half loaded model:

$$\begin{aligned} A_2(q^{-1}) &= 1 - 1.99185q^{-1} + 2.20265q^{-2} \\ &\quad - 1.84083q^{-3} + 0.89413q^{-4} \\ B_2(q^{-1}) &= 0.1027q^{-1} + 0.18123q^{-2} \end{aligned} \quad (3.28)$$

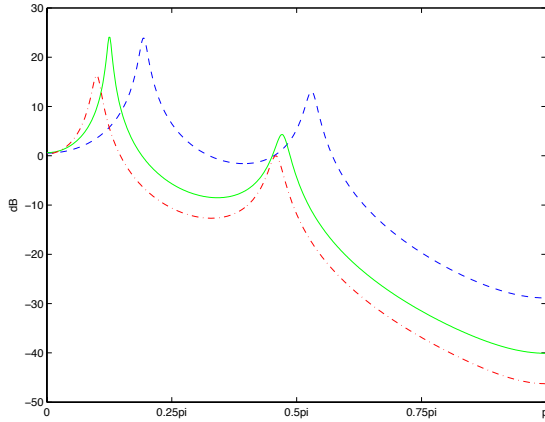


Fig. 3.4. Frequency characteristics: Fully loaded (dashed-dotted, red), Half loaded (solid, green) and Unloaded (dashed, blue)

Fully loaded model:

$$\begin{aligned} A_3(q^{-1}) &= 1 - 2.09679q^{-1} + 2.31962q^{-2} \\ &\quad - 1.93353q^{-3} + 0.87129q^{-4} \\ B_3(q^{-1}) &= 0.06408q^{-1} + 0.10407q^{-2} \end{aligned} \quad (3.29)$$

Benchmark specifications

A discrete-time 2DOF polynomial form RST controller (see Fig.3.1) has to be designed. The canonical form of the RST controller is given by:

$$R(q^{-1})u(t) = T(q^{-1})r(t) - S(q^{-1})y(t) \quad (3.30)$$

where $u(t)$ is the plant input, $y(t)$ the plant output, $r(t)$ the desired reference and R,S,T are polynomials in q^{-1} .

The controller should be designed to satisfy the following specifications:

1. A rise time (90% of the final value) of less than 1s.

2. Overshoot of less than 10%.
3. Rejection of 90% of the output disturbance \mathcal{S}_{3_i} filtered by $1/A_i$ in less than 1.2s.
4. Perfect rejection of a constant disturbance (using integral action).
5. Disturbance attenuation at low frequencies (less than 0.2Hz).
6. Maximum of output sensitivity function less than 6dB (modulus margin greater than 0.5).
7. A delay margin of at least 40 ms.
8. A maximum value of less than 10dB for the input sensitivity function \mathcal{S}_{5_i} at high frequencies (between 8 to 10 Hz).

Solution to the Benchmark Problem

The design procedure described in Section 3.3 is applied to the flexible transmission benchmark. The linearly parameterized 2DOF controller with RST structure given in (3.2), (3.3) and (3.4) is considered. For this particular example, to reduce the complexity of the controller, $n_T = 1$ is chosen, reducing the polynomial T to a simple gain. The gain in $T(q^{-1})$ is taken equal to the sum of the parameters of $S(q^{-1})$ giving a unit gain to the closed-loop system.

The fixed term $(1 - q^{-1})$ in $R(q^{-1})$ is to assure the integral action of the controller (spec. 4). The time-domain performances (spec. 1,2 and 3) are tuned using the following reference model:

$$\mathcal{M}(s) = \frac{\omega_n^2}{s^2 + 2\omega_n\xi s + \omega_n^2} \quad (3.31)$$

This leads to the following desired open-loop transfer functions:

$$L_{d_i}(s) = \frac{\omega_n^2}{s(s + 2\xi\omega_n)} \quad (3.32)$$

for $i=1,2,3$ (same desired open-loop transfer function for three models). Note that since the design is carried out in the frequency domain, the desired open-loop transfer function can be defined either in

continuous or in discrete time. Choosing $\omega_n = 3.2$ rad/s and $\xi = 0.7$ gives a reference model with a rise time of 0.8 s and 5% overshoot which easily satisfies the time-domain specifications (spec. 1 and 2).

The delay margin cannot be transformed into a convex constraint. However, this specification is usually met when other specifications are satisfied (spec. 7).

Because of two very oscillatory modes in the plant models, the output step disturbance filtered by $1/A_i$ will be very oscillatory such that spec. 3 cannot be met. The disturbance rejection time can be reduced indirectly by adding a bound on the infinity-norm of the closed-loop transfer function between the disturbance and output, \mathcal{S}_{3_i}/A_i . This constraint can be represented by :

$$\left\| \frac{\mathcal{S}_{3_i}}{A_i} \right\|_{\infty} < \gamma_i \quad (3.33)$$

and it can be considered in the proposed approach by taking a performance filter $W_{S_i} = 1/(\gamma_i A_i)$.

In addition, a performance filter

$$W_3(e^{-j\omega}) = \begin{cases} 1 & \text{for } 0 < \omega \leq 0.02\pi \\ 1/10^{6/20} = 0.5 & \text{for } 0.02\pi < \omega \leq \pi \end{cases} \quad (3.34)$$

is chosen in order to assure a maximum of less than 6dB (spec. 6) for the output sensitivity function (modulus margin of 0.5) and an attenuation band of 0.02π rad/s (spec. 5). These performances can be given by one weighting function for each model defined as follows:

$$W_{3_i}(e^{-j\omega}) = \max[|W_3(e^{-j\omega})|, |W_{S_i}(e^{-j\omega})|] \quad (3.35)$$

The specification for the input sensitivity function $|\mathcal{S}_{5_i}(e^{-j\omega})| < 10$ dB at high frequencies ($0.8\pi < \omega < \pi$ rad/s) can be presented as (spec. 8):

$$\|W_5 \mathcal{S}_{5_i}\|_{\infty} < 1 \quad (3.36)$$

where

$$W_5(e^{-j\omega}) = \begin{cases} 0 & \text{for } 0 < \omega \leq 0.8\pi \\ 1/10^{10/20} & \text{for } 0.8\pi < \omega \leq \pi \end{cases} \quad (3.37)$$

The controller is tuned based on the proposed method and by solving the optimization problem given in (3.25). The frequency response of the three models are computed at $N=500$ equally spaced frequency points between $1/N$ and π (Nyquist frequency).

Simulation Results

Fixing the number of controller parameters $n_S = 12$ (controller order equal to 11), the design variable γ_i to $10^{28/20}$ (equal to 28dB) for $i = 1, 2, 3$ and using L_{d_i} in (3.32), the first controller K_0 , satisfying almost all the specifications, is designed solving the optimization problem in (3.25).

In order to reduce the complexity of the controller, a new iteration is carried out. It has been shown that a closer $L_d(e^{-j\omega})$ to the optimal $L(e^{-j\omega}, \rho^*)$ will reduce the conservatism of the convex approximation. Therefore, a new desired open loop transfer function is defined as: $L_{d_i}(e^{-j\omega}) = K_0(e^{-j\omega})G_i(e^{-j\omega})$. It should be mentioned that the disturbance rejection time is the most critical specification to be met. So with this new L_{d_i} , a tighter bound for \mathcal{S}_{3_i}/A_i is also considered. It means that a smaller γ_i equal to 22dB, 24dB and 26dB, respectively is chosen (1dB higher than those obtained in the first iteration). By running the convex optimization problem with $n_S = 8$, an 7-th order controller K_1 satisfying 100% of the specifications is obtained. The order is further reduced to $n_S = 7$ by using $L_{d_i}(e^{-j\omega}) = K_1(e^{-j\omega})G_i(e^{-j\omega})$ and γ_i equal to 20dB, 24dB and 26dB, respectively. The final 6th-order controller is given by:

$$\begin{aligned} R(q^{-1}) &= 1 - q^{-1} \\ S(q^{-1}) &= 0.632 - 1.781q^{-1} + 1.895q^{-2} - 1.062q^{-3} \\ &\quad + 0.5247q^{-4} - 0.3399q^{-5} + 0.1887q^{-6} \\ T(q^{-1}) &= 0.05733 \end{aligned} \quad (3.38)$$

Figures 3.5 and 3.6 show that the specifications on the input sensitivity function \mathcal{S}_{5_i} and output sensitivity function \mathcal{S}_{3_i} are satisfied for the three models. Figure 3.7 shows the step and disturbance rejection responses. The details of achieved performances for the final controller are shown in Table 3.1.

Table 3.1. Performance of the controller

Specification	No load	Half load	Full load
Rise Time [s]	0.80	0.75	0.70
Overshoot[%]	3.87	3.92	6.56
Dist. rejection [s]	1.15	1.15	1.2
Maximum \mathcal{S} [dB]	5.93	4.41	5.12
Delay Margin [ms]	44	95	385
Maximum \mathcal{U} [dB]	9.20	9.86	9.99
Attenuation band [Hz]	0.204	0.206	0.200

Table 3.2 gives a joint evaluation of the performance and complexity of some controllers that have already been designed for the benchmark problem and compare them with the proposed controller. It can be observed that the proposed controller meets all specifications with the lowest complexity.

3.5 Application to an Industrial Double-Axis Positioning System

In this section, the proposed approach is applied to a double-axis LPMSM. The goal is to control the position of the mentioned system shown in Fig. 3.8, using an RST discrete-time controller with a sampling frequency of 6 kHz. This kind of systems have high dynamics (high accelerations and decelerations), high mechanical stiffness, reduced friction and high accuracy as there is no backlash and no

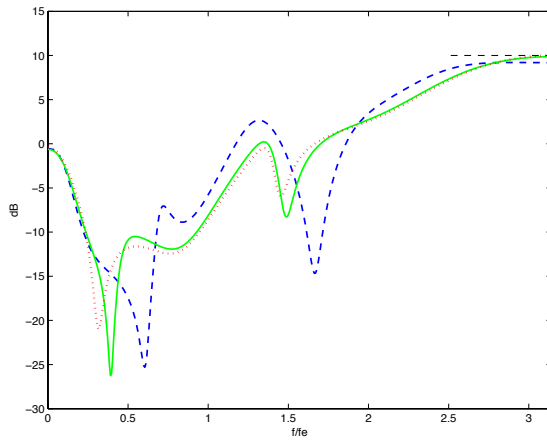


Fig. 3.5. \mathcal{U} of Unloaded (dashed, blue), Half loaded (solid, green) and Fully loaded (dashed-dotted, red) systems.

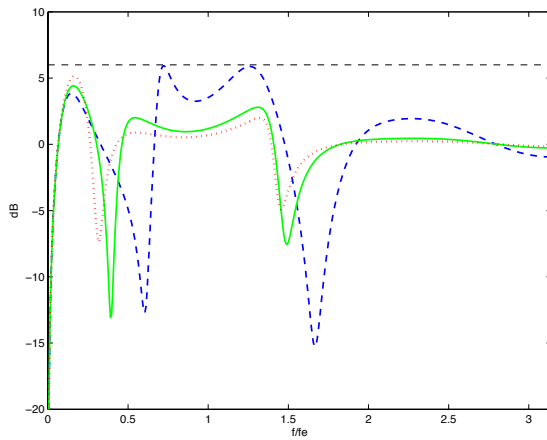


Fig. 3.6. \mathcal{S} of Unloaded (dashed, blue), Half loaded (solid, green) and Fully loaded (dashed-dotted, red) systems.

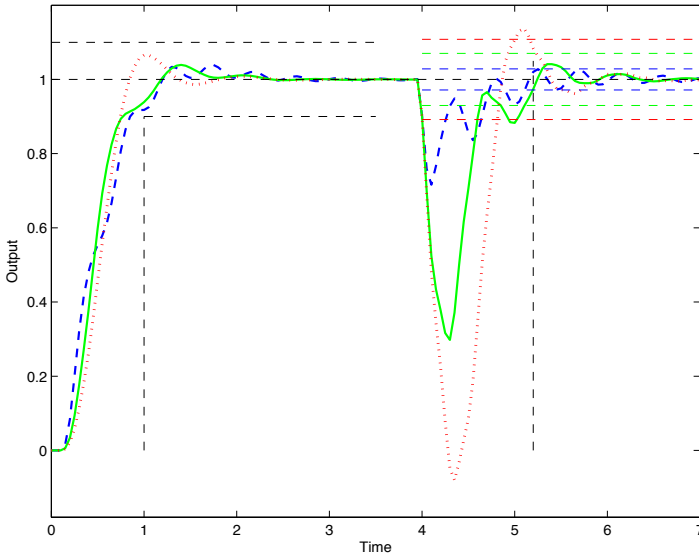


Fig. 3.7. Step and disturbance rejection of Unloaded (dashed, blue), Half loaded (solid, green) and Fully loaded (dashed-dotted, red) systems. The straight dashed lines show the intervals in which the responses should be located.

mechanical transmission. For simplicity, only the system identification and feedback design for the higher axis is analyzed when the motor is in three different positions at -0.16m , 0m and 0.16m of the x axis.

3.5.1 Non-parametric identification of the dynamics of the higher axis

A spectral model is obtained by exciting the higher axis with a sum of sinusoidal signals from 4.4 to 3000 Hz for each position of the x axis. Three different frequency response functions (FRF) $G_i(e^{-j\omega})$

Table 3.2. Comparison with other benchmark results

	Performance (%)	Complexity (order of R+S+T)
Proposed approach	100	7
[42]	100	16
[49]	100	20
[18]	98.80	11
[50]	98.61	14
[37]	97.71	9
[27]	97.48	9
[40]	97.12	12
[32]	94.38	35
[13]	91.82	16
[56]	72.35	15

are obtained for $i = 1, 2, 3$ which are shown in Fig. 3.9. Though the three frequency response functions are similar, the controller is designed using the multi-model uncertainty to show the effectiveness of the method with this type of systems.

3.5.2 RST controller design of the higher axis

The objective is to design an RST controller by tuning the polynomials S and T given in (3.3) and (3.4) using the proposed method. A second-order feedback controller with a second-order pre-compensator is designed choosing n_S and n_T equal to 3. The controller should stabilize the system at all i -th positions and reduce the settling time for an error band of $200nm$ for a given reference signal designed by the manufacturer. The signal has the form of a low-pass filtered step of 25 mm (the filter $F(j\omega)$ is given) which does not excite unwanted vibrations and avoids input saturation.

Since the design of the controller is carried out in the frequency domain, the weighting filters can be defined in continuous-time. A modulus margin of 0.5 is desirable to assure the robustness of the

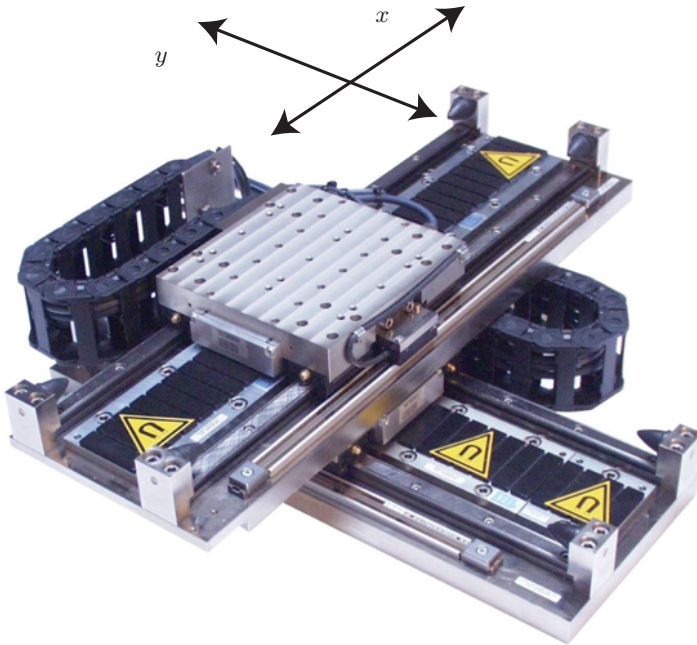


Fig. 3.8. Double-axis linear permanent magnet synchronous motor system

controller (i.e. maximum value of less than 6 dB of the magnitude of the output sensitivity functions \mathcal{S}_{3_i}). This is obtained choosing $W_{3_i}(j\omega) = 0.5$ for all ω and for all i . On the other hand, due to the friction appearing as a constant input disturbance, an integrator is needed in the controller to reject it. Therefore, the open-loop transfer functions should contain three integrators, one because of the controller and two others because of the plant (the system can be considered as 2 pure integrators). It is shown in [58] that internal cancelation between integrators and the zeros of the controller can be avoided by introducing the desired integrators in the weighting filters $W_{3_i}(j\omega)$. The desired bandwidth for the closed-loop disturbance

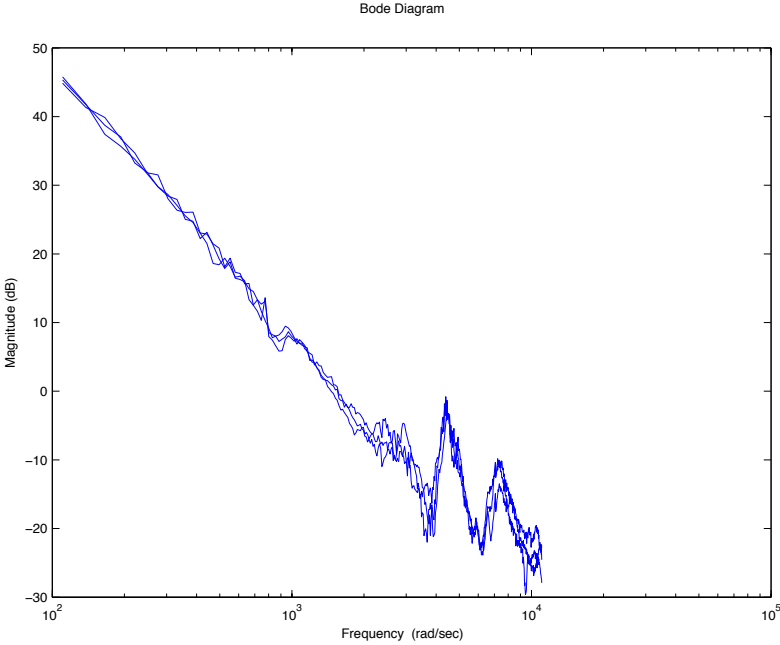


Fig. 3.9. FRF of the double-axis system at -0.16m , 0m and 0.16m of the x axis

rejection ω_c is 300 rad/s. As a result, the $W_{3_i}(j\omega)$ weighting filters are chosen as a triple integrator with a bandwidth of ω_c to assure the integral action. The combination of the robustness and performance conditions defines the following weighting filters:

$$W_{3_i}(j\omega) = \begin{cases} \frac{\omega_c^3}{(j\omega)^3} & \text{for } \left| \frac{\omega_c^3}{(j\omega)^3} \right| > 0.5 \\ 0.5 & \text{for } \left| \frac{\omega_c^3}{(j\omega)^3} \right| < 0.5 \end{cases} \quad (3.39)$$

for $i = 1, 2, 3$.

In order to reduce the tracking error and indirectly the settling time, a constraint on the weighted tracking functions $W_{6_i}\mathcal{S}_{6_i}$ are considered. It is desired to reduce the tracking error at the excited frequencies for this particular reference. For this reason, the given low-pass filtered step is used as weighted function W_{6_i} :

$$W_{6_i}(j\omega) = \frac{F(j\omega)}{j\omega} \quad (3.40)$$

Figure 3.11 and 3.12 show the inverse of the filters that have been chosen. A stabilizing controller tuned by the manufacturer is already available:

$$\begin{aligned} R_0(q^{-1}) &= 1 - q^{-1} \\ S_0(q^{-1}) &= 1.4661 - 2.7567q^{-1} + 1.3021q^{-2} \\ T_0(q^{-1}) &= 9.2439 - 26.0901q^{-1} + 24.6354q^{-2} - 7.7778q^{-3} \end{aligned} \quad (3.41)$$

Therefore, $L_{d_i}(e^{-j\omega})$ is chosen as $K_0(e^{-j\omega})G_i(e^{-j\omega})$ for $i = 1, 2, 3$ where $K_0(q^{-1}) = S_0(q^{-1})/R_0(q^{-1})$. This controller leads to

$$\|W_6\mathcal{S}_{6_0}\|_\infty = 0.361360 \quad (3.42)$$

The goal is to minimize the maximum value of $\|W_{6_i}\mathcal{S}_{6_i}\|_\infty$ for $i = 1, 2, 3$. In order to obtain the optimal controller, the optimization problem in (3.24) is solved repeating the constraints for each system using the bisection algorithm proposed in Remark 2 and the weighting filters given in (3.39) and (3.40). The optimization problem leads to

$$\|W_6\mathcal{S}_6\|_\infty = 0.217580 \quad (3.43)$$

The resulting controller is:

$$\begin{aligned} R_1(q^{-1}) &= 1 - q^{-1} \\ S_1(q^{-1}) &= 2.387724 - 4.526296q^{-1} + 2.145863q^{-2} \\ T_1(q^{-1}) &= 2.558529 - 4.874582q^{-1} + 2.323343q^{-2} \end{aligned} \quad (3.44)$$

The same problem is solved based on the method proposed in Chapter 2 using the two-step optimization and the bisection algorithm as in the example 2.4. This leads to:

$$\|W_6\mathcal{S}_{6_2}\|_\infty = 0.244481 \quad (3.45)$$

The resulting controller is:

$$\begin{aligned} R_2(q^{-1}) &= 1 - q^{-1} \\ S_2(q^{-1}) &= 2.283279 - 4.298835q^{-1} + 2.017491q^{-2} \\ T_2(q^{-1}) &= 2.404921 - 4.545919q^{-1} + 2.142933q^{-2} \end{aligned} \quad (3.46)$$

Figure 3.10 shows the final part of the movement for the desired reference signals. The outputs of the three different controllers at the three different positions are shown. The proposed controller has a less oscillatory behavior with a shorter settling time. Figure 3.11 and 3.12 show respectively the upper bounds ($1/W_{3_i}$ and $1/W_{6_i}$) and sensitivity functions \mathcal{S}_{3_i} and \mathcal{S}_{6_i} for each controller.

As expected, the proposed controller obtains a smaller maximum value for the weighted sensitivity functions than that obtained by using the 2 step approach. It should be mentioned that the controller designed by the manufacturer has not been designed for the same purpose.

3.6 Conclusions

In this chapter, the robust fixed-order RST controller design problem based on the shaping of the open-loop transfer function with H_∞ constraints on the closed-loop sensitivity functions is formulated as a convex optimization problem. Solving only one convex optimization problem, T and S polynomials of the RST controller with a fixed R polynomial are tuned for a SISO system. The approach is based on the minimization of the difference between the open-loop transfer function and a desired open-loop transfer function with constraints

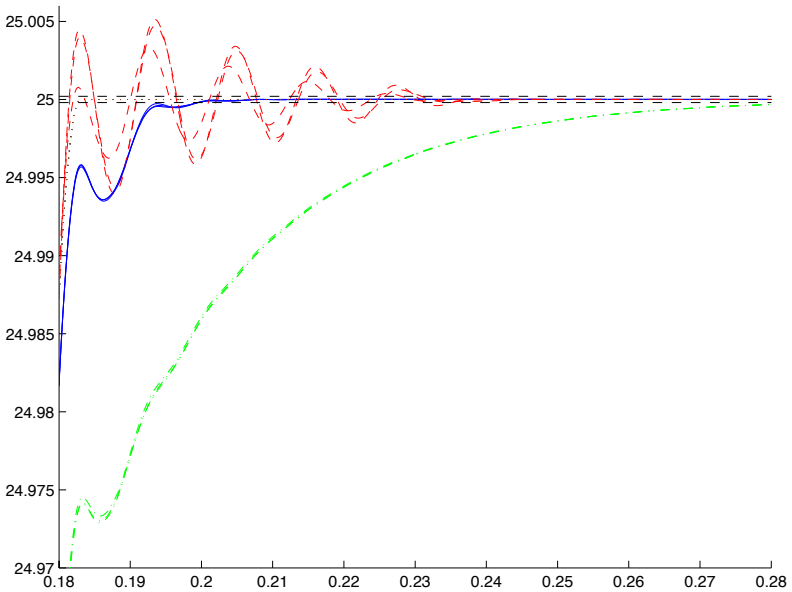


Fig. 3.10. Output of the system for three different positions: Reference signal (black, dashed-dotted), Proposed controller (solid, blue), 2 Step controller (dashed-dotted, green), Manufacturer's controller (dashed, red) and the error band for the settling time (dashed, black)

on the weighted sensitivity functions. These constraints are approximated with convex constraints in the Nyquist diagram. This method requires only the frequency response of the system. In contrast to the standard H_∞ controller design method, systems with time-delay can be considered directly by this method. The multi-model uncertainty can be directly taken into account by this approach without any approximation. Control problems where the performance is improved by minimizing the norm of a specific weighted sensitivity function can also be implemented using a bi-section algorithm.

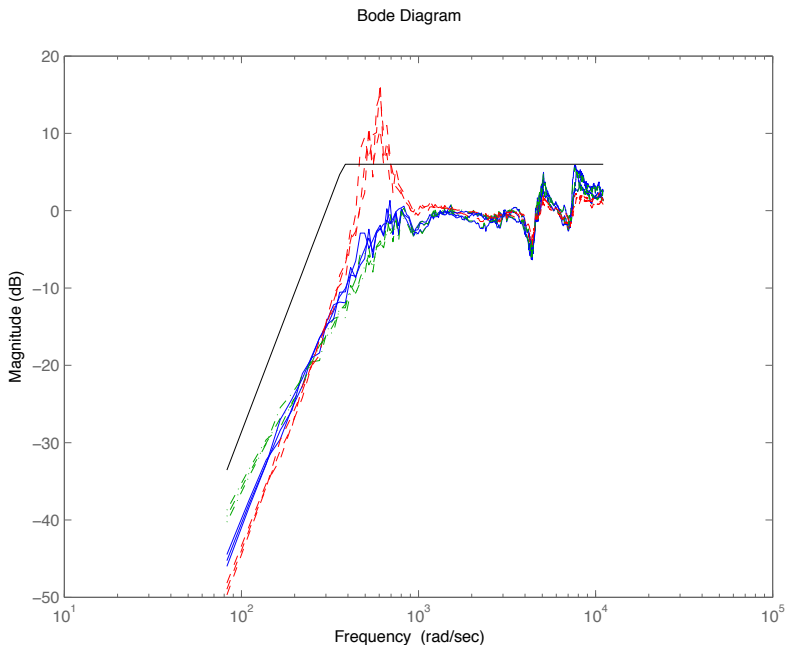


Fig. 3.11. The performance conditions on \mathcal{S}_{3_i} : Proposed controller (solid, blue), 2 Step controller (dashed-dotted, green), Manufacturer's controller (dashed, red) and $1/W_{3_i}$ (solid, black) for $i = 1, 2, 3$.

The effectiveness of the proposed approach has been shown by two simulation examples. This approach has been applied to an international benchmark problem for robust controller design [41] and a controller with only 7 parameters has been designed that meets all benchmark specifications. To the best of the authors knowledge, the proposed controller meets all the specifications with the lowest complexity amongst all controllers proposed for this system in the literature. Although the resulting controller has the smallest order among the benchmark solutions, it cannot be shown that there is no

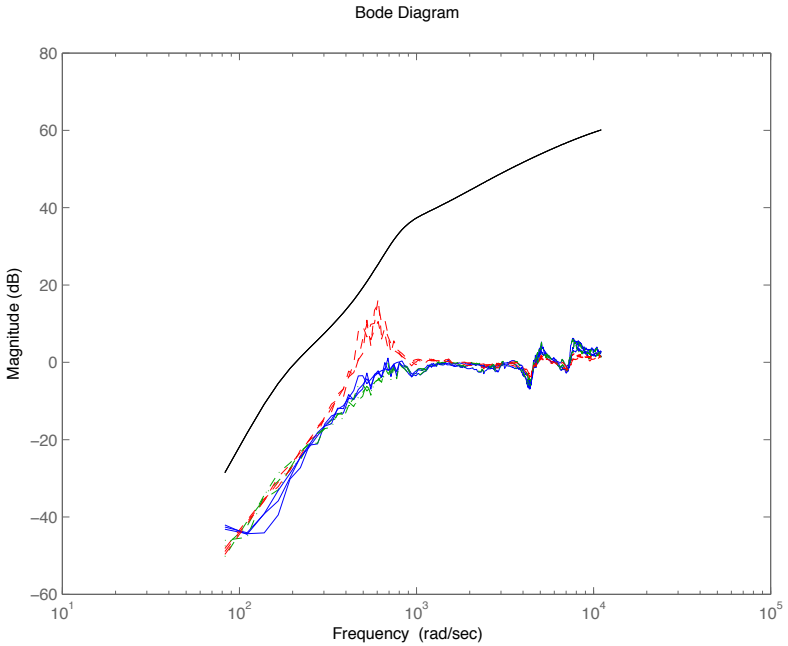


Fig. 3.12. The performance conditions on \mathcal{S}_{6_i} : Proposed controller (solid, blue), 2 Step controller (dashed-dotted, green), Manufacturer's controller (dashed, red) and $1/W_{6_i}$ (solid, black) for $i = 1, 2, 3$.

lower-order controller that can achieve the same performance. The method has also been applied on an industrial double-axis LPMSM system. It should be noted that the application considers a multi-model uncertainty for which a controller has been designed satisfying weighted closed-loop sensitivity constraints for all models.

Fixed-order H_∞ Controller Design for Spectral MIMO Models

4.1 Introduction

In this chapter, the method proposed in chapter 2 is extended to deal with LTI-MIMO systems. It is shown that fixed-order linearly parameterized MIMO controllers for MIMO nonparametric spectral models can be computed with H_∞ performance. The stability of the closed-loop system is guaranteed thanks to the Generalized Nyquist Stability criterion. It should be mentioned that the use of this criterion leads to a non-convex set on the controller parameters. In this chapter, a convex approximation of this set is given by a set of convex constraints in the Nyquist diagram based on Gershgorin bands. In this approach, decouplers and decoupled controllers are designed simultaneously by a convex optimization technique. The proposed method can be used for PID controllers as well as for higher order linearly parametrized controllers in discrete or continuous time. The case of unstable open-loop systems can be considered if a stabilizing controller is available.

This chapter is organized as follows: In Section 4.2, the class of models and controllers are introduced. Section 4.3 describes the control design methodology for MIMO systems based on the convex constraints in the Nyquist diagram which guarantees the Generalized

Nyquist Stability criterion and single-loop H_∞ -SISO performance. Section 4.4 shows some simulation results. Finally, Section 4.5 gives some concluding remarks.

4.2 Problem Formulation

4.2.1 Class of models

A set \mathcal{G} including m LTI-MIMO strictly proper continuous-time or discrete-time models with bounded infinity norm are considered:

$$\mathcal{G} = \{\mathbf{G}_i(j\omega); \quad i = 1, \dots, m; \quad \omega \in \mathbb{R}\} \quad (4.1)$$

where $\mathbf{G}_i(j\omega)$ is an $n_o \times n_i$ matrix of FRF or spectral models with n_i the number of inputs and n_o the number of outputs of the system.

In the sequel, it will be shown that ensuring closed-loop performance and stability for each member of the set \mathcal{G} leads to a set of convex constraints. Therefore, thanks to the properties of convex sets, by repeating the constraints for m models the robust performance and stability for the set \mathcal{G} will be guaranteed. For the sake of simplicity, henceforth, we derive the stability and performance conditions for a single nominal model \mathbf{G} . Obviously, the results can be applied to the class of model \mathcal{G} by repeating the constraints for every model in the set.

4.2.2 Class of controllers

Consider the class of multivariable controllers given by an $n_i \times n_o$ matrix $\mathbf{K}(s)$ whose elements $K_{pq}(s)$ for $p = 1, \dots, n_i$ and $q = 1, \dots, n_o$ are linearly parameterized. It means that $K_{pq}(s) = \rho_{pq}^T \phi_{pq}(s)$ where ρ_{pq}^T is the vector of parameters for $K_{pq}(s)$ and $\phi_{pq}(s)$ is the vector of stable transfer functions possibly with poles on the imaginary axis, chosen from a set of orthogonal basis functions. Obviously, PID matrix controllers belong to this set, whose non-diagonal elements principally decouple the system and whose diagonal elements

are designed to achieve some single-loop desired performances. As in previous chapters, the main property of this parameterization is that every component of the matrix $\mathbf{L}(j\omega, \rho) = \mathbf{G}(j\omega)\mathbf{K}(j\omega)$ can be written as a linear function of the controller parameters ρ :

$$\rho = [\rho_{11}, \dots, \rho_{1n_i}, \dots, \rho_{n_o1}, \dots, \rho_{n_on_i}] \quad (4.2)$$

4.2.3 Control problem

The shaping of the open-loop transfer function matrix with infinity norm constraints on the weighted closed-loop transfer functions of the diagonal elements is considered in this chapter. A $n_o \times n_o$ desired open loop transfer function matrix $\mathbf{L}_D(j\omega)$ is available representing all or a part of the desired specifications. For decoupling control problems, $\mathbf{L}_D(j\omega)$ can be defined as a diagonal matrix with $L_{Dq}(j\omega)$ as the q -th diagonal element for $q = 1, \dots, n_o$ where $L_{Dq}(j\omega)$ is a desired strictly proper open-loop transfer function for the q -th loop.

Consequently, the 2-norm of $\mathbf{L} - \mathbf{L}_D$ is minimized under infinity norm constraints on the weighted closed-loop transfer functions of the diagonal elements. Let the sensitivity function and complementary sensitivity function be defined $\mathbf{S}(s) = [\mathbf{I} + \mathbf{L}(s)]^{-1}$ and $\mathbf{T}(s) = \mathbf{L}(s)[\mathbf{I} + \mathbf{L}(s)]^{-1}$, respectively. For simplicity, the following optimization control problem is considered:

$$\begin{aligned} & \min_{\rho} \|\mathbf{L}(j\omega, \rho) - \mathbf{L}_D(j\omega)\|_2 \\ & \text{Subject to:} \\ & \| |W_{1q} \mathcal{S}_{qq}| + |W_{2q} \mathcal{T}_{qq}| \|_{\infty} < 1 \quad \text{for } q = 1, \dots, n_o \end{aligned} \quad (4.3)$$

where $\mathcal{S}_{qq}(s)$ is the q -th diagonal component of $\mathbf{S}(s)$ and $\mathcal{T}_{qq}(s)$ is the q -th diagonal component of $\mathbf{T}(s)$.

4.3 MIMO Controller Design in Nyquist Diagram

In this section, the loop shaping controller design method proposed in Chapter 2 is extended to MIMO systems to solve the nonconvex

control problem presented in (4.3). In contrast with the previous chapters, the interconnected loops should be considered to guarantee the stability of the feedback system.

4.3.1 Stability condition based on Gershgorin Bands

Let the open-loop system $\mathbf{L}(s)$ have no uncontrollable and/or unobservable unstable modes. Then, the Generalized Nyquist Stability criterion shows that the feedback system will be stable if and only if the net sum of anti-clockwise encirclements of the critical point $(-1 + j0)$ by the set of eigenvalues of the matrix $\mathbf{L}(j\omega)$ is equal to the total number of right-half plane poles of $\mathbf{L}(s)$.

The eigenvalues of the matrix $\mathbf{L}(j\omega, \rho)$ at each frequency ω are nonconvex functions of the controller parameters. A sufficient stability condition can be obtained by approximating the eigenvalues using the Gershgorin bands.

Let $\mathbf{L}(j\omega, \rho)$ be the open-loop $n_o \times n_o$ matrix with complex elements $L_{pq}(j\omega, \rho)$. For $q \in \{1, \dots, n_o\}$ we define

$$r_q(\omega, \rho) = \sum_{p=1, p \neq q}^{n_o} |L_{pq}(j\omega, \rho)| \quad (4.4)$$

which is a convex function with respect to the controller parameters. Let $D(L_{qq}(j\omega, \rho), r_q(\omega, \rho))$ be a circle centered at $L_{qq}(j\omega, \rho)$ with radius $r_q(\omega, \rho)$. Such a circle is called a Gershgorin band. Every eigenvalue of $\mathbf{L}(j\omega, \rho)$ lies within at least one of the Gershgorin bands $D(L_{qq}(j\omega, \rho), r_q(\omega, \rho))$ for $q = 1, \dots, n_o$ [51].

Proposition 4.1 [52]: *Consider that the elements of the $n_o \times n_o$ matrix $\mathbf{L}(j\omega) = \mathbf{G}(j\omega)\mathbf{K}(j\omega)$ satisfy*

$$|r_q(\omega)| < |1 + L_{qq}(j\omega)| \quad (4.5)$$

for $q = 1, \dots, n_o$ and for all ω on the Nyquist contour, where

$$r_q(\omega) = \sum_{p=1, p \neq q}^{n_o} |L_{pq}(j\omega)| \quad (4.6)$$

Let the q -th Gershgorin band of $\mathbf{L}(j\omega)$, which is composed of circles centered at $L_{qq}(j\omega)$ with radius $r_q(\omega)$, encircle the critical point $(-1 + j0)$, N_q times counterclockwise. Then, the negative feedback system is stable if and only if

$$\sum_{q=1}^{n_o} N_q = P_0 \quad (4.7)$$

where P_0 is the number of unstable poles of $\mathbf{L}(s)$.

For example, for an open-loop stable system, the closed-loop is stable if the set of the Gershgorin bands of radius $r_q(\omega, \rho)$ of the matrix $\mathbf{L}(j\omega, \rho)$ is strictly at the right hand side of a line passing through the critical point $(-1 + j0)$ for all ω and for $q = 1, \dots, n_o$. A line $d_q(\omega)$ could be used to divide the Nyquist diagram space in two half-planes, shown in Fig. 4.1. The slope of this line can be changed automatically to enlarge the set of admissible controllers using the desired strictly proper open-loop transfer function $L_{Dq}(s)$ for each q -th diagonal component. At each frequency ω , the line $d_q(\omega)$ which crosses the critical point $(-1 + j0)$ and is orthogonal to the line connecting the critical point $(-1 + j0)$ to $L_{Dq}(j\omega)$ is defined. For an open-loop stable system, if all Gershgorin bands for all frequencies are located on the same side of $L_{Dq}(j\omega)$ with respect to the lines $d_q(\omega)$, stability is guaranteed.

The proposed approach can also be applied to unstable systems. The main condition is that $\mathbf{L}_D(j\omega)$ should be a matrix of strictly proper transfer functions and the set of its eigenvalues has to encircle P_0 times the critical point $(-1 + j0)$, where P_0 is the number of unstable poles of $\mathbf{G}(s)$ (in our approach $K(s)$ has no unstable poles due to its parameterization).

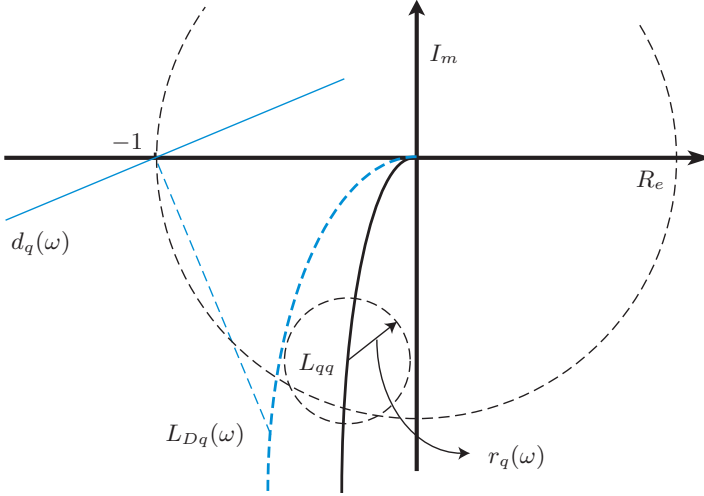


Fig. 4.1. Convex constraints for the Generalized Nyquist Stability criterion in Nyquist diagram

4.3.2 Main result

The main result of this chapter is presented in the following theorem:

Theorem 4.1 *Given the spectral model $\mathbf{G}(j\omega)$, the linearly parameterized controller $\mathbf{K}(s)$ defined in subsection 4.2.2 stabilizes the closed-loop system if*

$$|r_q(\omega, \rho)| |1 + L_{Dq}(j\omega)| - \text{Re}\{[1 + L_{Dq}^*(j\omega)][1 + L_{qq}(j\omega, \rho)]\} < 0 \\ \forall \omega \quad \text{for } q = 1, \dots, n_o \quad (4.8)$$

where the diagonal matrix $\mathbf{L}_D(j\omega)$ is chosen such that the number of counterclockwise encirclements of the critical point by the Nyquist plot of the set of its eigenvalues is equal to the number of unstable poles of $\mathbf{G}(s)$ and $L_{Dq}^*(j\omega)$ is the complex conjugate of $L_{Dq}(j\omega)$.

Proof: Since the real value of a complex number is less than or equal to its magnitude, we have:

$$\operatorname{Re}\{[1 + L_{Dq}^*(j\omega)][1 + L_{qq}(j\omega, \rho)]\} \leq |[1 + L_{Dq}^*(j\omega)][1 + L_{qq}(j\omega, \rho)]| \quad (4.9)$$

Then from (4.8) we obtain:

$$|r_q(\omega, \rho)| - |1 + L_{qq}(j\omega, \rho)| < 0 \quad \forall \omega \quad \text{for } q = 1, \dots, n_o \quad (4.10)$$

which leads directly to (4.5).

Now we should show that this controller stabilizes the system. From (4.8), we have:

$$\operatorname{Re}\{[1 + L_{Dq}^*(j\omega)][1 + L_{qq}(j\omega, \rho)]\} > 0 \quad \forall \omega \quad (4.11)$$

or $\operatorname{wno}\{[1 + L_{Dq}^*(j\omega)][1 + L_{qq}(j\omega, \rho)]\} = 0$, where wno stands for winding number around the origin. It should be mentioned that $L_{qq}(j\omega, \rho)$ is zero for the semicircle with infinity radius of the Nyquist contour so the wno of $1 + L_{qq}(j\omega, \rho)$ depends only on the variation of s on the imaginary axis. On the other hand, as $L_{Dq}(j\omega)$ is a strictly proper transfer function, it goes also to zero for this semicircle. Consequently, the wno of $1 + L_{Dq}^*(j\omega)$ is also determined by the variation of s on the imaginary axis. Therefore:

$$\sum_{q=1}^{n_o} \operatorname{wno}[1 + L_{Dq}(j\omega)] = \sum_{q=1}^{n_o} \operatorname{wno}[1 + L_{qq}(j\omega, \rho)] \quad (4.12)$$

Since $\mathbf{L}_D(j\omega)$ satisfies the Generalized Nyquist criterion, $\mathbf{L}(j\omega)$ will do so as well and all closed-loop systems are stable. ■

Remarks:

- The results of Theorem 4.1 are valid even if $L_{qq}(s, \rho)$ has some poles on the imaginary axis, say $\{jp_1, jp_2, \dots\}$. In this case $\omega \in \mathbb{R} - \{[p_1 - \epsilon, p_1 + \epsilon], [p_2 - \epsilon, p_2 + \epsilon], \dots\}$ where ϵ is a small positive

value. The stability is guaranteed if $L_{Dq}(s)$ contains the poles on the imaginary axis of $L_{qq}(s, \rho)$, because they will have the same behavior at the small semicircular detour of the Nyquist contour at these poles.

- According to this theorem $L_{Dq}(s)$ should contain the unstable poles (as well as the poles on the imaginary axis) of $L_{qq}(s)$. If these poles are unknown (when only the frequency response of the system $\mathbf{G}(j\omega)$ is available), but a stabilizing controller $\mathbf{K}_0(s)$ is available a reasonable choice for $\mathbf{L}_D(j\omega)$ is $\mathbf{G}(j\omega)\mathbf{K}_0(j\omega)$. In this case, $\mathbf{L}_D(j\omega)$ is no longer diagonal and $L_{Dq}(j\omega)$ in the above constraints should be replaced by the q -th eigenvalue, $\lambda_q(j\omega)$, of $\mathbf{L}_D(j\omega)$.

4.3.3 Optimization problem

The convex stability constraints shown in (4.8) adds some conservatism to the approach since the location of an eigenvalue is no longer considered at a point but inside the circle $D(L_{qq}(j\omega, \rho), r_q(\omega, \rho))$. To reduce this conservatism, the radius of this circle $r_q(\omega, \rho)$ should be minimized. This is equivalent to minimizing the magnitude of the off-diagonal components of the open-loop transfer function matrix $\mathbf{L}(j\omega, \rho)$. Therefore, the objective function minimizing the 2-norm of $\mathbf{L} - \mathbf{L}_D$ reduces the conservatism of the approach. This way, the off-diagonal elements of $\mathbf{L}(j\omega, \rho)$ are minimized, which helps to decouple the system. On the other hand, the two norm of $L_{qq} - L_{Dq}$ is minimized for $q = 1, \dots, n_o$, which ensures the single-loop closed-loop performances. It means that by one optimization decoupling controller and decoupled controlled systems are designed simultaneously.

In this decoupling control problem, the diagonal loops can be considered as independent *SISO* systems since a decoupler controller is designed. Hence, it is judicious to define performance constraint on diagonal loops. The infinity norm constraints in (4.3) are considered by following Theorem 2.1. The following optimization problem is proposed to solve the controller design problem:

$$\min_{\rho} \|\mathbf{L}(\rho) - \mathbf{L}_D\|_2$$

Subject to:

$$|r_q(\omega, \rho)| |1 + L_{Dq}(j\omega)| - R_e\{[1 + L_{Dq}^*(j\omega)][1 + L_{qq}(j\omega, \rho)]\} < 0$$

$$\forall \omega \quad \text{for } q = 1, \dots, n_o$$

$$|W_{1q}(j\omega)[1 + L_{Dq}(j\omega)]| + |W_{2q}(j\omega)L_{qq}(j\omega, \rho)[1 + L_{Dq}(j\omega)]|$$

$$- R_e\{[1 + L_{Dq}^*(j\omega)][1 + L_{qq}(j\omega, \rho)]\} < 0$$

$$\forall \omega \quad \text{and for } q = 1, \dots, n_o$$

(4.13)

where $r_q(\omega, \rho)$ is defined in 4.6.

A weighted norm of $\mathbf{L}(\rho) - \mathbf{L}_D$ can be minimized to obtain a controller with more decoupling effect or a better tracking of the desired open-loop transfer function in a given frequency range.

Remarks:

1. The multi-model uncertainty can be considered by repeating the constraints for each model of the uncertainty as presented in the optimization problem below:

$$\min \sum_{i=1}^m \|\mathbf{L}_i(\rho) - \mathbf{L}_{D_i}\|_2$$

Subject to:

$$|r_{q_i}(\omega, \rho)| |1 + L_{Dq_i}(j\omega)|$$

$$- R_e\{[1 + L_{Dq_i}^*(j\omega)][1 + L_{qq_i}(j\omega_k, \rho)]\} < 0$$

$$\text{for } i = 1, \dots, m; \quad \text{for } q = 1, \dots, n_o \text{ and } \forall \omega$$

$$|W_{1q_i}(j\omega)[1 + L_{Dq_i}(j\omega)]| + |W_{2q_i}(j\omega)L_{qq_i}(j\omega, \rho)[1 + L_{Dq_i}(j\omega)]|$$

$$- R_e\{[1 + L_{Dq_i}^*(j\omega)][1 + L_{qq_i}(j\omega, \rho)]\} < 0$$

$$\text{for } i = 1, \dots, m; \quad \text{for } q = 1, \dots, n_o \text{ and } \forall \omega$$

(4.14)

where $L_{Dq_i}^*(j\omega)$ is the complex conjugate of $L_{Dq_i}(j\omega)$.

2. The optimization problems in (4.13) and (4.14) are also an SIP problems. As in Section 2.3.4, a practical solution is to choose

a finite number of frequencies $\omega \in \{\omega_1, \omega_2, \dots, \omega_N\}$ to solve the problem. Practically, to obtain a quadratic objective function, the two norm is replaced by $\|\mathbf{L}(\rho) - \mathbf{L}_D\|_2^2$, which is approximated by:

$$\|\mathbf{L}(\rho) - \mathbf{L}_D\|_2^2 \approx \sum_{\omega} \|\mathbf{L}(j\omega, \rho) - \mathbf{L}_D(j\omega)\|_F \quad (4.15)$$

where $\|\cdot\|_F$ is the Frobenius norm. Thus, the following optimization problem is considered for the multi-model case:

$$\min \sum_{i=1}^m \sum_{k=1}^N \|\mathbf{L}_i(j\omega_k, \rho) - \mathbf{L}_{D_i}(j\omega_k)\|_F$$

Subject to:

$$\begin{aligned} & |r_{q_i}(\omega_k, \rho)| |1 + L_{Dq_i}(j\omega_k)| \\ & - R_e\{[1 + L_{Dq_i}^*(j\omega_k)][1 + L_{qq_i}(j\omega_k, \rho)]\} < 0 \\ & \text{for } k = 1, \dots, N; \text{ for } i = 1, \dots, m \text{ and for } q = 1, \dots, n_o \end{aligned}$$

$$\begin{aligned} & |W_{1q_i}(j\omega_k)[1 + L_{Dq_i}(j\omega_k)]| \\ & + |W_{2q_i}(j\omega_k)L_{qq_i}(j\omega_k, \rho)[1 + L_{Dq_i}(j\omega_k)]| \\ & - R_e\{[1 + L_{Dq_i}^*(j\omega_k)][1 + L_{qq_i}(j\omega_k, \rho)]\} < 0 \\ & \text{for } k = 1, \dots, N; \text{ for } i = 1, \dots, m \text{ and for } q = 1, \dots, n_o \end{aligned} \quad (4.16)$$

where $L_{Dq_i}^*(j\omega_k)$ is the complex conjugate of $L_{Dq_i}(j\omega_k)$.

4.4 Simulation Examples

In this section, the proposed algorithm is applied to the models of two industrial processes proposed in the literature.

4.4.1 Example 1

Consider the following process model proposed in [57]:

$$\mathbf{G}_1(s) = \begin{bmatrix} \frac{5e^{-3s}}{4s+1} & \frac{2.5e^{-5s}}{15s+1} \\ \frac{-4e^{-6s}}{20s+1} & \frac{e^{-4s}}{5s+1} \end{bmatrix} \quad (4.17)$$

where the time scale is given in minutes. A continuous-time PI controller should be tuned assuring 3 dB gain margin and $\pi/3$ phase margin. This system is not diagonally dominant and the variable pairings are not evident.

A solution to this problem is given in [57] where single loop tuning techniques are used to design the decentralized controller using the effective transfer function. This effective transfer function considers the coupling effects for a particular loop from the other closed loop. This results in the following controller:

$$\mathbf{K}_0(s) = \begin{bmatrix} 0.0233\left(1 + \frac{1}{4s}\right) & 0 \\ 0 & 0.1094\left(1 + \frac{1}{5s}\right) \end{bmatrix} \quad (4.18)$$

Equally spaced $N = 150$ frequency points between 0.01 rad/min and 10 rad/min are chosen to solve the optimization problem proposed in (4.16). The lower limit is greater than 0 because of the integrator. The upper limit is chosen sufficiently large so that the frequency response of the system is negligible at frequencies above the upper limit. The desired open-loop transfer function matrix $\mathbf{L}_D(s)$ is chosen as simple integrators at the diagonal elements with a bandwidth similar to those obtained with the controller proposed in [57]:

$$\mathbf{L}_D(s) = \begin{bmatrix} \frac{1}{30s} & 0 \\ 0 & \frac{1}{30s} \end{bmatrix} \quad (4.19)$$

which satisfies the specified gain and phase margins.

Only stability constraints are considered on the optimization problem given in (4.16), which results in the following controller:

$$\mathbf{K}_1(s) = \begin{bmatrix} \frac{0.002667s+0.002338}{s} & \frac{0.003439s-0.005726}{s} \\ \frac{-0.0004078s+0.008943}{s} & \frac{0.05531s+0.01166}{s} \end{bmatrix} \quad (4.20)$$

Figure 4.2 shows that the proposed method decouples the system almost perfectly, which is not the case for $\mathbf{K}_0(s)$. It should be noted that the controller proposed in [57] is a decentralized controller while that proposed in this paper is centralized. The complexity of the controller explains the better performances obtained with the proposed controller. However, even that the proposed method offers the possibility to design more complex controllers, the method remains simple and intuitive.

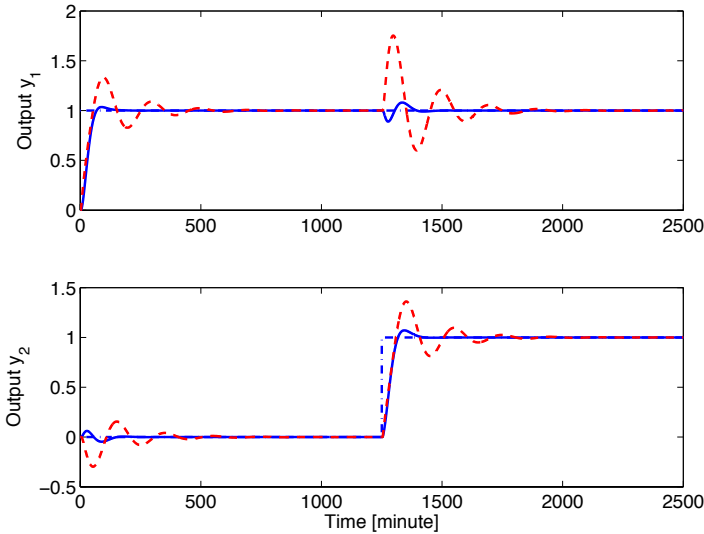


Fig. 4.2. Two output responses: Reference signal (blue, dash-dot), controller proposed in [57] (red dashed) and proposed controller (blue solid).

One of the most important advantages of the proposed approach is that systems with multi-model uncertainty can directly be considered. A second system with 100% higher values for the gains, time constants and time delays than those of the previous system $\mathbf{G}_1(s)$

is defined:

$$\mathbf{G}_2(s) = \begin{bmatrix} \frac{10e^{-6s}}{8s+1} & \frac{5e^{-10s}}{30s+1} \\ \frac{-8e^{-12s}}{40s+1} & \frac{2e^{-8s}}{10s+1} \end{bmatrix} \quad (4.21)$$

The following multiplicative uncertainty filters are defined for the diagonal elements of both systems, $\mathbf{G}_1(s)$ and $\mathbf{G}_2(s)$ by:

$$W_{2_q}(s) = 0.5 \frac{2s+1}{s+1} \quad \text{for } q = 1, 2 \quad (4.22)$$

A stabilizing PI MIMO controller is tuned to satisfy the robust performance condition in (2.11) for the diagonal elements of both systems, where the performance filter for both systems is given by $W_{1_q}(s) = 0.5$ for $q = 1, 2$.

The optimization problem proposed in (4.16) is solved by repeating the stability and robust performance constraints for $\mathbf{G}_2(s)$. This results in the following controller:

$$\mathbf{K}_2(s) = \begin{bmatrix} \frac{0.001851s+0.001348}{s} & \frac{0.002225s-0.003084}{s} \\ \frac{-0.0005015s+0.004521}{s} & \frac{0.03111s+0.006742}{s} \end{bmatrix} \quad (4.23)$$

This controller is stabilizing and satisfies the required H_∞ constraints for both systems. Figure 4.3 shows that, contrarily to $\mathbf{K}_1(s)$, controller $\mathbf{K}_2(s)$ decouples both systems. This was expected because $\mathbf{K}_1(s)$ was not designed for this purpose. It should be noted that $\mathbf{K}_0(s)$ does not even stabilize $\mathbf{G}_2(s)$.

4.4.2 Example 2

In this example, the proposed algorithm is applied to a multivariable LV100 gas turbine engine and the results are compared with those of two other data-driven controller approaches for multivariable systems in [26,47]. The objective is to tune a multivariable PI controller for a LV100 gas turbine engine to follow the reference model $\mathcal{M}_D(z)$. The

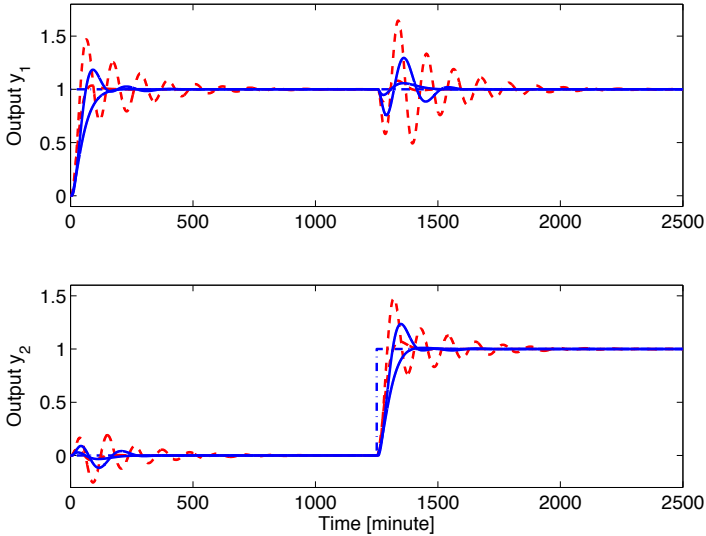


Fig. 4.3. Two output responses: Reference signal (blue, dash-dot), $\mathbf{K}_1(s)$ (red, dashed) and $\mathbf{K}_2(s)$ (blue, solid).

plant is represented by a continuous-time state-space model with five states, two inputs and two outputs. The model is discretized using Tustin's approximation with $T_s = 0.1s$ as the sampling period. Each experiment is performed with a measurement noise that is generated as a zero-mean, stationary white Gaussian sequence with variance $0.0025I$.

The given reference model is:

$$\mathcal{M}_D(z) = \begin{bmatrix} \mathcal{M}_{d_1}(z) & 0 \\ 0 & \mathcal{M}_{d_2}(z) \end{bmatrix} = \begin{bmatrix} \frac{0.4}{z-0.6} & 0 \\ 0 & \frac{0.4}{z-0.6} \end{bmatrix} \quad (4.24)$$

which is used to define our desired open-loop transfer function:

$$\begin{aligned} \mathbf{L}_D(z) &= \begin{bmatrix} \frac{\mathcal{M}_{d_1}(z)}{1-\mathcal{M}_{d_1}(z)} & 0 \\ 0 & \frac{\mathcal{M}_{d_2}(z)}{1-\mathcal{M}_{d_2}(z)} \end{bmatrix} \\ &= \begin{bmatrix} L_{d_1}(z) & 0 \\ 0 & L_{d_2}(z) \end{bmatrix} = \begin{bmatrix} \frac{0.4}{z-1} & 0 \\ 0 & \frac{0.4}{z-1} \end{bmatrix} \end{aligned} \quad (4.25)$$

An experiment is realized using the simulation conditions proposed in [26]. The results are compared with controller given in [47] designed using the iterative correlation-based controller tuning approach (CbT):

$$\mathbf{K}_{CbT}(z) = \begin{bmatrix} \frac{0.3636z-0.09866}{\frac{z-1}{18.69z-18.16}} & \frac{0.3653z-0.2691}{\frac{z-1}{-3.453z+2.652}} \end{bmatrix} \quad (4.26)$$

and the IFT controller provided in [26]:

$$\mathbf{K}_{IFT}(z) = \begin{bmatrix} \frac{0.248z-0.03}{\frac{z-1}{16.47z-15.91}} & \frac{0.38z-0.199}{\frac{z-1}{0.063z+0.054}} \end{bmatrix} \quad (4.27)$$

The CbT approach tunes diagonal and off-diagonal elements of the controller transfer function matrix simultaneously to satisfy desired closed-loop performance and to decouple the closed-loop outputs. This method is a time-domain data-driven approach using non-convex optimization which does not guarantee closed-loop stability. On the other hand, the IFT control method uses the unbiased gradient estimate of a quadratic control criterion using closed-loop experiment data to obtain a tuning algorithm. However, the number of experiments needed to estimate the gradient increases with the number of outputs and inputs of the system.

The sum of squared output errors (SSOE) is used for comparison of different controllers. This criterion is defined as:

$$SSOE = \frac{1}{N_t} \sum_{t=1}^{N_t} \varepsilon_{oe}^T(t) \varepsilon_{oe}(t) \quad (4.28)$$

where $N_t = 151$ is the data length and ε_{oe} the difference between the desired and the obtained outputs.

Model-based design

The optimization problem proposed in (4.16) only considering the stability constraints is solved with $N = 500$ equally spaced between ω_{\max}/N and ω_{\max} rad/s. The smallest frequency is greater than zero because of the integrator in the controller and ω_{\max} is chosen equal to the Nyquist frequency. The result of the optimization algorithm is :

$$\mathbf{K}_0(z) = \begin{bmatrix} \frac{0.3793z-0.098}{z-1} & \frac{0.3582z-0.25}{z-1} \\ \frac{20.22z-19.61}{z-1} & \frac{-2.876z+1.992}{z-1} \end{bmatrix} \quad (4.29)$$

with an SSOE equal to 0.0048. Figure 4.4 shows the experiment without noise where an almost perfect decoupling can be observed.

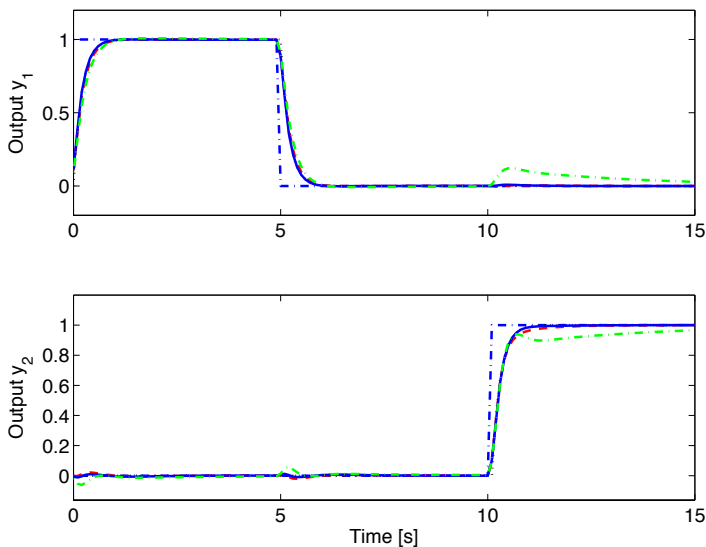


Fig. 4.4. Two output responses: Reference signal (blue, dash-dot), Reference model (black dotted), CbT (red dashed), IFT (green dash-dot) and proposed controller using the model (blue solid)

Data-driven design

To be fair on this comparison, a spectral model is identified based on the same rectangular reference signal used by the iterative methods previously mentioned. The ETFE method is used to identify the frequency function models based on the input/output measurements for the rectangular reference signal applied to each input while the other is not excited. As the input's spectral content is poor at high frequencies and as the signal to noise ratio is very low, the ETFE model is evaluated at $N = 500$ equally spaced frequency points between $1/N$ and $\omega_{\max} = 1$ rad/s for the optimization problem (this range of frequency defines the first lobe of the input spectrum). The resulting PI MIMO controller designed is :

$$\mathbf{K}(z) = \begin{bmatrix} \frac{0.3392z-0.05811}{z-1} & \frac{0.3581z-0.2572}{z-1} \\ \frac{20.38z-19.76}{z-1} & \frac{-3.299z+2.339}{z-1} \end{bmatrix} \quad (4.30)$$

Figure 4.5 shows that the system's outputs using the proposed controller are very close to the desired reference response except for the effect of noise. In addition, the closed-loop system is nearly fully diagonalized. The observed SSOE with the proposed controller is 0.0048, while those with the CbT and IFT controllers are 0.0050 and 0.0082 respectively. Even if IFT method has a noise-rejection objective function that could be advantageous in a noisy environment, the results are not so satisfying because it is not able to fully decouple the system, while the other methods do. This is more perceptible in Figure 4.6, where an experiment without noise is shown. At the instants 0s and 5s on y_2 and at instant 10s on y_1 , it is visible that the decoupling of the IFT controller is not as good as that proposed by the other approaches.

It should be noticed that global stability is guaranteed thanks to the Gershgorin bands considered as convex constraints in this approach, whereas the other data-driven approaches do not ensure the stability of the closed-loop system. The other advantage of the proposed approach is in terms of experimental cost. The CbT and IFT methods are iterative methods which are experimentally expensive.

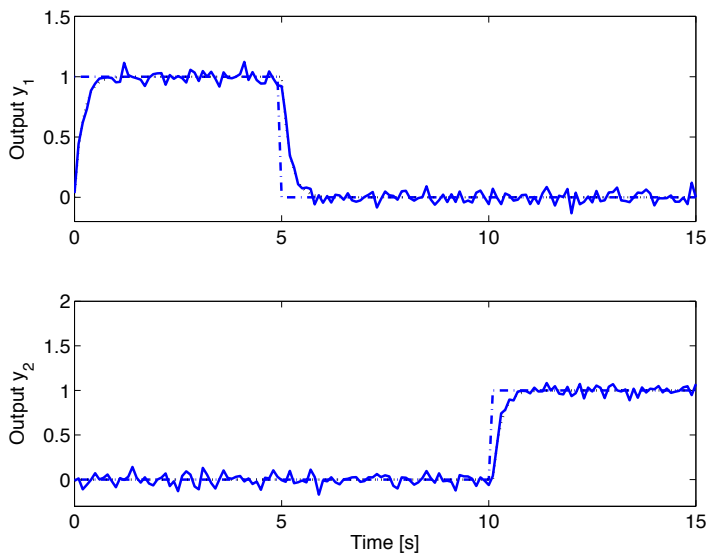


Fig. 4.5. Two output responses: Reference signal (blue, dash-dot), Reference model (black dotted) and proposed controller (blue solid)

The IFT controller is designed after 6 iterations with a total of 450 seconds of experimentation and CbT is obtained after 8 iterations (120 seconds), while the proposed method is designed based on an experiment of 20 seconds. Moreover, the computational complexity of this approach is very low.

4.5 Conclusions

A new decoupling fixed-order MIMO controller design method in the Nyquist diagram for spectral MIMO models based on the shaping of the open-loop matrix transfer function has been proposed in this chapter. The 2-norm of the difference between the open-loop and a

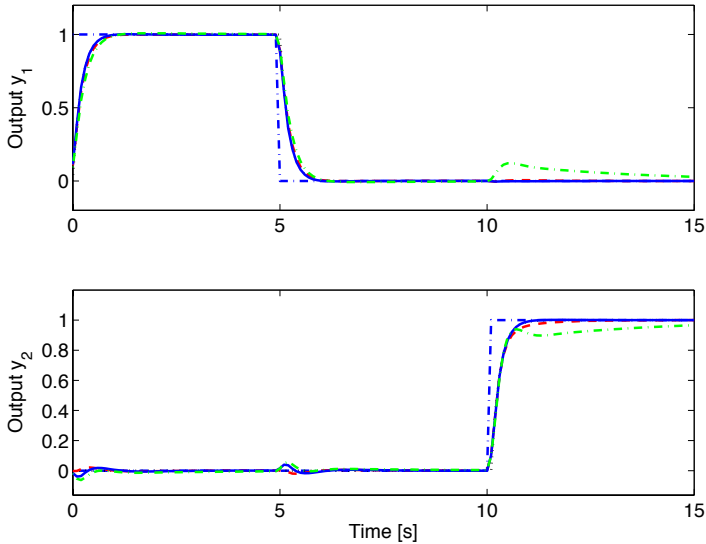


Fig. 4.6. Two output responses: Reference signal (blue, dash-dot), Reference model (black dotted), CbT (red dashed), IFT (green dash-dot) and proposed controller (blue solid)

desired open-loop matrix transfer functions is minimized under stability constraints to design a linearly parameterized decoupling controller. The method is based on an approximation of the nonconvex Generalized Nyquist Stability criterion by convex constraints using the Gershgorin bands. The controller is linearly parameterized and its denominator should be fixed a priori. However, this restriction ensures the stability of the controller and makes no problem for PID controller design as well as for higher order controllers.

The advantages of this approach are summarized below:

1. Only the frequency response of the system is needed and no parametric model is required. The method can be qualified as “data-driven” because the frequency response of the system can be

obtained directly by discrete Fourier transform from a set of periodic data. Of course, when a parametric model is given, the method can be also applied.

2. Simultaneously, the diagonal elements of the controller are tuned to satisfy some desired performances, while the off-diagonal elements are tuned to decouple the system.
3. Multi-model uncertainty can be handled easily by increasing the number of convex constraints. Most of the mentioned classical frequency-domain approaches cannot deal with this type of uncertainty.
4. If a stabilizing initial controller is known, unstable systems can be also considered with this approach.

Controller Design with Finite Number of Constraints

Many frequency-domain controller design methods including those presented in this thesis define the stability and performance specifications conditions at all frequencies of the frequency response function. In several cases, this control problem is transformed into an optimization problem where a finite number of decision variables (the parameters of the controller) should be optimized subject to an infinite number of constraints. This optimization problem is known as a Semi-Infinite Programming (SIP) problem which is difficult to solve and can even be NP-hard in many cases. Different numerical solutions exist in the literature to solve this type of problems (see [22] for a survey). In this chapter, three different approaches are proposed to deal with this type of optimization problems.

Typically, this problem is relaxed by considering only a finite number of those constraints. This converts the optimization problem into a Semi-Definite Programming (SDP) problem which can be solved with many standard solvers. Practically, if the number of constraints is large enough, this may lead to stable controllers with the desired performances. That the constraints are satisfied at certain frequencies does not imply, however, that the conditions are also satisfied between those frequencies. A randomized approach can also

be used to solve the problem. In this case, the solution satisfies the constraints for all frequencies with a high probability level. This is known as the *scenario approach* [2,7,8]. Nonetheless, it is possible to satisfy the constraints for all frequencies only using a finite number of frequencies if some assumptions are verified on the system. The difficulty, however, is knowing the minimum number of necessary frequencies. The system's behavior between the measured frequency samples is referred to in the sequel as its inter-grid behavior.

In [12], the set of all possible interpolants that corresponds to the system's measured frequency samples is defined with a prior assumption on the system's impulse response. The absolute value of the system's impulse response is assumed to be bounded by a decreasing exponential function that converges to zero. As a result, a bound for the difference between the linear interpolation model and all the possible interpolants between the frequency samples is obtained. This result cannot be applied for systems with integrators because the impulse response cannot be bounded with a decreasing exponential function that converges to zero. A similar problem is treated in [14]. A prior assumption is considered on the relative stability of the underlying system. This means that the real parts of the underlying system's poles are assumed to be greater than a chosen positive value. A frequency dependent bound is then given for all possible interpolants. This slightly reduces the conservatism compared to the previously mentioned constant bound proposed by [12]. These results have been applied to a controller design method presented in [15]. The main drawback of the approach is that non-parametric controllers are obtained. A second step of interpolation is needed to obtain a parametric controller to be implementable in a feedback loop.

This chapter is organized as follows: In Section 5.1 the *Approximate approach* is described where a finite number of constraints are considered to solve the SIP problem. The *Probabilistic approach* is presented in Section 5.2 where a randomized solution is given for the SIP problem. In Section 5.3 the *Exact approach* is introduced for discrete-time controller design problems where adding some conser-

vatism, the original SIP problem is transformed to a standard SDP problem. An example shows how the performance is affected when this conservatism is added in Section 5.4. Finally, some concluding remarks are given in Section 5.5.

5.1 Approximate Approach

Practically, the SIP problem can be solved choosing a sufficiently large number of frequencies N to define a finite set of constraints for $\omega \in \{\omega_1, \dots, \omega_N\}$. A sufficiently large number of frequency points means that the infinite number of constraints should be well represented by the chosen finite number of constraints.

The constraints given in the SIP problems are presented in the Nyquist diagram based on the open-loop frequency response of the system. Hence, it is assumed that if the open-loop frequency samples are a good representation of the open-loop frequency response, the finite set of constraints defined based on the open-loop frequency samples will also be a good representation of the infinite set of constraints. Consequently, N could be chosen such that for equally spaced frequency samples, the open-loop frequency response in the Nyquist diagram between two adjacent frequency samples can be well approximated by the linear interpolation.

However, the open-loop frequency response is not available since the controller is not known a priori. Practically, a value is chosen for N to solve the optimization problem. A posteriori, once the controller is available, it is verified if the open-loop frequency response $L(j\omega)$ between two adjacent frequency samples is well approximated by the linear interpolation in the Nyquist diagram. As an initial guess, N can be chosen such that the sampled frequency response $L_d(j\omega_k)$ for $k = 1, \dots, N$ is a complete representation of the underlying system $L_d(j\omega)$. This can be verified if the dual of Shannon's Theorem is satisfied. The dual of Shannon's Theorem, given below, shows that uniformly spaced discrete samples of the frequency

response of a signal are a complete representation of the frequency response if its Inverse Fourier Transform is a time-limited signal.

Theorem 5.1 Dual of Shannon's Theorem. $X(\omega)$ is completely determined by its ordinates at a series of points spaced by less than or equal to π/T_i if its Inverse Fourier Transform $x(t)$ is 0 for $t < -T_i$ and $t > T_i$.

Proof: $x(t)$ has non zero values for a period of $2T_i$. Therefore, it can be represented as a Fourier series expansion using any period $T_m \geq 2T_i$. The Fourier Transform expansion of $x(t)$ can be written as:

$$x(t) = \sum_{k=-\infty}^{\infty} A_k e^{jk2\pi \frac{t}{T_m}} \quad (5.1)$$

where $A_k = \frac{1}{T_m} \int_{-\frac{T_m}{2}}^{\frac{T_m}{2}} x(t) e^{-jk2\pi \frac{t}{T_m}} dt$. As $x(t)$ is 0 for $t < -\frac{T_m}{2}$ and $t > \frac{T_m}{2}$, the Fourier Transform is reduced to:

$$X(\omega) = \mathcal{F}\{x(t)\} = \int_{-\infty}^{\infty} x(t) e^{-j\omega t} dt = \int_{-\frac{T_m}{2}}^{\frac{T_m}{2}} x(t) e^{-j\omega t} dt \quad (5.2)$$

By comparison, $A_k = \frac{1}{T_m} X(k \frac{2\pi}{T_m})$. Hence, this implies that $X(\omega)$ can be fully represented by its samples.

$$X(\omega) = \frac{1}{T_m} \int_{-\frac{T_m}{2}}^{\frac{T_m}{2}} \left[\sum_{k=-\infty}^{\infty} X(\omega_k) e^{j\omega_k t} \right] e^{-j\omega t} dt \quad (5.3)$$

where $\omega_k = k \frac{2\pi}{T_m}$. ■

Consequently, if the open-loop transfer function $L_d(j\omega)$ is negligible for $\omega > \omega_{max}$ and if its impulse response is time limited (between $-T_i$ and T_i), then $L_d(j\omega)$ is completely represented by $L_d(j\omega_k)$ where $\omega_k = (k-1) \frac{\omega_{max}}{N-1}$ for $k = 1, \dots, N$ and $N \geq \frac{\omega_{max} T_i}{\pi} + 1$. For example, consider that the desired open-loop transfer function $L_d(s) = \frac{1}{s+1}$ is defined for a control problem. In this particular example, $\omega_{max} = 100$

rad/s and $T_i = 10$ s can be considered. The dual of Shannon's Theorem shows that $L_d(j\omega)$ is completely represented by $L_d(j\omega_k)$ where $N = 320$ and $\omega_k = (k - 1)\frac{\omega_{max}}{N-1}$. Hence, the control problem can be solved taking equally spaced N frequencies between 0 and ω_{max} rad/s.

The optimization problems to be solved have been already presented in (2.49), (3.25) and (4.16).

5.2 Probabilistic Approach

If the spectral models are obtained from a set of noisy data, then the frequency-domain uncertainty sets are defined with a probability level. In this case, even a feasible solution to the SIP will guarantee the stability and the required performance with a probability level. Therefore, it is more reasonable to use a randomized approach to solve the SIP problem. According to the results of [2, 7, 8] with a reasonable number N of randomly chosen frequency samples, the optimal solution ρ^* to the convex optimization problem will satisfy the constraints for all frequencies with a high probability level. This is known as the *Scenario approach*. In order to be more precise, let the violation probability $V(\rho^*)$ be defined as the probability that for $\omega_0 \in \mathbb{R}$ the convex constraints are not satisfied for ρ^* . Then it can be shown that:

$$\mathcal{P}\{V(\rho^*) > \epsilon\} \leq \sum_{i=0}^{n-1} \binom{N}{i} \epsilon^i (1 - \epsilon)^{N-i} \leq \eta \quad (5.4)$$

where $\mathcal{P}\{\cdot\}$ stands for the probability of an event, n is the number of design parameters, the *violation parameter* ϵ is a satisfying level and η is a *confidence parameter*. To make the result in (5.4) more useful, the following explicit expression is provided in [2]:

$$N \geq \frac{1}{\epsilon} \left(\ln \frac{1}{\eta} + n - 1 + \sqrt{2(n-1) \ln \frac{1}{\eta}} \right) \quad (5.5)$$

Then, with probability no smaller than $1 - \eta$, the solution satisfies all constraints but at most an ϵ -fraction. Actually, the value of N returned by (5.5) can be conservative. However, it offers the possibility to recognize that η plays a key role because selecting $\eta = 0$ leads to $N = \infty$, but practically has marginal importance since its logarithm appears in (5.5).

Consider, for example, PID controller design ($n = 3$) with $N = 500$ frequency points. Then, using (5.4), having a violation probability of greater than $\epsilon = 0.01$ has a probability of less than 0.1234. This upper bound goes exponentially to zero with N . Therefore, the upper bound can be reduced to 0.0027 for $N = 1000$ and to 4.2×10^{-7} for $N = 2000$.

The optimization problems to be solved are the same as those proposed for the *Approximate approach*. The only difference is that in this case the N frequencies are randomly chosen which assures that constraints are satisfied with a chosen violation and probability level.

5.3 Exact Approach

The *Approximate approach* and *Probabilistic approach* guarantee that the stability and performance conditions are satisfied at the evaluated N frequencies samples. However, this is not the case for all the frequencies between the frequency samples. To assure the stability and performance constraints, the behavior of the open-loop frequency response between the frequency samples should be analyzed, which is known as inter-grid behavior.

In this section, first the inter-grid behavior of a frequency response of a discrete-time system is analyzed using only its discrete samples. Then, the results are extended to discrete-time systems containing an integrator. Finally, these results are implemented in the loop-shaping discrete-time controller design method for discrete-time systems proposed in the previous chapters.

5.3.1 Analysis of the inter-grid behavior

Inter-grid uncertainty

Based on the results shown in [12], the frequency response samples of a discrete-time system are used to define an uncertainty bound. This bound represents all possible interpolants between the samples.

Assume that we have N frequency response samples, $X(e^{-j\omega_k})$ for $k = 1, \dots, N$ of the original frequency response $X(e^{-j\omega})$ of a discrete-time system between 0 and the Nyquist frequency ω_N spaced by $\frac{\omega_N}{N-1}$. Let the linear interpolation frequency response model $X_\lambda(e^{-j\omega})$ be defined between two consecutive frequency response samples $X(e^{-j\omega_k})$ and $X(e^{-j\omega_{k+1}})$:

$$X_\lambda(e^{-j\omega}) = \lambda X(e^{-j\omega_k}) + (1 - \lambda)X(e^{-j\omega_{k+1}}) \quad \text{for } \omega_k < \omega < \omega_{k+1} \quad (5.6)$$

where ω is defined as $\omega = \lambda\omega_k + (1 - \lambda)\omega_{k+1}$ and:

$$\lambda = \frac{\omega - \omega_{k+1}}{\omega_k - \omega_{k+1}} \quad \lambda \in [0, 1] \quad (5.7)$$

Since $\left| \frac{d^2 X_\lambda(e^{-j\omega})}{d\omega^2} \right| = 0$, if the impulse response $x(h)$ of the discrete-time system satisfies $|x(h)| \leq M\beta^{-h}$, it is shown in [12] that:

$$|X_\lambda(e^{-j\omega}) - X(e^{-j\omega})| \leq \delta \quad (5.8)$$

where

$$\delta = \frac{M\beta(\beta + 1)}{2(\beta - 1)^3} \left(\frac{\omega_{k+1} - \omega_k}{2} \right)^2 = \frac{1}{2} \frac{M\beta(\beta + 1)}{(\beta - 1)^3} \left(\frac{\omega_N}{2(N - 1)} \right)^2 \quad (5.9)$$

Inter-grid uncertainty with integrators

If the discrete-time system contains an integrator, (a pole at 1), its impulse response $x(h)$ cannot be bounded by a decreasing exponential function that converges to zero. In this case, a similar approach can be applied nonetheless.

In the sequel, it is considered that the discrete-time system has only one integrator. For simplicity, the discrete-time integrator $\frac{1}{1-e^{-j\omega}}$ is approximated by $\frac{1}{j\omega}$. However, in Appendix A the results considering the discrete-time integrator without approximation are given.

The frequency response $\tilde{X}(e^{-j\omega})$ of the discrete-time system is approximated by:

$$\tilde{X}(e^{-j\omega}) = \frac{X(e^{-j\omega})}{1-e^{-j\omega}} \approx \frac{X(e^{-j\omega})}{j\omega} \quad (5.10)$$

where $X(e^{-j\omega})$ is the frequency response of the discrete-time system without integral part. The impulse response $x(h)$ of the discrete-time system without the integral term is bounded $|x(h)| \leq M\beta^{-h}$. This bounds $|X_\lambda(e^{-j\omega}) - X(e^{-j\omega})|$ as in (5.9). However, now the goal is to find a bound δ_{int} for $|\tilde{X}_\lambda(e^{-j\omega}) - \tilde{X}(e^{-j\omega})|$ based on the bound on $|X_\lambda(e^{-j\omega}) - X(e^{-j\omega})|$. Note that the linear interpolation model $\tilde{X}_\lambda(e^{-j\omega})$ between the frequency samples $\tilde{X}(e^{-j\omega_k})$ is defined as:

$$\tilde{X}_\lambda(e^{-j\omega}) = \lambda \frac{X(e^{-j\omega_k})}{j\omega_k} + (1-\lambda) \frac{X(e^{-j\omega_{k+1}})}{j\omega_{k+1}} \quad \text{for } \omega_k < \omega < \omega_{k+1} \quad (5.11)$$

Using the linear interpolation models, the bound for $|\tilde{X}_\lambda(e^{-j\omega}) - \tilde{X}(e^{-j\omega})|$ can be bounded as follows:

$$\begin{aligned} |\tilde{X}_\lambda(e^{-j\omega}) - \tilde{X}(e^{-j\omega})| &\leq \left| \tilde{X}_\lambda(e^{-j\omega}) - \frac{X_\lambda(e^{-j\omega})}{j\omega} \right| \\ &+ \left| \frac{X_\lambda(e^{-j\omega})}{j\omega} - \tilde{X}(e^{-j\omega}) \right| \quad \text{for } \omega_k < \omega < \omega_{k+1} \quad (5.12) \end{aligned}$$

Now, each term of the previous bound is analyzed separately. From (5.6) and (5.7), the following equation is obtained:

$$\begin{aligned} \frac{X_\lambda(e^{-j\omega})}{j\omega} &= \frac{\omega - \omega_{k+1}}{\omega_k - \omega_{k+1}} \frac{X(e^{-j\omega_k})}{j\omega} + \left(1 - \frac{\omega - \omega_{k+1}}{\omega_k - \omega_{k+1}}\right) \frac{X(e^{-j\omega_{k+1}})}{j\omega} \\ &\quad \text{for } \omega_k < \omega < \omega_{k+1} \quad (5.13) \end{aligned}$$

Then, if λ from (5.7) is replaced in (5.11) and combined with (5.13), the following equation is obtained:

$$\begin{aligned} \left| \tilde{X}_\lambda(e^{-j\omega}) - \frac{X_\lambda(e^{-j\omega})}{j\omega} \right| &= \left| \frac{\omega - \omega_{k+1}}{\omega_k - \omega_{k+1}} X(e^{-j\omega_k}) \frac{\omega_k - \omega}{\omega_k \omega} - \right. \\ &\quad \left. \frac{\omega_k - \omega}{\omega_k - \omega_{k+1}} X(e^{-j\omega_{k+1}}) \frac{\omega - \omega_{k+1}}{\omega_{k+1} \omega} \right| \\ &= \left| \frac{(\omega - \omega_{k+1})(\omega_k - \omega)}{(\omega_k - \omega_{k+1})\omega} \right| \left| \frac{X(e^{-j\omega_k})}{\omega_k} - \frac{X(e^{-j\omega_{k+1}})}{\omega_{k+1}} \right| \\ &\quad \text{for } \omega_k < \omega < \omega_{k+1} \end{aligned} \quad (5.14)$$

which has a maximum value when $\omega = \sqrt{\omega_k \omega_{k+1}}$. Then, (5.14) can be bounded by:

$$\begin{aligned} \left| \tilde{X}_\lambda(e^{-j\omega}) - \frac{X_\lambda(e^{-j\omega})}{j\omega} \right| &\leq \left| \frac{(\sqrt{\omega_k \omega_{k+1}} - \omega_{k+1})(\omega_k - \sqrt{\omega_k \omega_{k+1}})}{(\omega_k - \omega_{k+1})\sqrt{\omega_k \omega_{k+1}}} \right| \times \\ &\quad \left| \frac{X(e^{-j\omega_k})}{\omega_k} - \frac{X(e^{-j\omega_{k+1}})}{\omega_{k+1}} \right| \\ &= \left| \frac{(\sqrt{\omega_k} - \sqrt{\omega_{k+1}})^2}{\omega_k - \omega_{k+1}} \right| \left| \frac{X(e^{-j\omega_k})}{\omega_k} - \frac{X(e^{-j\omega_{k+1}})}{\omega_{k+1}} \right| \\ &= \left| \frac{\omega_k - \omega_{k+1}}{(\sqrt{\omega_k} + \sqrt{\omega_{k+1}})^2} \right| \left| \frac{X(e^{-j\omega_k})}{\omega_k} - \frac{X(e^{-j\omega_{k+1}})}{\omega_{k+1}} \right| \\ &\quad \text{for } \omega_k < \omega < \omega_{k+1} \end{aligned} \quad (5.15)$$

Replacing $\omega_{k+1} - \omega_k$ by $\frac{\omega_N}{N-1}$:

$$\begin{aligned} \left| \tilde{X}_\lambda(e^{-j\omega}) - \frac{X_\lambda(e^{-j\omega})}{j\omega} \right| &\leq \frac{1}{N-1} \frac{\omega_N}{(\sqrt{\omega_k} + \sqrt{\omega_{k+1}})^2} \left| \frac{X(e^{-j\omega_k})}{\omega_k} - \frac{X(e^{-j\omega_{k+1}})}{\omega_{k+1}} \right| \\ &\quad \text{for } \omega_k < \omega < \omega_{k+1} \end{aligned} \quad (5.16)$$

On the other hand, the second term of the bound is a direct result from the previous subsection:

$$\left| \frac{X_\lambda(e^{-j\omega})}{j\omega} - \tilde{X}(e^{-j\omega}) \right| = \left| \frac{1}{j\omega} (X_\lambda(e^{-j\omega}) - X(e^{-j\omega})) \right| \leq \left| \frac{1}{j\omega_k} \right| \delta$$

for $\omega_k < \omega < \omega_{k+1}$ (5.17)

Therefore, the bound δ_{int} for the difference between the linear interpolation model $\tilde{X}_\lambda(e^{-j\omega})$ and all possible interpolants between the frequency samples of the frequency response of the discrete-time system $\tilde{X}(e^{-j\omega})$ when the discrete-time system contains an integrator, is given by:

$$\delta_{int}(\omega) = \frac{1}{N-1} \frac{\omega_N}{(\sqrt{\omega_k} + \sqrt{\omega_{k+1}})^2} \left| \frac{X(e^{-j\omega_k})}{\omega_k} - \frac{X(e^{-j\omega_{k+1}})}{\omega_{k+1}} \right| + \left| \frac{1}{j\omega_k} \right| \delta$$

for $\omega_k < \omega < \omega_{k+1}$ (5.18)

Remark: It should be noted that these bounds are conservative but decrease rapidly while N is increased. For the no integrator case, the bound δ in (5.9) decreases by a factor of $1/(N-1)^2$ while for the case with one integrator, the bound δ_{int} in (5.18) decreases by a factor of $1/(N-1)$.

5.3.2 Controller design method

The inter-grid behavior of a frequency response function can be analyzed following Subsection 5.3.1. To integrate these bounds in the open-loop shaping controller design method proposed in the previous chapters, $X(e^{-j\omega})$ or $\tilde{X}(e^{-j\omega})$ should be replaced by the open-loop frequency response $L(e^{-j\omega}, \rho)$ (a function of the controller parameters). However, the controller is not known a priori (ρ is not known), so these results cannot be applied directly. Thus, the results presented in Subsection 5.3.1 should be integrated in the controller design method taking into account the inter-grid behavior as a function of the controller parameters ρ .

The main idea is to define linear constraints on controller parameters to bound the impulse response of the open-loop discrete-time system $L(e^{-j\omega}, \rho)$. Then, the graphical interpretation of the bound for the difference between the linear interpolation model and the open-loop frequency response is used to define new convex constraints in the Nyquist diagram. These new constraints assure that the frequency condition is satisfied for all frequencies between the frequency samples. It should be noted that only a finite number of convex constraints are used in the optimization problem.

Controller design (no integrator)

Consider that $G(e^{-j\omega})$ is a causal discrete-time LTI-SISO system with bounded infinity norm. A linearly parameterized discrete-time controller should be tuned given by:

$$K(e^{-j\omega}, \rho) = \rho^T \phi(e^{-j\omega}) \quad (5.19)$$

where

$$\rho^T = [\rho_1, \rho_2, \dots, \rho_n] \quad (5.20)$$

$$\phi^T(e^{-j\omega}) = [\phi_1(e^{-j\omega}), \phi_2(e^{-j\omega}), \dots, \phi_n(e^{-j\omega})] \quad (5.21)$$

n is the number of controller parameters and $\phi_i(e^{-j\omega}), i = 1, \dots, n$ are stable transfer functions with no poles at 1 chosen from a set of orthogonal basis functions. It is clear that PD controllers belong to this set.

$L(e^{-j\omega}, \rho) = K(e^{-j\omega}, \rho)G(e^{-j\omega})$ is the open-loop transfer function of the system. The inter-grid behavior between the open-loop frequency response samples depend on its impulse response $\ell(h, \rho)$. This impulse response can be computed with the Discrete-Time Inverse Fourier Transform of the open-loop frequency response $L(e^{j\omega}, \rho)$:

$$\ell(h, \rho) = \frac{1}{2\pi} \int_{-\pi}^{\pi} L(e^{-j\omega}, \rho) e^{j\omega h} d\omega \quad h = 0, \dots, \infty \quad (5.22)$$

The impulse response $\ell(h, \rho)$ can be bounded by $|\ell(h, \rho)| \leq M\beta^{-h}$ at the discrete-time instants $h = 0, \dots, N_\ell - 1$ where N_ℓ is chosen sufficiently large. The bandwidth of the desired open-loop transfer function $L_d(j\omega)$ can be used to choose the value of N_ℓ . This bound is presented as linear constraint on controller parameter ρ . In order to simplify the computations, the integration can be approximated with the desired precision based on the Inverse Discrete Fourier Transform given by:

$$\ell(h, \rho) \approx \frac{1}{N_d} \sum_{k=1}^{N_d} L(e^{-j\omega_k}, \rho) e^{j\omega_k h} \text{ for } h = 0, \dots, N_\ell - 1 \quad (5.23)$$

Note that $N_d \geq N$ should be chosen where N is the number of frequency samples of $L(e^{-j\omega_k}, \rho)$ such that the dual of Shannon's Theorem is satisfied. This assures that the discrete frequency samples $L(e^{-j\omega_k}, \rho)$ for $k = 1, \dots, N_d$ are a complete representation of $L(e^{-j\omega}, \rho)$. For simplicity, N_d and N_ℓ are chosen equal to N which gives:

$$\ell(h, \rho) \approx \frac{1}{N} \sum_{k=1}^N L(e^{-j\omega_k}, \rho) e^{j\omega_k h} \text{ for } h = 0, \dots, N - 1 \quad (5.24)$$

Then, the impulse response $\ell(h, \rho)$ can be bounded with a decreasing exponential function converging to zero using the following linear constraints:

$$\ell(h, \rho) \leq M\beta^{-h} \quad \text{for } h = 0, \dots, N - 1 \quad (5.25)$$

$$\ell(h, \rho) \geq -M\beta^{-h} \quad \text{for } h = 0, \dots, N - 1 \quad (5.26)$$

If the above mentioned constraints are satisfied, smoothness assumptions can be considered as in Subsection 5.3.1.

Note that the constraints are linear because the controller to be designed is linearly parameterized. Furthermore, it should be noted that the precision of the approximation of (5.22) by (5.23) can be

increased by increasing N_d without increasing the number of constraints in (5.25) and (5.26).

Now, the inter-grid behavior of $L(e^{-j\omega_k}, \rho)$ for $k = 1, \dots, N$ can be defined for all ω using the constant bound given in (5.9). It should be noted that this bound is defined around the following linear interpolation model:

$$L_\lambda(e^{-j\omega}, \rho) = \lambda L(e^{-j\omega_k}, \rho) + (1 - \lambda)L(e^{-j\omega_{k+1}}, \rho) \\ \text{for } \omega_k < \omega < \omega_{k+1} \quad (5.27)$$

For simplicity, an open-loop shaping controller design problem with constraint on one weighted closed-loop sensitivity function is considered. The 2-norm of $L - L_d$ is minimized under the closed-loop sensitivity function condition $\|W_1 \mathcal{S}\|_\infty < 1$ where $\mathcal{S} = (1 + L)^{-1}$.

In Chapter 2 it is shown that the constraint $\|W_1 \mathcal{S}\|_\infty < 1$ can be approximated by the following linear constraint:

$$|W_1(e^{-j\omega})[1 + L_d(e^{-j\omega})] - \\ R_e\{[1 + L_d^*(e^{-j\omega})][1 + L(e^{-j\omega}, \rho)]\}| < 0 \quad \forall \omega \quad (5.28)$$

where $L_d^*(e^{-j\omega})$ is the complex conjugate of $L_d(e^{-j\omega})$.

This constraint assures that the point $L(e^{-j\omega}, \rho)$ is on the side of $d(\omega)$ excluding the critical point for all ω (see Fig.5.1). The line $d(\omega)$ is defined orthogonal to the line connecting the critical point $(-1+0j)$ to $L_d(e^{-j\omega})$ and tangent to the circle centered at the critical point with radius of $W_1(e^{-j\omega})$.

The infinite number of constraints defined in (5.28) can be approximated with a finite number of constraints adding some conservatism. Therefore, based on the equally spaced finite set of frequencies $\omega \in \{\omega_1, \dots, \omega_N\}$, an *uncertainty area* is defined in the Nyquist diagram for each pair of ω_k and ω_{k+1} around the interpolation model (5.27). The *uncertainty area* bounds all possible interpolants between the frequency samples. If the *uncertainty area* described in Figure 5.1 is on the side of the line $d(\omega)$ excluding the critical point, the

frequency-domain condition is also satisfied for all frequencies between ω_k and ω_{k+1} . The infinite number of constraints in (5.28) defined for all $\omega \in [0, \omega_N]$ can be replaced by the following finite number of constraints:

$$\begin{aligned}
& |W_1(e^{-j\omega_k})[1 + L_d(e^{-j\omega_k})]| + |\delta[1 + L_d(e^{-j\omega_k})]| - \\
& \quad R_e\{[1 + L_d^*(e^{-j\omega_k})][1 + L(e^{-j\omega_k}, \rho)]\} < 0 \\
& \quad \text{for } k = 1, \dots, N-1 \\
& |W_1(e^{-j\omega_k})[1 + L_d(e^{-j\omega_k})]| + |\delta[1 + L_d(e^{-j\omega_k})]| - \\
& \quad R_e\{[1 + L_d^*(e^{-j\omega_k})][1 + L(e^{-j\omega_{k+1}}, \rho)]\} < 0 \\
& \quad \text{for } k = 1, \dots, N-1
\end{aligned} \tag{5.29}$$

where $L_d^*(e^{-j\omega_k})$ is the complex conjugate of $L_d(e^{-j\omega_k})$. These constraints assure that the *uncertainty area* is at the side of $d(\omega)$ excluding the critical point.

The new convex optimization approach in which the approximation of the 2-norm of $L - L_d$ is minimized under the linear constraints proposed in (5.26), (5.25) and (5.29) is given below:

$$\min_{\rho} \sum_{k=1}^N |L(e^{-j\omega_k}, \rho) - L_d(e^{-j\omega_k})|^2$$

Subject to:

$$\begin{aligned}
& |W_1(e^{-j\omega_k})[1 + L_d(e^{-j\omega_k})]| + |\delta[1 + L_d(e^{-j\omega_k})]| - \\
& \quad R_e\{[1 + L_d^*(e^{-j\omega_k})][1 + L(e^{-j\omega_k}, \rho)]\} < 0 \\
& \quad \text{for } k = 1, \dots, N-1 \\
& |W_1(e^{-j\omega_k})[1 + L_d(e^{-j\omega_k})]| + |\delta[1 + L_d(e^{-j\omega_k})]| - \\
& \quad R_e\{[1 + L_d^*(e^{-j\omega_k})][1 + L(e^{-j\omega_{k+1}}, \rho)]\} < 0 \\
& \quad \text{for } k = 1, \dots, N-1
\end{aligned} \tag{5.30}$$

$$\begin{aligned}
\ell(h, \rho) &\leq M\beta^{-h} & \text{for } h = 0, \dots, N-1 \\
\ell(h, \rho) &\geq -M\beta^{-h} & \text{for } h = 0, \dots, N-1
\end{aligned}$$

where $\ell(h, \rho)$ is defined in (5.24).

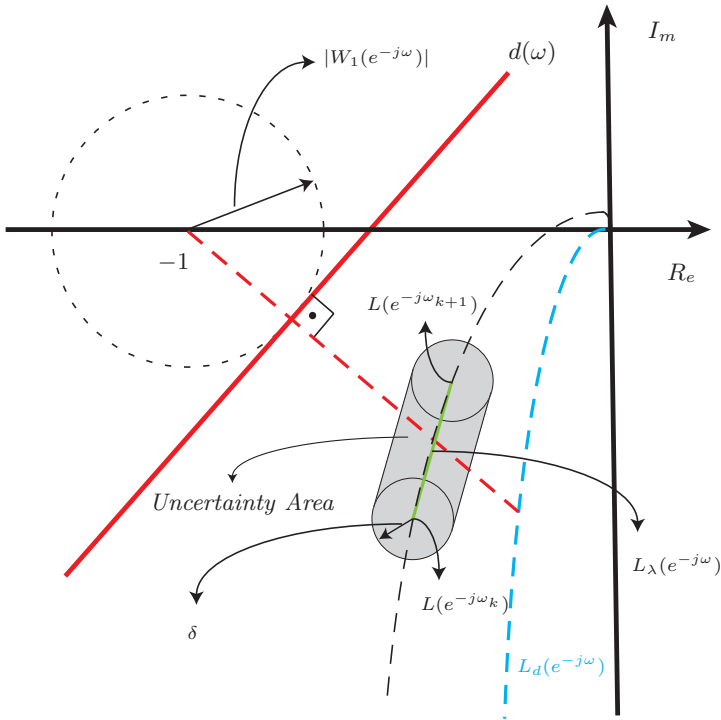


Fig. 5.1. Convex constraints guaranteeing inter-frequency behavior in Nyquist diagram

Controller design (with integrator)

For control problems where the open-loop system contains an integrator, $\phi(e^{-j\omega})$ defined in (5.21) can contain transfer functions with poles at 1. The open-loop frequency response of the system is approximated by:

$$\tilde{L}(e^{-j\omega}, \rho) = \rho^T \phi(e^{-j\omega}) G(e^{-j\omega}) = \frac{L(e^{-j\omega}, \rho)}{1 - e^{-j\omega}} \approx \frac{L(e^{-j\omega}, \rho)}{j\omega} \quad (5.31)$$

Note that, $L(e^{-j\omega}, \rho)$ is the open-loop frequency response of the system without the integral part.

The bound $\delta_{int}(\omega)$ given in (5.18) depends on the controller parameters ρ and it is defined around the following linear interpolation model:

$$\tilde{L}_\lambda(e^{-j\omega}, \rho) = \lambda \frac{L(e^{-j\omega_k}, \rho)}{j\omega_k} + (1 - \lambda) \frac{L(e^{-j\omega_{k+1}}, \rho)}{j\omega_{k+1}} \quad \text{for } \omega_k < \omega < \omega_{k+1} \quad (5.32)$$

In this case, figure 5.1 also describes graphically the constraints for controller design if $L(e^{-j\omega_k})$ and $L(e^{-j\omega_{k+1}})$ are replaced by $\tilde{L}(e^{-j\omega_k})$ and $\tilde{L}(e^{-j\omega_{k+1}})$ respectively, $L_\lambda(e^{-j\omega})$ is replaced by $\tilde{L}_\lambda(e^{-j\omega})$ and δ is replaced by $\delta_{int}(\omega, \rho)$. Note that, in this case, the *uncertainty area* depends on the controller parameter ρ . This means that the linear constraints in (5.29) are now replaced by the following convex constraints:

$$\begin{aligned} & |W_1(e^{-j\omega_k})[1 + L_d(e^{-j\omega_k})]| + |\delta_{int}(\omega_k, \rho)[1 + L_d(e^{-j\omega_k})]| - \\ & \quad R_e\{[1 + L_d^*(e^{-j\omega_k})][1 + \tilde{L}(e^{-j\omega_k}, \rho)]\} < 0 \\ & \quad \text{for } k = 1, \dots, N - 1 \end{aligned} \quad (5.33)$$

$$\begin{aligned} & |W_1(e^{-j\omega_k})[1 + L_d(e^{-j\omega_k})]| + |\delta_{int}(\omega_k, \rho)[1 + L_d(e^{-j\omega_k})]| - \\ & \quad R_e\{[1 + L_d^*(e^{-j\omega_k})][1 + \tilde{L}(e^{-j\omega_{k+1}}, \rho)]\} < 0 \\ & \quad \text{for } k = 1, \dots, N - 1 \end{aligned}$$

The optimization problem proposed in (5.30) is slightly modified giving the following convex optimization problem:

$$\min_{\rho} \sum_{k=1}^N |\tilde{L}(e^{-j\omega_k}, \rho) - L_d(e^{-j\omega_k})|^2$$

Subject to:

$$\begin{aligned} |W_1(e^{-j\omega_k})[1 + L_d(e^{-j\omega_k})]| + |\delta_{int}(\omega_k, \rho)[1 + L_d(e^{-j\omega_k})]| - \\ R_e\{[1 + L_d^*(e^{-j\omega_k})][1 + \tilde{L}(e^{-j\omega_k}, \rho)]\} < 0 \\ \text{for } k = 1, \dots, N - 1 \end{aligned} \quad (5.34)$$

$$\begin{aligned} |W_1(e^{-j\omega_k})[1 + L_d(e^{-j\omega_k})]| + |\delta_{int}(\omega_k, \rho)[1 + L_d(e^{-j\omega_k})]| - \\ R_e\{[1 + L_d^*(e^{-j\omega_k})][1 + \tilde{L}(e^{-j\omega_{k+1}}, \rho)]\} < 0 \\ \text{for } k = 1, \dots, N - 1 \end{aligned}$$

$$\begin{aligned} \ell(h, \rho) &\leq M\beta^{-h} & \text{for } h = 0, \dots, N - 1 \\ \ell(h, \rho) &\geq -M\beta^{-h} & \text{for } h = 0, \dots, N - 1 \end{aligned}$$

where

$$\delta_{int}(\omega_k, \rho) = \frac{\frac{\omega N}{N-1}}{(\sqrt{\omega_k} + \sqrt{\omega_{k+1}})^2} \left| \frac{L(e^{-j\omega_k}, \rho)}{\omega_k} - \frac{L(e^{-j\omega_{k+1}}, \rho)}{\omega_{k+1}} \right| + \left| \frac{1}{j\omega_k} \right| \delta \quad (5.35)$$

and $\ell(h, \rho)$ is computed based on N samples of the open-loop frequency response $L(e^{-j\omega_k}, \rho)$ (which does not contain the integrator).

It should be noted that the optimization problem proposed in (5.30) contains only linear constraints while that proposed in (5.34) contains linear and convex constraints (because δ_{int} is a function of ρ but δ is not). The optimization problem in (5.30) can be solved very efficiently even with thousands of constraints by standard quadratic programming. On the other hand, an SDP solver is needed to solve the optimization problem in (5.34) (e.g. SeDuMi [54]).

5.4 Simulation Results

A simulation example is presented in this section where a discrete-time PD controller is designed. The idea is to show the conservatism of the *Exact approach* in comparison with the *Approximate approach*

in a controller design problem. At the same time, it is shown how this conservatism is reduced when the number of frequency samples used in the *Exact approach* is increased.

The following continuous-time transfer function system is considered:

$$G(s) = \frac{1}{(s+1)(s+2)} \quad (5.36)$$

which is discretized using Tustin approximation with $T_s = 0.1$ s as sampling period. The following PD controller should be tuned for this system:

$$K(z) = \frac{\rho_1 z + \rho_0}{z} \quad (5.37)$$

The goal is to design a controller minimizing the 2-norm of $L - L_d$ with a modulus margin of at least 0.5 ($W_1(z) = 0.5$) where $L_d(s) = \frac{1}{s+1}$ is chosen (which is also discretized using Tustin approximation). The impulse response of $L_d(s)$ is e^{-t} which let us define $\beta = 1$ and $M = 1$. However, β and M are chosen 10% higher than these values, giving $\beta = 1.1$ and $M = 1.1$. The Nyquist frequency ω_N is $\frac{\pi}{T_s}$ rad/s.

Based on the *Exact approach*, the optimization problem presented in (5.30) is solved with N equally spaced frequency samples between 0 and ω_N rad/s for different values of N . The results are shown in Table 5.1 for N equal to 50, 100, 1000, 10000 and 100000. It should be noted that the computation of the impulse response of the open-loop system is not accurate for high values of h for some chosen values of N . Therefore, only the constraints bounding the impulse response for which the bound $M\beta^{-h}$ is higher than 10^{-4} are considered. Looking at the Table 5.1, it can be seen that the 2-norm of $L - L_d$ is reduced when N is increased. This result is expected because the inter-grid uncertainty δ is decreasing when N is increased which reduces the conservatism of the approach. However, the computational cost (TC) is also increased.

As expected, if the same control problem is solved using the *Approximate approach*, better performances can be obtained for the same number of data N . The results are shown in Table 5.2. Note that using the *Exact approach*, if N is large enough, the results are

Table 5.1. *Exact approach*

N	$\ L - L_d\ _2$	ρ_1	ρ_0	TC [s]
50	Not feasible			
100	Not feasible			
1000	0.1769	11.0329	-10.997	2.5
10000	0.1445	11.3952	-10.9894	12.49
100000	0.0440	12.0155	-10.0977	730

the same as those obtained with the *Approximate approach* with a different computational cost.

Table 5.2. *Approximate approach*

N	$\ L - L_d\ _2$	ρ_1	ρ_0	TC [s]
50	0.0441	12.0260	-10.0888	0.81
100	0.0440	12.0213	-10.0926	0.82
1000	0.0440	12.0162	-10.0971	0.83
10000	0.0440	12.0156	-10.0976	2.5
100000	0.0440	12.0155	-10.0977	148.04

5.5 Conclusions

In this chapter, three different approaches to solve the SIP optimization problems in the context of controller design are proposed. The proposed approaches transform the original SIP optimization problem with an infinite number of convex constraints to an SDP optimization problem with a chosen finite number of convex constraints. The *Approximate approach* and *Probabilistic approach* assure that the constraints are only satisfied for the chosen constraint. However, the *Probabilistic approach* gives a probability level for which the solution will satisfy all the convex constraints of the original problem

with a given violation level. On the other hand, the *Exact approach* using only a finite number of constraints assures that all the constraints are satisfied. This is made possible by defining a frequency uncertainty in the Nyquist diagram which considers the inter-grid behavior of the open-loop transfer function. This approach is applicable to the controller design methods proposed in this thesis. In this approach, the inter-grid behavior is used to satisfy desired stability and performance constraints between the samples. Convex constraints are defined to bound the impulse response of the open-loop system. This allows one to include smoothness assumptions which are used to bound the difference between the linear interpolation model and all possible interpolants between the frequency samples of the open-loop system. Additionally, it is shown how this bound is reduced when the number of frequency samples is increased. These results are integrated in an H_∞ controller design method proposed in Chapter 2 where a linearly parameterized controller is designed by convex optimization.

The simulation results show that based on the *Exact approach*, using a finite number of frequency samples, the stability and performance conditions can be satisfied even for frequencies between the samples. The conservatism of the approach decreases if the number of frequency samples increases. Consequently, the complexity of the optimization problem increases. The same results can be obtained with much less computational complexity by only verifying the constraints at the available frequency samples based on the *Approximate approach*. It should be noted that in this case, there is no guarantee that the conditions are verified between the frequency samples.

Conclusions

6.1 Summary

In this thesis, a new method for the design of fixed-order linearly parameterized controllers is proposed. The method consists of shaping the open-loop transfer function in the Nyquist diagram by convex optimization with infinity norm constraints on the weighted closed-loop sensitivity functions. This new controller design method designs controllers for systems using either parametric models or frequency-domain data. Moreover, it can also directly treat multi-model systems and systems with frequency-domain uncertainties.

In Chapter 2, a method to design fixed-order linearly parameterized controllers for SISO systems is proposed. The open-loop transfer function is shaped by minimizing its difference with a desired open-loop transfer function subject to constraints on the weighted closed-loop sensitivity functions. The nonconvex constraints on the closed-loop sensitivity functions are approximated by convex constraints on the controller parameters using the desired open-loop transfer function. Hence, the robust control problem is presented as a convex optimization problem.

In Chapter 3, an extension of the method to design 2DOF controllers with an RST structure for SISO systems is presented. The

shaping of the open-loop transfer function with H_∞ constraints on the weighted closed-loop sensitivity functions is proposed as a convex optimization problem. The T and S polynomials of the RST controller with a fixed R polynomial are tuned by a single convex optimization.

In Chapter 4, the method is extended to design decoupling fixed-order MIMO linearly parameterized controllers for MIMO systems. The shaping of the open-loop matrix transfer function is proposed with constraints in order to satisfy the Generalized Nyquist Stability criterion. The nonconvex stability constraints are approximated by convex constraints using the Gershgorin bands.

In Chapter 2, 3 and 4, the different control problems are presented as SIP optimization problems where a finite number of decision variables (the parameters of the controller) should be optimized subject to an infinite number of constraints. In Chapter 5, three different approaches are proposed to solve this type of optimization problems by relaxing the original infinite number of constraints to a finite number of constraints. The *Approximate approach* and *Probabilistic approach* assure only that the chosen constraints are satisfied. The solution using the *Probabilistic approach* satisfies the unseen constraints with a certain probability which depends on N . However, the *Exact approach* assures that the solution satisfies all the constraints even if only a finite number of constraints are considered. This is possible by defining a frequency uncertainty area in the Nyquist diagram which envelops the inter-grid behavior of the open-loop transfer function.

This methodology is tested on numerous simulations examples. The method is applied to an international benchmark problem for robust controller design for which the proposed controller meets all the specifications with the lowest complexity of all the controllers proposed for the system in the literature. Additionally, the method is used to design a 2DOF controller with an RST structure for an industrial double-axis LPMSM high-precision positioning system. The simulations and the experimental results illustrate the effectiveness of the method.

6.2 Perspectives

There are a number of interesting extensions that arise from this work. These are briefly presented below:

- The methods proposed in this thesis design linearly parameterized controllers or RST controllers with a fixed R polynomial. This means that the denominators of the controllers are chosen a priori. Thus, it would be potentially useful to extend the method to have also the denominators of the controllers as decision variables on the convex optimization problems.
- The proposed MIMO controller design method considers stability conditions of the interconnected loops with H_∞ constraints on the decoupled diagonal SISO loops. The original MIMO H_∞ controller design problem has not been considered because it has not been possible to approximate MIMO H_∞ constraints to convex constraints. Basically, these constraints are a function of the singular value of the weighted closed-loop transfer function matrix, for which was not possible to find a convex approximation. An extension of the method to consider MIMO H_∞ constraints would be interesting.
- The proposed methods are formulated as optimization problems with an infinite number of constraints. An approach has been proposed to assure that the solution satisfies all the constraints even using a finite number of constraints. This is possible if the impulse response of the discrete-time open-loop system is bounded with a decreasing exponential function that converges to zero. This can be guaranteed with a finite number of linear constraints added on the optimization problem. This is possible if discrete-time control problems are considered since its impulse response is a discrete-time signal. For continuous-time systems, the impulse response is also continuous-time signal for which infinity number of constraints are needed to bound it. It would be interesting to find another approach to consider control problems for continuous-time systems.

Additionally, the proposed approach for discrete-time systems adds some conservatism. This conservatism decreases if the chosen number of finite constraints is increased. However, even for a very large number of constraints the added conservatism is high. A new approach adding less conservatism and guaranteeing that the solution satisfies all the constraints would be useful.

A

Exact Approach with Integrators

A.1 Inter-grid behavior

Assume that we have N samples $\bar{X}(e^{-j\omega_k})$ for $k = 1, \dots, N$ of the original frequency response of the discrete-time system $\bar{X}(e^{-j\omega})$ between 0 and the Nyquist frequency ω_N spaced by $\frac{\omega_N}{N-1}$. The frequency response $\bar{X}(e^{-j\omega})$ is given by:

$$\bar{X}(e^{-j\omega}) = \frac{X(e^{-j\omega})}{1 - e^{-j\omega}} \quad (\text{A.1})$$

where $X(e^{-j\omega})$ is the frequency response of the discrete-time system without the integral part.

As in Subsection 5.3.1, it is assumed that impulse response $x(h)$ of the discrete-time system without the integral part $X(e^{-j\omega})$ is bounded $|x(h)| \leq M\beta^{-h}$. This bounds $|X_\lambda(e^{-j\omega}) - X(e^{-j\omega})|$ as in (5.9). However, now the goal is to find a bound δ_{int} for $|\bar{X}_\lambda(e^{-j\omega}) - \bar{X}(e^{-j\omega})|$ based on the bound on $|X_\lambda(e^{-j\omega}) - X(e^{-j\omega})|$. Note that the linear interpolation model $\bar{X}_\lambda(e^{-j\omega})$ between the frequency samples $\bar{X}(e^{-j\omega_k})$ is defined as:

$$\bar{X}_\lambda(e^{-j\omega}) = \lambda \frac{X(e^{-j\omega_k})}{1 - e^{-j\omega_k}} + (1 - \lambda) \frac{X(e^{-j\omega_{k+1}})}{1 - e^{-j\omega_{k+1}}} \quad \text{for } \omega_k < \omega < \omega_{k+1} \quad (\text{A.2})$$

The bound is obtained with the help of an intermediate frequency function $\tilde{X}(e^{-j\omega})$, which approximates the discrete integrator $\frac{1}{1 - e^{-j\omega}}$ by $\frac{1}{j\omega}$. $\tilde{X}(e^{-j\omega})$ is defined as follows:

$$\tilde{X}(e^{-j\omega}) = \frac{X(e^{-j\omega})}{j\omega} \quad (\text{A.3})$$

An intermediate linear interpolation model is defined between the approximated frequency response samples $\tilde{X}(e^{-j\omega_k})$ as follows:

$$\tilde{X}_\lambda(e^{-j\omega}) = \lambda \frac{X(e^{-j\omega_k})}{j\omega_k} + (1 - \lambda) \frac{X(e^{-j\omega_{k+1}})}{j\omega_{k+1}} \quad \text{for } \omega_k < \omega < \omega_{k+1} \quad (\text{A.4})$$

Using the intermediate frequency responses $\tilde{X}(e^{-j\omega})$ and $\tilde{X}_\lambda(e^{-j\omega})$, the bound is divided in four different terms as follows:

$$\begin{aligned} |\bar{X}_\lambda(e^{-j\omega}) - \tilde{X}(e^{-j\omega})| &\leq \left| \bar{X}_\lambda(e^{-j\omega}) - \tilde{X}_\lambda(e^{-j\omega}) \right| \\ &\quad + \left| \tilde{X}_\lambda(e^{-j\omega}) - \frac{X_\lambda(e^{-j\omega})}{j\omega} \right| \\ &\quad + \left| \frac{X_\lambda(e^{-j\omega})}{j\omega} - \frac{X_\lambda(e^{-j\omega})}{1 - e^{-j\omega}} \right| \\ &\quad + \left| \frac{X_\lambda(e^{-j\omega})}{1 - e^{-j\omega}} - \bar{X}(e^{-j\omega}) \right| \quad \text{for } \omega_k < \omega < \omega_{k+1} \end{aligned} \quad (\text{A.5})$$

Now, each of these terms are bounded independently:

- The error between the linear interpolation model and the approximated interpolation model is always maximum when ω is ω_k or ω_{k+1} . Hence, this error is bounded by:

$$\left| \bar{X}_\lambda(e^{-j\omega}) - \tilde{X}_\lambda(e^{-j\omega}) \right| \leq \left| \frac{1}{1 - e^{-j\omega_k}} - \frac{1}{j\omega_k} \right| |X(e^{-j\omega_k})| \quad (\text{A.6})$$

for $\omega_k < \omega < \omega_{k+1}$

or by:

$$\left| \bar{X}_\lambda(e^{-j\omega}) - \tilde{X}_\lambda(e^{-j\omega}) \right| \leq \left| \frac{1}{1-e^{-j\omega_{k+1}}} - \frac{1}{j\omega_{k+1}} \right| |X(e^{-j\omega_{k+1}})|$$

for $\omega_k < \omega < \omega_{k+1}$

(A.7)

- The bound for the second term $\left| \tilde{X}_\lambda(e^{-j\omega}) - \frac{X_\lambda(e^{-j\omega})}{j\omega} \right|$ has already been defined in (5.16).
- The bound for the third term $\left| \frac{X_\lambda(e^{-j\omega})}{j\omega} - \frac{X_\lambda(e^{-j\omega})}{1-e^{-j\omega}} \right|$ is transformed to:

$$\begin{aligned} \left| \frac{X_\lambda(e^{-j\omega})}{j\omega} - \frac{X_\lambda(e^{-j\omega})}{1-e^{-j\omega}} \right| &= \left| \left(\frac{1}{j\omega} - \frac{1}{1-e^{-j\omega}} \right) X_\lambda(e^{-j\omega}) \right| \\ &= \left| \frac{1}{j\omega} - \frac{1}{1-e^{-j\omega}} \right| |X_\lambda(e^{-j\omega})| \end{aligned}$$
(A.8)

for $\omega_k < \omega < \omega_{k+1}$

where $\left| \frac{1}{j\omega} - \frac{1}{1-e^{-j\omega}} \right|$ is the approximation error of the integral part which has its maximum for $\omega = \omega_{k+1}$. Since $|X_\lambda(e^{-j\omega})|$ is the linear interpolation model, its maximum value is given when ω is ω_k or ω_{k+1} . Hence, (A.8) is bounded by:

$$\left| \frac{X_\lambda(e^{-j\omega})}{j\omega} - \frac{X_\lambda(e^{-j\omega})}{1-e^{-j\omega}} \right| \leq \left| \frac{1}{j\omega_{k+1}} - \frac{1}{1-e^{-j\omega_{k+1}}} \right| |X(e^{-j\omega_k})|$$
(A.9)

for $\omega_k < \omega < \omega_{k+1}$

or by:

$$\left| \frac{X_\lambda(e^{-j\omega})}{j\omega} - \frac{X_\lambda(e^{-j\omega})}{1-e^{-j\omega}} \right| \leq \left| \frac{1}{j\omega_{k+1}} - \frac{1}{1-e^{-j\omega_{k+1}}} \right| |X(e^{-j\omega_{k+1}})|$$

for $\omega_k < \omega < \omega_{k+1}$

(A.10)

- Finally, the bound of the fourth term is a direct result from Sub-section 5.3.1:

$$\begin{aligned} \left| \frac{X_\lambda(e^{-j\omega})}{1-e^{-j\omega}} - \bar{X}(e^{-j\omega}) \right| &= \left| \frac{1}{1-e^{-j\omega}} (X_\lambda(e^{-j\omega}) - X(e^{-j\omega})) \right| \\ &\leq \left| \frac{1}{1-e^{-j\omega_k}} \right| \delta \quad \text{for } \omega_k < \omega < \omega_{k+1} \end{aligned} \quad (\text{A.11})$$

Therefore, combining the different bounds for each term, three bounds δ_{int} are defined which bounds the difference between the linear interpolation model $\bar{X}_\lambda(e^{-j\omega})$ and all possible interpolants between the frequency samples when the frequency response contains an integrator :

$$\begin{aligned} \delta_{int_1}(\omega) &= \frac{1}{N-1} \frac{\omega_N}{(\sqrt{\omega_k} + \sqrt{\omega_{k+1}})^2} \left| \frac{X(e^{-j\omega_k})}{\omega_k} - \frac{X(e^{-j\omega_{k+1}})}{\omega_{k+1}} \right| \\ &\quad + 2 \left| \frac{1}{1-e^{-j\omega_k}} - \frac{1}{j\omega_k} \right| |X(e^{-j\omega_k})| + \left| \frac{1}{1-e^{-j\omega_k}} \right| \delta \end{aligned} \quad (\text{A.12})$$

for $\omega_k < \omega < \omega_{k+1}$

$$\begin{aligned} \delta_{int_2}(\omega) &= \frac{1}{N-1} \frac{\omega_N}{(\sqrt{\omega_k} + \sqrt{\omega_{k+1}})^2} \left| \frac{X(e^{-j\omega_k})}{\omega_k} - \frac{X(e^{-j\omega_{k+1}})}{\omega_{k+1}} \right| \\ &\quad + 2 \left| \frac{1}{1-e^{-j\omega_{k+1}}} - \frac{1}{j\omega_{k+1}} \right| |X(e^{-j\omega_{k+1}})| + \left| \frac{1}{1-e^{-j\omega_k}} \right| \delta \end{aligned} \quad (\text{A.13})$$

for $\omega_k < \omega < \omega_{k+1}$

$$\begin{aligned} \delta_{int_3}(\omega) &= \frac{1}{N-1} \frac{\omega_N}{(\sqrt{\omega_k} + \sqrt{\omega_{k+1}})^2} \left| \frac{X(e^{-j\omega_k})}{\omega_k} - \frac{X(e^{-j\omega_{k+1}})}{\omega_{k+1}} \right| \\ &\quad + \left| \frac{1}{1-e^{-j\omega_{k+1}}} - \frac{1}{j\omega_{k+1}} \right| |X(e^{-j\omega_{k+1}})| \end{aligned} \quad (\text{A.14})$$

$$+ \left| \frac{1}{1-e^{-j\omega_k}} - \frac{1}{j\omega_k} \right| |X(e^{-j\omega_k})| + \left| \frac{1}{1-e^{-j\omega_k}} \right| \delta$$

for $\omega_k < \omega < \omega_{k+1}$

A.2 Controller design method with integrator

The idea is the same as in Subsection 5.3.2. Linear constraints are used to bound the impulse response. Then, this allows to use the bounds presented in (A.12), (A.13) and (A.14). These bounds define a frequency-domain uncertainty which is integrated in the convex constraints of the controller design method.

To integrate the bounds (A.12), (A.13) and (A.14) in the open-loop shaping controller design method, $X(e^{-j\omega})$ or $\bar{X}(e^{-j\omega})$ should be replaced by the open-loop frequency response with an integrator $\bar{L}(e^{-j\omega}, \rho)$ and without an integrator $L(e^{-j\omega}, \rho)$ respectively. $\bar{L}(e^{-j\omega}, \rho)$ and $L(e^{-j\omega}, \rho)$ are defined as follows:

$$\bar{L}(e^{-j\omega}, \rho) = \rho^T \phi(e^{-j\omega}) G(e^{-j\omega}) = \frac{L(e^{-j\omega}, \rho)}{1 - e^{-j\omega}} \quad (\text{A.15})$$

The new bounds are introduced into the optimization problem proposed in (5.34). The constraints are defined using the three different bounds to assure that the constraints are verified between the frequency samples for the worst case. The following convex optimization problem is considered:

$$\min_{\rho} \sum_{k=1}^N |\bar{L}(e^{-j\omega_k}, \rho) - L_d(e^{-j\omega_k})|^2$$

Subject to:

$$|W_1(e^{-j\omega_k})[1 + L_d(e^{-j\omega_k})]| + |\delta_{int_p}(\omega_k, \rho)[1 + L_d(e^{-j\omega_k})]| -$$

$$R_e\{[1 + L_d^*(e^{-j\omega_k})][1 + \bar{L}(e^{-j\omega_k}, \rho)]\} < 0$$

for $k = 1, \dots, N - 1$ and for $p = 1, 2, 3$

$$|W_1(e^{-j\omega_k})[1 + L_d(e^{-j\omega_k})]| + |\delta_{int_p}(\omega_k, \rho)[1 + L_d(e^{-j\omega_k})]| -$$

$$R_e\{[1 + L_d^*(e^{-j\omega_k})][1 + \bar{L}(e^{-j\omega_{k+1}}, \rho)]\} < 0$$

for $k = 1, \dots, N - 1$ and for $p = 1, 2, 3$

$$\ell(h, \rho) \leq M\beta^{-h} \quad \text{for } h = 0, \dots, N - 1$$

$$\ell(h, \rho) \geq -M\beta^{-h} \quad \text{for } h = 0, \dots, N - 1 \quad (\text{A.16})$$

where

$$\begin{aligned} \delta_{int_1}(\omega) &= \frac{1}{N-1} \frac{\omega_N}{(\sqrt{\omega_k} + \sqrt{\omega_{k+1}})^2} \left| \frac{L(e^{-j\omega_k})}{\omega_k} - \frac{L(e^{-j\omega_{k+1}})}{\omega_{k+1}} \right| \\ &+ 2 \left| \frac{1}{1-e^{-j\omega_k}} - \frac{1}{j\omega_k} \right| |L(e^{-j\omega_k})| + \left| \frac{1}{1-e^{-j\omega_k}} \right| \delta \end{aligned} \quad (\text{A.17})$$

for $\omega_k < \omega < \omega_{k+1}$

$$\begin{aligned} \delta_{int_2}(\omega) &= \frac{1}{N-1} \frac{\omega_N}{(\sqrt{\omega_k} + \sqrt{\omega_{k+1}})^2} \left| \frac{L(e^{-j\omega_k})}{\omega_k} - \frac{L(e^{-j\omega_{k+1}})}{\omega_{k+1}} \right| \\ &+ 2 \left| \frac{1}{1-e^{-j\omega_{k+1}}} - \frac{1}{j\omega_{k+1}} \right| |L(e^{-j\omega_{k+1}})| + \left| \frac{1}{1-e^{-j\omega_k}} \right| \delta \end{aligned} \quad (\text{A.18})$$

for $\omega_k < \omega < \omega_{k+1}$

$$\begin{aligned}
\delta_{int_3}(\omega) &= \frac{1}{N-1} \frac{\omega_N}{(\sqrt{\omega_k} + \sqrt{\omega_{k+1}})^2} \left| \frac{L(e^{-j\omega_k})}{\omega_k} - \frac{L(e^{-j\omega_{k+1}})}{\omega_{k+1}} \right| \\
&+ \left| \frac{1}{1-e^{-j\omega_{k+1}}} - \frac{1}{j\omega_{k+1}} \right| |L(e^{-j\omega_{k+1}})| \\
&+ \left| \frac{1}{1-e^{-j\omega_k}} - \frac{1}{j\omega_k} \right| |L(e^{-j\omega_k})| + \left| \frac{1}{1-e^{-j\omega_k}} \right| \delta
\end{aligned} \tag{A.19}$$

for $\omega_k < \omega < \omega_{k+1}$

and $\ell(h, \rho)$ is computed based on the open-loop transfer function $L(e^{-j\omega_k}, \rho)$ (which does not contain the integrator) and $L_d^*(e^{-j\omega_k})$ is the complex conjugate of $L_d(e^{-j\omega_k})$.

References

- [1] H. Akcay and B. Ninness. Orthonormal basis functions for modeling continuous-time systems. *Signal Processing*, 77:261–274, 1999.
- [2] T. Alamo, R. Tempo, and A. Luque. *Perspectives in Mathematical System Theory, Control, and Signal Processing*. Springer-Verlag, London, 2010.
- [3] B. D. O. Anderson. Windsurfing approach to iterative control design. In P. Albertos and A. Sala, editors, *Iterative Identification and Control: Advances in Theory and Applications*,. Springer-Verlag, Berlin, 2002.
- [4] K. J. Åström and B. Wittenmark. *Adaptive Control*. Addison-Wesley, 1989.
- [5] K.J. Aström and B. Wittenmark. *Computer Controlled Systems: Theory and Design*. Prentice Hall, Englewood Cliffs NJ, 1984.
- [6] G. F. Bryant and G. D. Halikias. Optimal loop shaping for systems with large parameter uncertainty via linear programming. *International Journal of Control*, 62:557–568, 1995.
- [7] G. Calafiore and M. C. Campi. Uncertain convex programs: randomized solutions and confidence levels. *Mathematical Programming Ser. B*, 102(1):25–46, 2005.

- [8] G. Calafiore and M. C. Campi. The scenario approach to robust control design. *IEEE Transactions on Automatic Control*, 51(5):742–753, May 2006.
- [9] Y. Chait, Q. Chen, and C. V. Hollot. Automatic loop-shaping of QFT controllers via linear programming. *Journal of Dynamic Systems, Measurement and Control*, 121(3):351–357, September 1999.
- [10] D. Chen and D. E. Seborg. Multiloop PI/PID controller design based on Gershgorin bands. *IEE Proceedings on Control Theory and Applications*, 149(1), January 2002.
- [11] J. Crowe and M.A. Johnson. Automated PI control tuning to meet classical performance specifications using a phase locked loop identifier. In *IEEE American Control Conference*, pages 2186–2191, Arlington, USA, 2001.
- [12] D. de Vries. *Identification of Model Uncertainty for Control Design*. PhD thesis, Delft University of Technology, Delft, The Netherlands, 1994.
- [13] C. Decker, A. Ehrlinger, P. Boucher, and D. Dumur. Application of constrained receding horizon predictive control to a benchmark problem. *European Journal of Control*, 1(2):157–165, 1995.
- [14] A.J. den Hamer, S. Weiland, and M. Steinbuch. Worst-case inter frequency grid behavior of transfer functions identified via finite frequency response data. In *European Control Conference*, pages 466–471, Budapest, Hungary, 2010.
- [15] A.J. den Hamer, S. Weiland, M. Steinbuch, and G.Z. Angelis. Stability and causality constraints on frequency response coefficients applied for non-parametric h_2 and h_∞ control synthesis. In *Conference on Decision and Control*, pages 3670–3675, Cancun, Mexico, 2008.
- [16] T. E. Djaferis. *Robust Control Design: A Polynomial Approach*. Kluwer Academic Publishers, Massachusetts, USA, 1995.
- [17] C. J. Doyle, B. A. Francis, and A. R. Tannenbaum. *Feedback Control Theory*. Mc Millan, New York, 1992.

- [18] G. Ferreres and V. Fromion. H_∞ control for a flexible transmission system. *European Journal of Control*, 5:185–192, 1999.
- [19] D. Garcia, A. Karimi, and R. Longchamp. PID controller design for multivariable systems using Gershgorin bands. In *IFAC World Congress*, Prague, July 2005.
- [20] D. Garcia, A. Karimi, and R. Longchamp. Robust PID controller tuning with specifications on the infinity-norm of sensitivity functions. *IET Control Theory Applications*, 1(1), 2006.
- [21] A. F. Gilbert, A. Yousef, K. Natarajan, and S. Deighton. Tuning of PI controllers with one-way decoupling in 2x2 MIMO systems based on finite frequency response data. *Journal of Process Control*, 13:553–567, 2003.
- [22] M. A. Goberna and M. A. Lopez. Linear semi-infinite programming theory: An updated survey. *European Journal of Operational Research*, 143(2):390–405, December 2002.
- [23] E. Grassi and K. Tsakalis. PID controller tuning by frequency loop shaping. In *35th IEEE Conference on Decision and Control*, pages 4776–4781, Kobe, Japan, 1996.
- [24] G. D. Halikias, A. C. Zolotas, and R. Nandakumar. Design of optimal robust fixed-structure controllers using the quantitative feedback theory approach. *Proceedings of the Institution of Mechanical Engineers, Part I: Journal of Systems and Control Engineering*, 221(4):697–716, 2007.
- [25] P. S. C. Heuberger, P. M. J. Van Den Hof, and B. Wahlberg. *Modelling and Identification with Rational Orthogonal Basis Functions*. Springer, 2004.
- [26] H. Hjalmarsson. Efficient tuning of linear multivariable controllers using iterative feedback tuning. *International Journal of Adaptive Control and Signal Processing*, 13(8):553–572, 1999.
- [27] H. Hjalmarsson, S. Gunnarsson, and M. Gevers. Model free tuning of a robust regulator for a flexible transmission system. *European Journal of Control*, 1(2):134–140, 1995.
- [28] W. K. Ho and Wen Xu. Multivariable PID controller design based on the direct nyquist array method. In *IEEE American Control Conference*, Philadelphia, Pennsylvania, 1998.

- [29] I. M. Horowitz. *Synthesis of Feedback Systems*. Academic Press, 1963.
- [30] I. M. Horowitz. *Quantitative Feedback Theory (QFT)*. QFT Publications Boulder, Colorado, 1993.
- [31] Y. S. Hung and A. G. J. MacFarlane. *Multivariable feedback: A quasiclassical approach*. Springer Verlag, N. Y., 1982.
- [32] N. W. Jones and D. J. N. Limebeer. A digital H_∞ controller for a flexible transmission system. *European Journal of Control*, 1(2):134–140, 1995.
- [33] L. C. Kammer, R. R. Bitmead, and P. L. Bartlett. Direct iterative tuning via spectral analysis. *Automatica*, 36(9):1301–1307, 2000.
- [34] A. Karimi, D. Garcia, and R. Longchamp. PID controller tuning using Bode’s integrals. *IEEE Transactions on Control Systems Technology*, 11(6):812–821, 2003.
- [35] A. Karimi, M. Kunze, and R. Longchamp. Robust controller design by linear programming with application to a double-axis positioning system. *Control Engineering Practice*, 15(2):197–208, February 2007.
- [36] L. H. Keel and S. P. Bhattacharyya. Controller synthesis free of analytical models: Three term controllers. *IEEE Transactions on Automatic Control*, 53(6):1353–1369, July 2008.
- [37] O. Kidron and O. Yaniv. Robust control of uncertain resonant systems. *European Journal of Control*, 1(2):104–112, 1995.
- [38] H. Kwakernaak. Symmetries in control system design. In A. Isidori, editor, *Trends in Control*. Springer Verlag, London, 1995.
- [39] I. D. Landau and A. Karimi. Robust digital control using pole placement with sensitivity function shaping method. *International Journal of Robust and Nonlinear Control*, 8(2):191–210, 1998.
- [40] I. D. Landau, A. Karimi, A. Voda, and D. Rey. Robust digital control of flexible transmission using the combined pole placement/sensitivity function shaping method. *European Journal of Control*, 1(2):122–133, 1995.

- [41] I. D. Landau, D. Rey, A. Karimi, A. Voda, and A. Franco. A flexible transmission system as a benchmark for robust digital control. *European Journal of Control*, 1(2):77–96, 1995.
- [42] J. Langer and A. Constantinescu. Pole placement design using convex optimisation criteria for the flexible transmission benchmark. *European Journal of Control*, 5:193–207, 1999.
- [43] L. Ljung. *System Identification - Theory for the User*. Prentice Hall, NJ, USA, second edition, 1999.
- [44] W. L. Luyben. Simple method for tuning SISO controllers in multivariable systems. *Ind. Eng. Chem. Des. Dev.*, 25:654–660, 1986.
- [45] A. G. J. MacFarlane. Commutative controller: a new technique for the design of multivariable control systems. *Electronic Letters*, 6:121–123, 1970.
- [46] P. Mäkilä. Approximation of stable systems by laguerre filters. *Automatica*, 26:333–345, 1990.
- [47] L. Mišković, A. Karimi, D. Bonvin, and M. Gevers. Correlation-based tuning of decoupling multivariable controllers. *Automatica*, 43(9):1481–1494, 2007.
- [48] P. Nordfeldt and T. Hägglund. Decoupler and PID controller design of TITO systems. *Journal of Process Control*, 16:923–936, 2006.
- [49] M. Nordin and P. Gutman. Digital QFT design for the benchmark problem. *European Journal of Control*, 1(2):97–103, 1995.
- [50] A. Oustaloup, B. Mathieu, and P. Lanusse. The CRONE control of resonant plants: Application to a flexible transmission. *European Journal of Control*, 1(2):113–121, 1995.
- [51] H. H. Rosenbrock. *State-space and multivariable theory*. London Nelson, 1970.
- [52] H. H. Rosenbrock. *Computer-aided control system design*. Academic Press, 1974.
- [53] M. J. Sidi. A combined QFT/ H_∞ design technique for TDOF uncertain feedback systems. *International Journal of Control*, 75(7):475–489, 2002.

- [54] J. F. Sturm. Using SeDuMi 1.02, a Matlab toolbox for optimization over symmetric cones. *Optimization Methods and Software*, 11:625–653, 1999.
- [55] D. Vaes, J. Swevers, and P. Sas. Optimal decoupling for MIMO-controller design with robust performance. In *IEEE American Control Conference*, Boston, USA, 2004.
- [56] D. J. Walker. Control of a flexible transmission - a discrete time H_∞ approach. *European Journal of Control*, 1(2), 1995.
- [57] Q. Xiong and WJ. Cai. Effective transfer function method for decentralized control system design of multi-input multi-output processes. *Journal of Process Control*, 16:773–784, 2006.
- [58] K. Zhou. *Robust and Optimal control*. Prentice Hall, New Jersey, 1996.

Curriculum Vitæ

GALDOS Gorka

E-mail: gorka.galdos@gmail.com

Date of birth: 23rd July 1980

Nationality: Basque

Education

- 2005 - 2010: **Doctoral studies and research** at the Automatic Control Laboratory, Swiss Federal Institute of Technology Lausanne (EPFL).
- 2002 - 2005: **Master of Science in Mechanical Engineering**, EPFL.
- 1998 - 2002: **Bachelor of Science in Mechanical Engineering**, Mondragon Unibertsitatea, Arrasate, Gipuzkoa (Spain).

Publications

Published:

- A. Karimi and G. Galdos. Fixed-order H_∞ Controller Design for Nonparametric Models by Convex Optimization. *Automatica* 46 (8) August 2010: 1388-1394.
- G. Galdos, A. Karimi and R. Longchamp. H_∞ Controller Design for Spectral MIMO Models by Convex Optimization. In *Proceed-*

- ings of the European Control Conference 2009*, pages 2863-2868, Budapest, Hungary, August 2009.
- A. Karimi, G. Galdos and R. Longchamp. Robust fixed-order H_∞ Controller Design for Spectral Models by Convex Optimization. *Proceedings of the 47th IEEE Conference on Decision and Control*, pages 921-926, Cancun, Mexico, December 2008.
 - G. Galdos, A. Karimi and R. Longchamp. Robust Loop Shaping Controller Design for Spectral Models by Quadratic Programming. In *Proceedings of the 46th IEEE Conference on Decision and Control*, pages 171-176, New Orleans, LA, USA, December 2007.

Accepted:

- G. Galdos, A. Karimi and R. Longchamp. H_∞ Controller Design for Spectral MIMO Models by Convex Optimization. *Accepted for publication in Journal of Process Control 2010*.
- G. Galdos, A. Karimi and R. Longchamp. Robust Controller Design by Convex Optimization based on Finite Frequency Samples of Spectral Models. *Proceedings of the 49th IEEE Conference on Decision and Control*, Atlanta, Georgia, USA, December 2010.

Submitted:

- G. Galdos and A. Karimi. A solution to the flexible transmission benchmark by convex optimization. *Submitted to Journal of Vibration and Control*.
- G. Galdos, A. Karimi and R. Longchamp. RST Controller Design for Spectral Models by Convex Optimization with Application to a Double-Axis Positioning System. *Proceedings of the 18th IFAC World Congress*, Milan, Italy, August 2011.